INTERACTIONS OF RADIANT ENERGY WITH SMALL PARTICLES

IN HOT, HIGH PRESSURE GASES

A THESIS

Presented to

The Faculty of the Graduate Division

by

William Lee Partain, Jr.

In Partial Fulfillment

of the Requirements for the Degree

Doctor of Philosophy

in the School of Nuclear Engineering

Georgia Institute of Technology

August, 1970

In presenting the dissertation as a partial fulfillment of
the requirements for an advanced degree from the Georgia
Institute of Technology, I agree that the Library of the
Institute shall make it available for inspection and
circulation in accordance with its regulations governing
materials of this type. I agree that permission to copy
from, or to publish from, this dissertation may be granted
by the professor under whose direction it was written, or,
in his absence, by the Dean of the Graduate Division when
such copying or publication is solely for scholarly purposes
and does not involve potential financial gain. It is under-
stood that any copying from, or publication of, this dis-
sertation which involves potential financial gain will not
be allowed without written permission.

7/25/68

INTERACTIONS OF RADIANT ENERGY WITH SMALL PARTICLES

IN HOT, HIGH PRESSURE GASES

Approved:

Date approved by Chairman: 8/20/70

ACKNOWLEDGMENTS

I am especially grateful to Dr. J. R. Williams, my thesis advisor, for his assistance and encouragement during the course of this work. My thesis committee members, Dr. J. D. Clement, Dr. J. R. Stevenson, Dr. C. Orr, and Dr. R. A. Pierotti, have encouraged me in this research and provided invaluable professional support. Their suggestions and assistance are greatly appreciated. I wish to thank Dr. C. J. Roberts of the School of Nuclear Engineering for his encouragement towards a career in nuclear engineering.

I have acquired many good friends during this work. I am especially thankful to Dr. Arkal Shenoy who encouraged and aided me during the initial stages of this research. Mr. Won Guk Hwang gave many hours of unselfish assistance while studying at Georgia Tech. I appreciate the help given by my fellow nuclear engineering graduate students Tony Garrett and Steve Thompson.

I would like to thank Mr. Harold Huey of the Engineering Experiment Station machine shop for his assistance in the equipment design, and Mr. Finn Scarboro, also of the machine shop, for his excellent work

TABLE OF CONTENTS

TABLE OF CONTENTS (Concluded)

LIST OF ILLUSTRATIONS

LIST OF ILLUSTRATIONS (Continued)

LIST OF ILLUSTRATIONS (Concluded)

SUMMARY

Aerosols of submicron-sized refractory particles are currently being considered as coolants for gas core reactors and for thermal radiation shielding in nuclear rocket nozzles. In order to be useful for these applications, the particles should be strongly absorbing in the ultraviolet, visible and near infrared regions of the spectrum and should withstand high temperatures at high pressures without reacting or vaporizing. Submicron-sized particles of refractory metals generally satisfy both of these requirements.

The ability of dispersed particles to absorb thermal radiation is determined by the extinction parameter, the scattering parameter and the angular scattering characteristics of the particles. Measurements are needed of these heat transfer parameters as functions of temperature, pressure, and incident radiant energy wavelength in order to evaluate the propellant heating in gas core nuclear rocket engines.

Measurements of the extinction parameter of tungsten-hydrogen aerosols were made as a function of wavelength from 2500 Å to 5800 Å at pressures to 115 atmospheres and temperatures to 2500°K. High pressure hydrogen, first unseeded and then seeded, was heated in a furnace employing an electrically heated tungsten strip. Radiant energy from a high pressure mercury arc was passed through the furnace, and measurements of the transmitted radiation and of the aerosol density yielded the extinction parameter for the tungsten-hydrogen aerosol at the selected tempera-

ture and pressure.

The measured extinction parameter at room temperature for all pressures to 115 atmospheres compared well with the theoretical value of the extinction parameter calculated using the Mie theory. The extinction parameter was observed to increase with pressure at temperatures above about 1000°K. Whereas the extinction parameter had been shown earlier to increase about a factor of two, from room temperature to 2000°K, at one atmosphere pressure, the increase was found to be about a factor of four at about 10 atmospheres and much greater at 100 atmospheres pressure. According to the Mie theory, the breaking up of particle agglomerates could account for part of this increase, but not all. Several physical processes are discussed that might be expected to enhance photon extinction beyond that predicted by the Mie theory.

CHAPTER I

INTRODUCTION

Purpose of Research

The objective of this investigation was to examine the radiant heat attenuation of an aerosol which closely duplicated the gas core nuclear reactor propellant. In the gas core reactor, heat is emitted as radiant energy from the central core of fissioning uranium gas and is absorbed in a surrounding flow of hydrogen which is seeded with refractory metal particles to enhance the radiant energy absorption. This experiment utilized a hydrogen aerosol heated to temperatures as high as $2500^{\circ}K$ and under pressures up to 100 atmospheres. The hydrogen aerosol was produced by dispersing submicron sized particles of refractory metals in hydrogen gas. The principal property that was measured was the ability of the aerosol to attenuate a beam of broad spectrum, visible and ultraviolet, light passing through it with the attenuation being measured as a function of wavelength. Other characteristics of the aerosol that were examined included the nature and extent of chemical reactions between the seed material and the hydrogen and the degree of dispersion obtained in the seed material before and after heating.

Chemical equilibrium calculations and vapor pressure data for the refractory metals indicate that tungsten is the best seed material for the gas core nuclear rocket concept. For this reason it was the principal seed material used in the experiment.

The Gas Core Nuclear Reactor

Manned interplanetary exploration is very costly even if the solid core nuclear rocket is used. There is current evidence that the public is not willing to spend the amount of money necessary to accomplish extensive manned missions to other planets. The use of a gaseous core nuclear rocket having only a conservative value for the specific impulse of 1500 seconds could make this type of exploration economically feasible. In a very general sense the reduction in cost of a mission is related to the exponential of the specific impulse.

The advantage of a solid core nuclear rocket over a chemical rocket results from the use of hydrogen as the propellant rather than the H_2O formed in the combustion process of a liquid oxygen-liquid hydrogen rocket engine. The specific impulse, a measure of the performance of a rocket engine, is proportional to $\sqrt{T/M}$ where T is the temperature of the propellant and M is the molecular weight of the propellant. The theoretical increase in specific impulse for the solid core nuclear rocket compared to a chemical rocket is a factor of three, but a lower operating temperature necessitated by the structural matrix of the fuel in a solid core nuclear rocket and the actual use of more hydrogen than needed for combustion in the chemical rocket makes the difference more nearly two than three. Present solid core nuclear rockets have specific impulses on the order of 800 seconds. Other concepts have been proposed which would allow a higher operating temperature. The dust bed nuclear reactor concept[1,2] eliminates the use of a structural matrix for the fuel in favor of small uranium fuel particles held in a band near the walls of the rocket cavity by centrifugal force. A specific impulse on the order of 1100

seconds could be realized. The liquid core nuclear rocket[3] holds the liquid uranium in place by centrifugal force and the hydrogen propellant is allowed to bubble through. Temperatures of about 5000°K might be obtained with corresponding specific impulses of approximately 1600 seconds.

The nuclear rocket concept that offers the highest temperatures is the gaseous core nuclear rocket.[4,5,6] The average temperature of the propellant would of the order of $10,000^{\circ}$K to $30,000^{\circ}$K. The specific impulse realized could be greater than 2000 seconds and if the propellant temperature approached $30,000^{\circ}$K enough of the hydrogen would be ionized that a rapid increase in the specific impulse, due to the low mass of the electrons, would be obtained leading to a value near 5000 seconds.

The technical difficulties associated with the development of the gas core nuclear rocket are not greater than those associated with the dust bed or liquid core nuclear rocket and thus emphasis of future nuclear rocket development is on it. There are several designs for the gas core nuclear rocket. The two most representative concepts receiving attention are the co-axial flow and light bulb concepts. The co-axial flow concept shown in Figure 1 is being investigated at the NASA Lewis Research Center. This concept envisions a central core of fissioning uranium gas that will be flowing much slower than the hydrogen flowing around the central core. There would need to be a propellant to fuel mass flow separation of at least 100 to 1. Lanzo[8] at NASA/Lewis has achieved this flow separation using a two dimensional system of air to air, but the Reynolds numbers for the two flows were quite low.

The other concept, that of the nuclear light bulb reactor[9] is being supported by the Joint AEC-NASA Space Nuclear Propulsion Office,
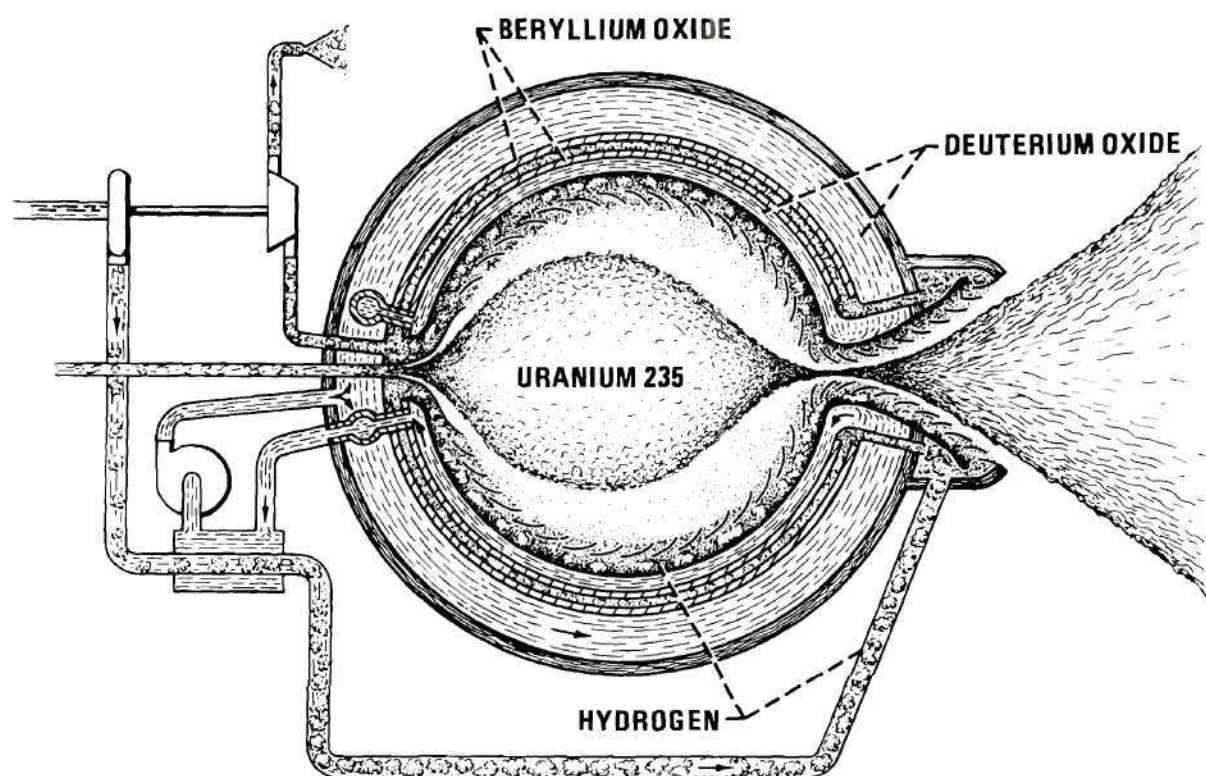
Figure 1. NASA/Lewis Gas Core Nuclear Rocket Co-axial Flow Concept

Washington, D.C. One of the prime contractors for this work is United Aircraft Laboratories. The heart of this concept is a transparent partition containing the uranium plasma with the hydrogen propellant flowing outside of the partition. For this reason, this concept is a closed cycle concept in that the fuel does not become mixed with the working fluid, while the previous concepts are known as open cycle. The current design of the closed cycle includes a partition constructed of quartz tubes through which hydrogen for cooling would be passed and a neon gas boundary flow injected tangentially into the uranium plasma from the tubes in order to prevent deposition of the gaseous uranium on the quartz walls.

Both of these gas core reactor concepts have in common the requirement of transferring thermal radiant energy from the uranium fuel region to the hydrogen. Hydrogen at lower temperatures is transparent to radiation of wavelengths longer than 1216 Å where the first transition in the Lyman series occurs. The hydrogen molecule can absorb infrared radiation, but, as indicated by the experimentally derived data[10,11] on uranium plasmas shown in Figure 2, most of the emission spectrum is concentrated below 7000 Å. As the hydrogen is heated, more of the hydrogen molecules occupy excited states and can absorb radiation of longer wavelengths. Figure 3 is a plot of the absorption coefficient for pure hydrogen with respect to wavelength of the radiation and with temperature as the parameter. Above 8000°K the absorption by the hydrogen becomes significant and sufficient to attenuate the radiant energy from a uranium plasma. For propellant temperatures below this point some other mechanism of heat transfer needs to be
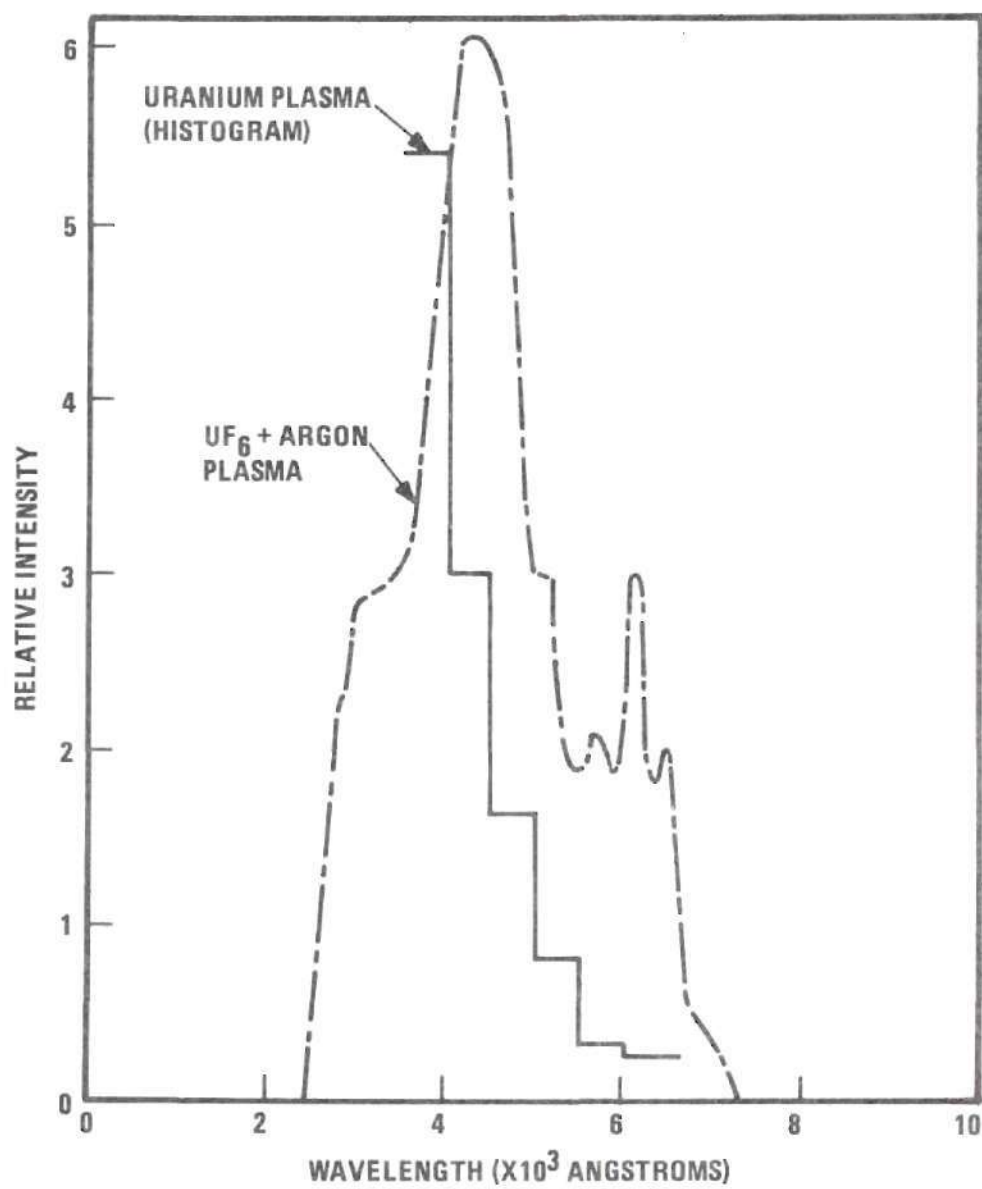
Figure 2. Experimental Emission Spectra of Uranium Plasma at about 8000°K (References 10 and 11)
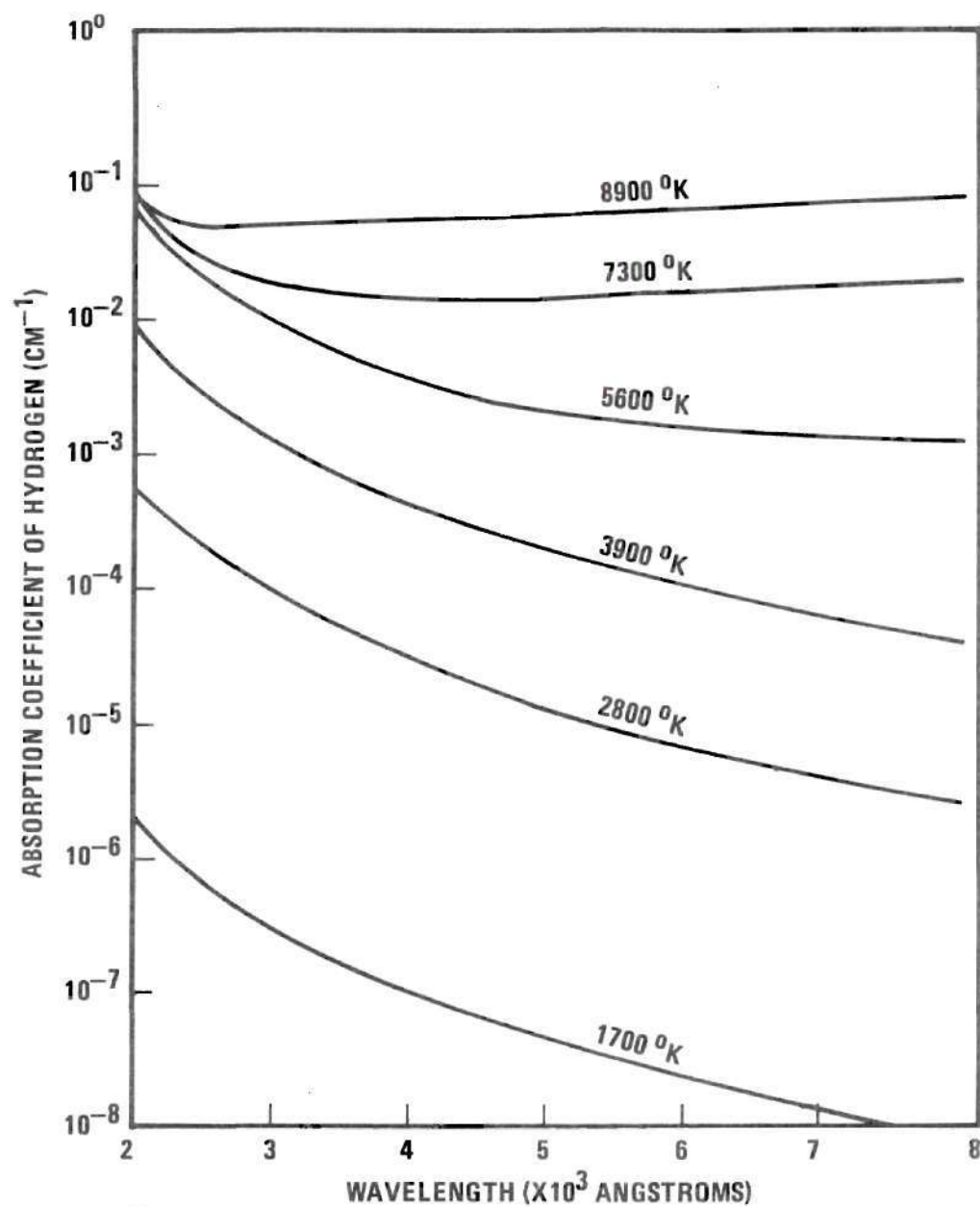
Figure 3.   Absorption Coefficient of Pure H_2 at 100 Atmospheres (Reference 16)

employed. The hydrogen could be seeded with a gas that would absorb in the 900-7000 Å region but the process would be line absorption and the integrated absorption would not be very large. Seeding by small particles is favored because they give a very broad absorption that varies uniformly with wavelength. There are several criteria that seed particles have to meet. Their optical absorption must be large so that a particle to propellant mass ratio smaller than one percent will be sufficient to absorb the radiant energy. The neutron absorption cross section must be low to prevent excessive uranium fuel inventories in the reactor cavity. A material with a high vaporization temperature and a low vapor pressure is desirable. The chemical reaction rate with hydrogen must be very small. These considerations indicate that submicron-sized refractory metal particles are the best candidates. Carbon was favored early in the development of the gas core nuclear reactor concept. However, Shenoy and Partain[12,13] have shown it to have a reaction rate with hydrogen that makes it unsuitable for a seed material until more experimental work is conducted with larger size carbon particles. Carbon is attractive, except for the chemical reaction, because it has a low density and low molecular weight and is highly absorbing.

Other materials such as alumina and silica which would seem to offer these advantages, being known as good attenuators of light, are unsatisfactory because they are almost purely scattering and absorb very little light. Also, high temperature, high pressure hydrogen tends to reduce the oxide refractory materials.

Heat transfer mechanisms in the gas core reactor are complex. In the central region of the cavity is the gaseous uranium core which is

essentially opaque to radiant energy.[14] As a result of this opacity radiant energy is emitted from very near the surface of the uranium plasma which may have approximately a spherical geometry in the case of the co-axial flow concept. The temperature in the interior of the uranium plasma may extend up to $100,000^{\circ}K$, but the temperature profile is very severe and a skin temperature of $15,000^{\circ}K$ is expected.[15] The seeded propellant closest to the core and that near the nozzle would have been heated to the point that no solid particles exist and the radiant energy absorption would be that due to the heated hydrogen and the vaporized or chemically reacted seed material. Krascella[16] has calculated the absorption of pure hydrogen as a function of pressure, temperature, and wavelength. Patch[17] has also calculated the absorption of hydrogen for the same parameters and compared his results with those of Krascella. Krascella[18] has also calculated the Rosseland mean opacity of tungsten vapor using a semiempirical model. The Rosseland mean opacity is an average of the spectral absorption coefficient over the spectrum. In the event that it becomes feasible to use graphite seed, the Rosseland mean opacity of carbon-hydrogen reaction products has been calculated by Main.[19]

At this point (before considering the solid seed particles) the propellant is considered to be a grey gas. Assuming a spherical geometry (approximate geometry of the co-axial flow concept) a two dimensional radiant heat transfer analysis could be made with the data available. The two dimensional problem is due to the flowing hydrogen propellant. The difficulties are, first, that the propellant is more nearly a colored gas than a grey gas, and therefore, absorbs preferentially

with wavelength; and second that the opacity of the hydrogen varies with the temperature. The hydrogen opacity has a positive temperature (T) dependence of between T^2 to T^4. The confidence level of the theoretically derived data also varies with temperature and wavelength. The data accumulated for heat transfer studies in the gas core nuclear reactor were examined by Patch[20] and the assumptions and confidence level behind the calculations discussed. The data appear less accurate in the temperature range of 3000-7000°K. This is also true of the particle opacity measurements. To date, no one has applied all of these data to a solution of the radiant energy transfer. The work that appears to be most applicable was done by Monsler[21] in which he examined the conditions under which a system similar to that of the gas core nuclear rocket would not have a stable, steady state solution. Given the proper conditions of high heat fluxes, optically thick gas, and a strong positive dependence of opacity on temperature and pressure, he has shown that an unstable system of radiation driven shock waves can result.

Near the walls of the reactor cavity and near the hydrogen propellant entrance, the seed material would be in the form of submicron sized particles in dynamic equilibrium with the hydrogen. The opacity of this aerosol is due to the seed material since the hydrogen is transparent in these cooler zones. The seed material serves to transfer the radiant energy to the hydrogen and to shield the containment walls from a high heat flux. The particles attenuate the radiant energy by two processes: scattering and absorption. Only the absorption process serves to heat the hydrogen propellant, but the scattering is equally important since it tends to increase the average path length traveled by a photon. The

steady state radiant energy transport equation for small particles suspended in a transparent medium is given by,

$$\frac{1}{\rho}\frac{dI(\lambda,\Omega)}{ds} = -\mu_e(\lambda)I(\lambda,\Omega) + j(\lambda) + \mu_s(\lambda)\int_0^{4\pi} I(\lambda,\Omega')p(\lambda,\cos\theta)\frac{d\Omega'}{4\pi}$$

where

I = the intensity of radiant energy in a unit wavelength interval at λ traveling in direction Ω

s = distance

Ω = solid angle

j = emission coefficient

p = scattering amplitude function

θ = angle of scattering

ρ = density of the aerosol

It is seen from this equation that the four important parameters one must know in order to evaluate radiant heat transfer through particle-seeded gases are:

$\mu_e(\lambda)$ the extinction parameter

$\mu_s(\lambda)$ the scattering parameter

$p(\lambda,\cos\theta)$ the scattering amplitude function

and $j(\lambda)$ the emission coefficient

These parameters must be known over the applicable temperature, wavelength, and pressure range. In addition, $p(\lambda,\cos\theta)$ must be known for scattering angles of 0 to 180 degrees.

In order to predict these heat transfer parameters theoretically, the complex index of refraction must be known over the wavelength range

of interest. The research that has been done on the theoretical and experimental determination of these heat transfer parameters is summarized in the Background chapter. There are sufficient theoretical values of the heat transfer parameters available to permit a "first attempt" at the solution to the complete heat transfer problem in the gas core nuclear reactor. Three areas that theory does not cover are irregularly shaped particles, the physical changes in the aerosol due to chemical reactions, and the change in the radiant energy interaction process when the particles are heated enough to become thermionically emitting. All three areas must be examined as a function of incident radiation wavelength, temperature and pressure.

This experimental investigation examines μ_e, the extinction parameter, in these three areas which deviate significantly from theory. The purpose of this introductory section is to present the context in which this investigation was conducted.

Other Applications of the Research

The gaseous core nuclear reactor concept was originally conceived as the next step in nuclear rocket propulsion, but it may find superior justification as the heat source for a magnetohydrodynamic power generation plant. Several studies[22,23,24] have recently been conducted on the characteristics of such a system. The MHD generator has received a great deal of attention in the past because of its simplicity of design, high efficiency and high power density for high temperature working fluids. The very hot working fluid of the gaseous core nuclear reactor combines well with the MHD system which is capable of using such high temperature

heat sources.

The primary hindrance to the development of MHD power plants has been the low electrical conductivity of the gas working fluid. A conductivity in the neighborhood of 100 mhos/m is desired. The research on higher conductivities in the past decade has focused on the promise of nonequilibrium ionization where the electrons are heated to a higher temperature than the gas by the use of a magnetically induced electric field. This work on nonequilibrium ionization has been directed toward solid-core nuclear reactor heat sources using noble gases, such as argon, in a closed cycle. Nonequilibrium ionization in a combustion device is not practical because the very large electron-atom and electron-molecule collision cross sections which exist in combustion products make it virtually impossible to obtain a condition of unequal electron and gas temperatures.[22] Still the results from experiments seeking to develop the nonequilibrium ionization have in general been disappointing.[25] The answer may lie with the gaseous core nuclear reactor which can provide a higher working fluid temperature and a high degree of ionization from the radiation present in the reactor cavity. The radiation should preferentially heat the electrons, increasing the nonequilibrium ionization.[26]

The fact that a gas core nuclear reactor requires a seed material consisting of small particles to transfer the radiant energy to the gas working fluid is also an advantage in the MHD application since the particles would enhance the electrical conductivity of the fluid by supplying additional electrons by thermionic emission.[27,28]

The gaseous reactor MHD generator could serve as a topping cycle for large ground based power plants to considerably improve their

efficiency. The exhaust from the MHD generator could be used to produce steam for conventional turbines before being returned to the reactor. Another important application for the gaseous reactor MHD generator may be in a space electrical power system which reauires a high radiator temperature.

Rosa[29] indicates the gaseous reactor may prevent MHD technology from becoming obsolete. It appears to be the best heat source which is capable of allowing the MHD generator to realize its true inherent advantages. Likewise an urgent need for more efficient electrical power generation, such as the gaseous reactor MHD system could supply, may be the necessary impetus for further research into gaseous reactors. A gaseous core nuclear reactor incorporated into a ground base power system with uranium separation from the working fluid could provide valuable operational experience for a gaseous core nuclear rocket engine.

There are many other applications for the use of small particles in a radiant heat transfer situation. The problem of radiant energy transfer from a very hot rocket exhaust plume containing metallic particles to the space vehicle has been investigated by Rochelle[30] and Carlson.[31] The earlier analytical calculations of this heat transfer problem[32-34] made use of simplifying assumptions such as plane parallel geometry or isotropic scattering. Love[35] applied Monte Carlo calculational techniques to the scattered radiant energy from the rocket exhaust plume. He used experimentally derived scattering amplitude function data. Use of the data described in this report coupled with experimentally measured scattering parameter data and scattering amplitude function data would permit more accurate calculations for the exhaust plume from a gaseous core nuclear

rocket. Williams and Byrn[36] applied the general purpose Monte Carlo transport program, CAVEAT,[37] to calculate the heat deposition in the propellant region and the heat flux reaching the cavity liner. The uranium emission spectrum from reference 10 was combined with the wavelength dependent absorption coefficients for uranium calculated by Parks[38] to obtain the thermal emission spectrum of $10,000^{\circ}K$ uranium at the surface of the core. The data described in this report were used to obtain the absorptive properties of the seeded hydrogen propellant. An absorbing layer of particle-seeded gas may also be used for shielding re-entry vehicles[39] from the intense heat generated upon entering the atmosphere. Howell[40] has shown that a seeded propellant layer next to the inner wall of a rocket nozzle will reduce the radiant heat flux at the nozzle wall by two orders of magnitude. This may make possible rocket engines which can operate with higher temperature propellants and thereby have higher performance.

CHAPTER II

BACKGROUND

Theory

Since this investigation involves measuring the ability of small particles dispersed in hydrogen to absorb radiant energy and explaining the characteristics of the aerosol at the time of measurement, including dynamic processes such as chemical reactions and aerosol kinetics, it is convenient to consider the theoretical background for the system in three sections corresponding to the natural divisions of the system: aerosols, the interaction of radiant energy with submicron-sized particles, and chemical reactions.

Aerosols

The properties of aerosols vary according to the size of the particles. A study was made of the characteristics of aerosols that contain particles of about one micron diameter or less and the forces acting between the particles. Most of the information quoted is based on a bound collection of papers edited by Davies,[41] a bound collection of papers edited by Green and Lane,[42] and Particulate Technology by Orr.[43]

There are two general ways to form particulate clouds. One is a condensation process in which clusters of molecules come together to build up particles of colloidal dimensions. An example of this is the burning of hydrocarbons in an oxygen-lean environment to produce small carbon particles. The second method is the dispersion method where a

solid material is ground into small particles, or more commonly, chemi-
cally produced as small particles and then mechanically dispersed.

There are three characteristics of aerosols that are especially
relevant to this experiment. They are the rate of particle coagulation,
the rate of particle deposition on containment walls, and the size dis-
tribution of the particles constituting an aerosol.

The first concern, even before considering coagulation, is to ob-
tain good dispersion of a powdered seed material. Powders of particles
with radii greater than 10 microns are quite readily dispersed by com-
pressed air to form aerosols with completely disagglomerated particles.
The dispersion becomes increasingly difficult with decreasing particle
size, and for powders of particles with radii of less than 0.5 micron
complete dispersion has not yet been achieved.[41] In addition to the
particle size, their shape is of great importance. Plate and needle
shaped particles are less readily dispersed than spherical ones. The
powders of hard substances are more readily dispersed than those of soft
materials. The presence of moisture in powders impairs their dispersion
greatly, but if the powders are too dry, they also disperse less readily
due to high triboelectric charges. The best way to transmit mechanical
force to the individual particles in a powder is to pass the aerosol of
large aggregates through a nozzle where the shear forces exerted on the
gas can be transmitted to the aggregates. This is not mechanically effi-
cient, but it is very difficult if not impossible to transmit the force
to the individual particles by any kind of mechanical mixing process. A
mechanical mixing process can be very important in forming a consistent
aerosol of the large aggregates which can then be delivered to the nozzle.

After a well-dispersed aerosol has been formed it will immediately begin to coagulate. The simplest form of coagulation is the collision of particles under Brownian motion. When two particles collide they almost invariably stick together. The coagulation rate in this case is roughly proportional to the square of the particle number density. Seldom is this the only coagulation process in effect. Especially in the case of a mechanically dispersed powder, the electrical charges on the particles are one of the most important factors in the coagulation process. The mechanical dispersion of the particles creates charged particles, but the amount of charge depends on many variables such as the moisture content of the powder, whether or not the dispersion nozzle is grounded, and the nature of the charge on the particle (unipolar or bipolar). All natural or artificially generated aerosols are to some extent electrically charged. The electrical charge may also be acquired when gaseous ions, produced by such agents as ionizing radiation, high voltage discharge, or high temperature are captured by the particle.

If an aerosol consisted of particles all with the same sign charge and in a unipolar charge state, the particles would tend to repel each other and therefore retard coagulation. This is more nearly a theoretical condition, however, since the particles are rarely all of the same charge. And even if the particles are unipolar charged, when they come sufficiently close to each other they can create a mirror charge in another particle and induce a bipolar charge state. Van der Waals forces must be taken into account since they aid coagulation by attracting particles when they come sufficiently close without having them actually touch. A chain-like aggregate is usually a good indication that coagulation

is taking place due to bipolar charged particles.

Aerosol particles in an electric field have an induced charge which causes them to behave as dipoles. Fuchs[41] reviewed the theory and experimental data for this type of coagulation. He concluded that very high electric fields are required to increase the coagulation rate significantly, but that at high aerosol concentrations and electric fields, long threadlike aggregates are formed. Because the dipole strength increases with aggregate length, the coagulation rate can actually increase with time even though the number concentration is decreasing. The only use of a high electric field in this research is the use of a Van de Graaff generator to induce a charge on particles and deposit them on electron microscope grids for inspection. These charged particles are so quickly attracted to the grounded electron microscope grids that it is unlikely they would have experienced an extensive coagulation during that time interval. Chain-like aggregates would indicate that such a coagulation process is occurring and would warrant a comparison with samples obtained by a thermal deposition process.

When a thermal gradient is set up in an aerosol, particles will move along the gradient under the influence of the differential molecular bombardment giving rise to radiometer forces. These particles are driven away from a hot surface and deposited on a cold one in the vicinity. This phenomenon is important in this research because of the need to sample the heated aerosol in order to determine its density and the degree of dispersion after heating.

Photophoresis is a phenomenon similar to the thermally generated

radiometer force just described. An intense beam of light will generally cause particles to move either in the direction of the radiation flux or against it. Since the principal energy form in the gaseous core nuclear reactor is visible and ultraviolet light this phenomenon may have to be taken into account. Photophoresis is very weak with good reflectors of radiation such as calcium cloride, antimony trioxide, and magnesium oxide, but very strong with strong absorbers like lamp black, iron filings, potash alum, and dyestuffs. Keng and Orr[44] investigated photophoresis for lamp black and observed some very interesting boundary effects, indicating that particles would not cross the boundary of an intense beam of light.

The size distribution of aerosols is important when measuring the extinction parameter. There are several distributions that can be used to describe particles and the way in which the particle was produced influences to a great extent the distribution that it will most closely follow. The log-normal distribution is commonly used, but again each group of particles should be examined as to source so as to apply the best distribution function to them. The approach used in this research has been to sample the aerosols and make electron micrographs which show the degree of agglomeration, the average size of the particle, and to some extent the size distribution. This method is really only applicable if a good random sample is obtained. An electrostatic precipitator was used to obtain the samples in this investigation. In general, an electrostatic sampling device does not produce a random sample since the charge and mass of the particle dictate the linear distance at which the particle should

settle from the entrance region.   However, tests with the electro-static device used in this research resulted in random collection. This is apparently due to the charge being given to the particles by a needle in the center of a box of approximately 200 cubic centimeters volume.

The references describe a coagulation process due to acoustic waves in an aerosol. This phenomenon has been used in conjunction with aerosol generation experiments as part of this research since the sound waves tend to form very large agglomerates which fluidize easily when gas is passed through them and the fluidized agglomerates can be deliv-ered to a shear producing nozzle. If this is not done with difficult-to-disperse powders, such as tungsten powder, large chunks of powder will tend to be transported to the nozzle where they clog the opening.

In general the science of aerosols has been approached in an em-pirical manner (e.g. making electron micrographs to determine size distri-bution) since the aerosol undergoes so many processes that it is almost impossible to predict from theory the state of the aerosol subsequently. A good intuitive grasp of the relative importance of phenomena such as charge-induced coagulation and thermal migration is important in design-ing an experiment like the one used in this investigation.

Interactions of Radiant Energy With Submicron-Sized Particles

When radiant energy of wavelength λ interacts with a particle of diameter λ/π, the ability of the particle to absorb this radiation is near a maximum. The energy absorption and the subsequent heating of the particle depends on the ohmic heating of the particle by the free elec-trons that have been excited by the incident radiation. In the two extremes, a perfect insulator and a perfect conductor, no energy would be deposited.

In the case of the insulator the electromagnetic wave would be reflected from the tightly bound electrons and in the case of a perfect conductor re-emission in the original form would take place because no ohmic heating could occur. Metallic particles are better able to absorb radiant energy because they are conducting and have significant resistivity.

In addition to absorption, radiant energy is scattered without change in wavelength by the particle. The scattering is the sum of three processes, reflection from the surface of the particle, refraction of light transmitted through the particle, and diffraction due to the interference of the electromagnetic wave as it passes by the edge of the particle. The cross-section for diffraction is approximately equal to the geometric cross-section of the particle. Since the reflection, refraction, and absorption are competing processes on the surface of a particle, the total cross-section of these processes is approximately equal to the geometrical cross-section. The total interaction of the radiant energy is the sum of the absorption and scattering processes, with a cross-section of approximately two geometrical cross-sections, and can be termed the attenuation or extinction process.

The extinction process as it has just been described is greatest for the case where the diameter of the particle is on the order of the wavelength λ divided by π. Thus, the absorption of radiant energy in the near infrared, visible, and ultraviolet regions of the spectrum is greatest for submicron sized particles of diameters in the range of 0.05 to 0.5 microns. The scattering from a particle in this size range

has a complicated angular dependence. Particles much larger give highly
forward scattering and particles much smaller give nearly *isotropic scat-
tering* which is known as Rayleigh scattering.

For particles as large as the wavelength or larger, the cross-
sections are proportional to the square of the radius, whereas the mass
is proportional to the cube of the radius, so the cross-sections per
unit mass of particle material are inversely proportional to the particle
radius, as is illustrated by Figures 4-6.

For particles much smaller than the wavelength of the incident
thermal radiation the total attenuation falls off rapidly and approaches
the value of the absorption-reflection process which also decreases. In
this instance the previous discussion concerning diffraction scattering
is no longer applicable, since the diffraction scattering is negligible
for such small particles. The very small particles can be totally ab-
sorbing (if there is no reflection, e.g. carbon) but the absorption para-
meter is smaller than that realized at the optimum size.

There are three significant mechanisms by which radiant energy
interacts with a gas containing particles: (1) absorption by the gas,
(2) absorption by the particles suspended in the gas, and (3) scattering
by the particles. The importance of each of these three mechanisms de-
pends on the composition, temperature and pressure of the gas, the com-
position, sizes and shapes of the particles, the particle number density,
and the spectrum of the radiant energy.

The attenuation of a beam of monochromatic radiant energy by a
gas containing particles is governed by the expression

$$I(\lambda,x) = I(\lambda,o) \, e^{-k_T(\lambda)x} \tag{1}$$

where $k_T(\lambda)$ is the total linear attenuation coefficient for radiant energy of wavelength λ, and x is the distance the beam traverses through the seeded gas. The total linear attenuation coefficient for all three interaction processes is equal to the sum of the linear attenuation coefficients for each process separately, that is,

$$k_T(\lambda) = k_a^g(\lambda) + k_a^P(\lambda) + k_s^P(\lambda) \tag{2}$$

where $k_a^g(\lambda)$ is the linear attenuation coefficient due to absorption by the gas alone, $k_a^P(\lambda)$ is the linear attenuation coefficient due to absorption by the particles, and $k_s^P(\lambda)$ is the linear attenuation coefficient due to scattering by the particles. $k_a^P(\lambda)$ and $k_s^P(\lambda)$ are proportional to the number density of the particles as long as the particles are randomly oriented and the average distance between the particles is much greater than their effective radius, so it is convenient to define the absorption parameter $\mu_a(\lambda)$ by

$$\mu_a(\lambda) = \frac{k_a^P(\lambda)}{\rho} \text{ and } \mu_s(\lambda) = \frac{k_s^P(\lambda)}{\rho} \tag{3}$$

where ρ is the particle density in grams of particles per cubic centimeter of aerosol. $\mu_a(\lambda)$ is also called the mass absorption coefficient. The totality of processes by which energy is removed from a beam by a particle cloud is called extinction, so the extinction parameter is given by

$$\mu_e(\lambda) = \mu_a(\lambda) + \mu_s(\lambda) \, . \tag{4}$$

The absorption, scattering, and extinction parameters are independent of the concentration of particles.

One may now consider the absorption of radiant energy by particle-seeded gases to be the sum of two independent processes; absorption by the gas itself and absorption due to the particles in the gas. The absorption coefficient of the gas, $k_a^g(\lambda)$, depends only on the composition, temperature, and pressure of the gas; whereas the absorption and scattering parameters of the particles, $\mu_a(\lambda)$ and $\mu_s(\lambda)$, depend on the composition, sizes, and shapes of the particles. Thus, $k_a^g(\lambda)$ may usually be determined for the pure gas and $\mu_a(\lambda)$ and $\mu_s(\lambda)$ for the particles in any transparent medium and then $k_T(\lambda)$ is calculated for the particle-seeded gas using equation 2 and 3. However, this procedure becomes difficult, if not impossible, when the composition of the gas and the sizes and shapes of the particles are changed by chemical reactions between the particles and the gas.

The basic mechanisms of radiant energy absorption by particle clouds and by gases are quite different. Since atoms and molecules of a gas absorb radiant energy in discrete quanta, the absorption coefficient of a gas may change many orders of magnitude over a wavelength interval of a few Angstroms. The familiar absorption spectra of various gases attest to the wide variations of $k_a^g(\lambda)$ as λ is changed.

Whereas gases tend to absorb in lines and bands, the absorption and scattering characteristics of real particle clouds vary gradually with the wavelength of the incident radiant energy. Thus, $\mu_a(\lambda)$ and $\mu_s(\lambda)$ are uniformly varying functions of wavelength. Scattering enhances energy absorption in particle clouds by increasing the average path

length traversed by the radiant energy. However, in any given unit volume of aerosol, the particle-gas mixture is heated only by absorption, not by scattering. For this reason it is convenient to define the absorption coefficient of the aerosol, $k_a(\lambda)$ by

$$k_a(\lambda) = k_a^g(\lambda) + k_a^p(\lambda) = k_a^g(\lambda) + \rho\mu_a(\lambda) \quad . \tag{5}$$

Then the scattering coefficient for the aerosol is equal to the scattering coefficient of the particles alone, since scattering by the gas is negligible.

$$k_s(\lambda) = k_s^p(\lambda) = \rho\mu_s(\lambda) \quad . \tag{6}$$

The effect of scattering depends not only on the value of $\mu_s(\lambda)$ but also on the angular dependence of the scattered energy.

The Mie theory,[45] published in 1908, is the best known and most useful theory which describes the absorption and scattering of electromagnetic radiant energy by particles. It applies to homogeneous spherical particles of any diameter situated in a homogeneous transparent non-magnetic medium. Mie solved Maxwell's equations with the appropriate boundary conditions and evaluated the total scattered energy as well as the total energy removed from an incident beam, thus arriving at the scattering and extinction cross sections, σ_s and σ_e. Excellent discussions of the derivation of the Mie Equations are found in the literature.[46-50]

Krascella[51] applied a transformation procedure developed by Aden[52] to the Mie equations to calculate the effect of particle size, wavelength, and particle temperature on particle opacity in those regions of the ultraviolet, visible, and infrared spectra for which complex index of refraction

data were available. Shenoy[12] used Krascella's program to extend these calculations to other types of particles and to a broader wavelength range.

Svatos[53] has recently published a solution to Maxwell's equations for extinction by flattened ellipsoids; however, at present there is no theory that accurately predicts absorption and scattering characteristics of irregularly shaped particles. Submicron-sized particles of refractory materials are generally highly irregular in shape, so the Mie theory can only be used as an approximation to the absorption and scattering characteristics of these particles.

Since the Mie theory calculates the extinction cross section, σ_e, and the scattering cross section, σ_s, the absorption cross section is given by $\sigma_a = \sigma_e - \sigma_s$, and the extinction, absorption, and scattering parameters are given by

$$\mu_e = \frac{\sigma_e}{\rho_p V}, \ \mu_a = \frac{\sigma_a}{\rho_p V}, \ \text{and} \ \mu_s = \frac{\sigma_s}{\rho_p V} \tag{7}$$

where ρ_p is the mass density of the particle material and V is the volume of the spherical particle.

Mie's solution, though derived for a single sphere, also applies to absorption and scattering by any number of spheres, provided that they are all of the same diameter and composition and provided also that they are randomly distributed and separated from each other by distances that are large compared to the particle radius. Under these circumstances there are no coherent phase relationships between the light that is scattered by the different spheres, and the total scattered energy is equal

to the energy scattered by one sphere multiplied by their total number.
Similarly, for a distribution of sizes, the energy scattered by the
spheres of each particular size may be summed to obtain the total scat-
tered energy.

Calculations using the Mie theory require a knowledge of the par-
ticle radius, wavelength of the radiant energy, and the complex index
of refraction of the spherical particles. The relationship between the
complex index of refraction $n = n_1 + in_2$, the conductivity σ, the di-
electric constant ϵ, and the permeability μ is given by the equations

$$n_1^2 = \frac{1}{2} \mu \epsilon \left[(1 + 4\sigma^2 \epsilon^{-2} \nu^{-2})^{\frac{1}{2}} + 1 \right] , \tag{8}$$

and

$$n_2^2 = \frac{1}{2} \mu \epsilon \left[(1 + 4\sigma^2 \epsilon^{-2} \nu^{-2})^{\frac{1}{2}} - 1 \right] , \tag{9}$$

where ν is the frequency.

The Mie theory is very useful in studying the effect of the par-
ticle parameters on the extinction and scattering cross sections and in
predicting the theoretical values for the measured extinction parameter.
Shenoy[12] has varied the input data to the Mie program written by Krascella
and generated the particle size dependence of the heat transfer parameters
for several cases. Figure 4 shows the size dependence of the extinction,
absorption and scattering parameters of submicron carbon particles at a
temperature of 2240°K and for two wavelengths, 2000 Å and 6000 Å, of in-
cident thermal radiation. The existence of an optimum size is apparent,
as is the sharp decrease in the scattering as the particles become very
small. Figure 5 presents similar results for silicon and tungsten.

Non-conductive particles such as magnesium oxide, aluminum oxide, or silica, have scattering parameters several orders of magnitude higher than their absorption parameters, so they scatter much more thermal radiation than they absorb. Figure 6 shows the extinction, absorption, and scattering parameters of aluminum oxide calculated by Plass[54] using the Mie theory.

Chemical Reactions

A literature survey was conducted to obtain information on the reaction of hydrogen with possible seed material candidates, such as, tungsten, molybdenum, silicon, tungsten carbide, silicon carbide, titanium, and carbon. The literature revealed that no reaction occurred between the metals and hydrogen other than the formation of complex hydrides that are important from a strength of materials point, but are not important in the choice of a seed material. Roback[55] of United Aircraft Laboratories made a similar study of the literature and arrived at the same conclusion.

While the melting point and boiling point of a material that is nonreactive with hydrogen are important, the most important criteria in picking a seed material from the chemical viewpoint is the vapor pressure at the high temperatures. Masser[56] made a survey of the vapor-pressure data for 13 refractory materials having low thermal neutron absorption cross sections and extrapolated the available vapor-pressure data to 1000 atmospheres. He found that tungsten was superior to the other materials (carbon, cerium, molybdenum, niobium, niobium carbide, platinum, ruthenium, silicon, tungsten, vanadium, yttrium, zirconium, and zirconium carbide) with a temperature of 9340°K at 1000 atmospheres
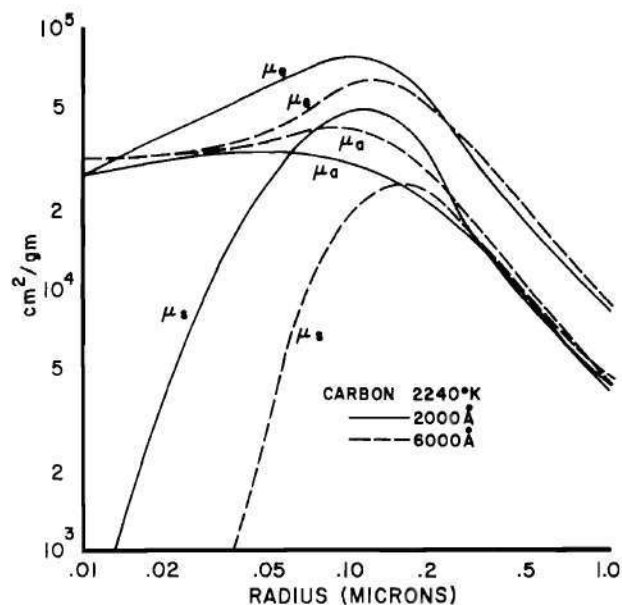
Figure 4. Mie Theory Calculations of the Extinction, Absorption, and Scattering Parameters of Submicron Carbon Particles (Ref. 12)
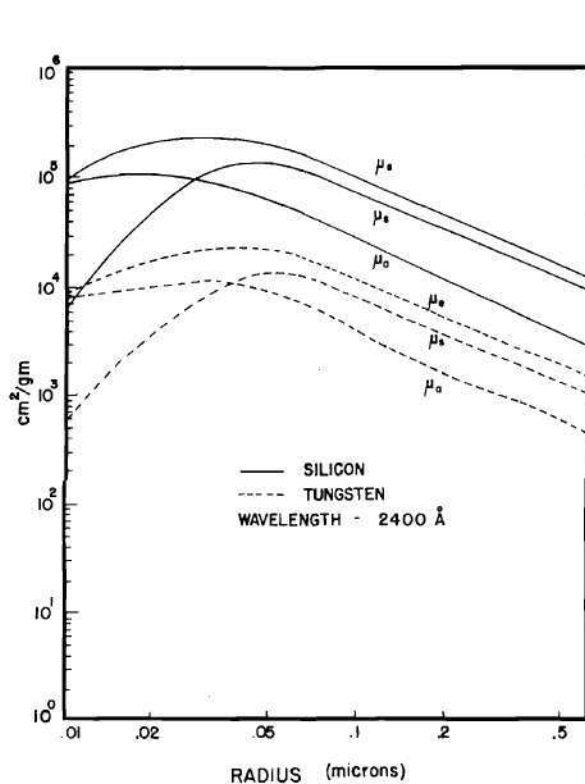
Figure 5. Extinction, Absorption and Scattering Parameters of Submicron Silicon and Tungsten Particles Calculated Using the Mie Theory (Ref. 12)
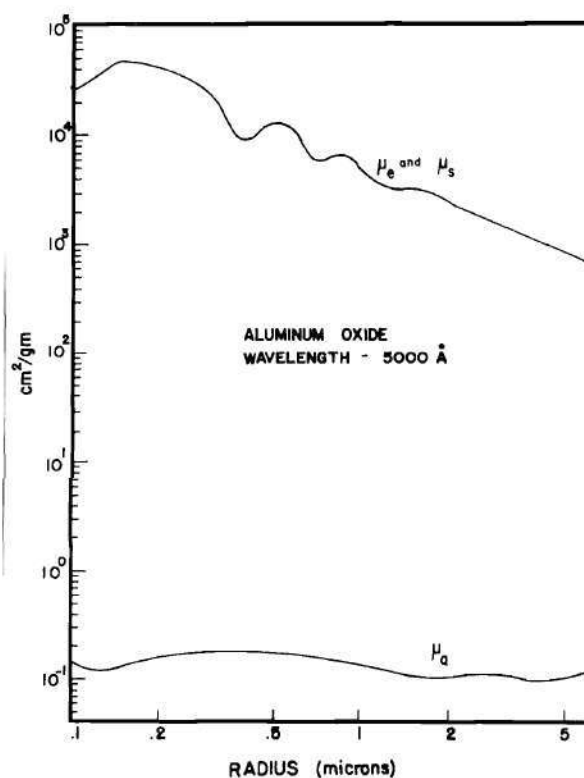
Figure 6. Extinction, Absorption, and Scattering Parameters of Aluminum Oxide Particles Calculated Using the Mie Theory (Plass, G.N., Applied Optics, 3:7, 867 (1964))

pressure. Roback did a similar investigation and extrapolation of the vapor pressure data. In addition Roback performed equilibrium composition calculations on the products of reaction of hydrogen with the oxides, nitrides, carbides, and borides of titanium and zirconium. He assumed two percent of the seed material was introduced into the hydrogen stream at a pressure of 1000 atmospheres. The results of the calculation indicated that TiC, TiN, TiB_2, and TiO_2 were completely vaporized or dissociated for the conditions described above at temperatures of 3540, 3410, 3450, and $2800^{\circ}K$, respectively. If these vaporization temperatures are compared with that obtained for titanium metal itself, namely, $3400^{\circ}K$, it is seen that the carbide, nitride, and boride offer slight advantages over the metal. The results of the zirconium calculations indicated that ZrC, ZrB_2, ZrN, and ZrO_2 vaporized at temperatures of 3820, 3200, 3650, and $3040^{\circ}K$, respectively. Since the vaporization temperature of zirconium is $4390^{\circ}K$ these compounds would offer only the advantage of a higher melting temperature than zirconium. Roback indicated the compounds of the other refractory metals could be expected to show a similar behavior.

Carbon, of course, does react with hydrogen. Duff and Bauer[57] used the readily available thermodynamic data for hydrocarbons to make a theoretical study of the formation of 71 reaction products of graphite and hydrogen at pressures from 0.1 to 10 atmospheres and temperatures from 500 to $5000^{\circ}K$. Main[19] has performed a more recent theoretical study in which he calculated the equilibrium compositions (in order that he could calculate the spectral absorption coefficients and Planck and Rosseland mean absorption coefficients) for carbon-hydrogen mixtures at total gas pressures of 100, 500, and 1000 atmospheres, gas temperatures of

1600, 2200, 3000, 4000, 5000, 6500, 8000, and 10,000°K, with carbon/hydrogen mass ratios of 0.005, 0.01, and 0.05, a total of 72 cases. The composition calculations included 65 species of which one was solid graphite, but the calculations showed that no condensed carbon, either solid or liquid, was present in any of the mixtures. The principal species in the mixtures were H_2 and CH_4 at the lower temperatures, and H_2, H, C, C_2, CH, C_2H, and C_2H_2, at the higher temperatures.

Marteney[58] examined the possibility of using carbon particles as a seed material. By making equilibrium composition calculations he determined that a weight ratio of carbon to hydrogen greater than 0.73 would be required at the optimum temperature, 2500°K, in order for any free carbon to exist, and that the amount of free carbon decreased very rapidly as the temperature was increased. Duff and Bauer, Main, and Marteney have all assumed an equilibrium condition. Marteney justifies his assumption:

> Particles which have been heated by thermal radiation cause heating of the surrounding gas by laminar conduction of the heat to gaseous atoms located in the vicinity of the particle. If the ratio of the thermal conductivity of the gas to the diffusivity of the gas (Lewis number) is on the order of unity, which is the case for most gases, then the diffusion of any vapor formed by the chemical interaction of the particle material and the surrounding gas should occur as rapidly as the conduction of heat from the particle to the surrounding gases. Therefore, it would appear unlikely that nonequilibrium mixtures of reaction products would occur locally and it can be assumed that the particle materials should be in thermodynamic equilibrium with the surrounding gases.

If, contrary to Marteney's supposition, a non-equilibrium condition could exist whereby a carbon particle might reach the vaporization temperature before reacting, then carbon would still be of interest as a seed material. A literature search for reaction rate data resulted only in data for large samples, although not as much as would have been expected,

and revealed no reaction rate data for carbon in colloidal form. This form refers to particles from approximately 10 Å to 1 micron in diameter. Particles in this size range can possess physical properties with different values than obtained from larger specimens. For example, the specific heat of colloidal particles is often different from that of larger particles. The distribution of chemically active zones are such that edge effects may also be different for materials in a colloidal form. For these reasons data that are experimentally determined from large sample experiments may not be directly applicable to submicron sized particles of these materials.

Several of the investigations[59-64] reviewed were not as applicable as that of Clarke and Fox[65] who showed that at 0.1 atm pressure, the sublimation temperature is as low as 2280°K. They observed a first order reaction rate and determined activation energies from 30 to 51 kcal/mole. The best reaction rate data available are that of Chi and Landahl.[66]

Their experiment measured the rate of weight loss and surface recession of graphite samples. The graphite materials studied were HAIM (Great Lakes Carbon Corporation), ATJ and AUC (Carbon Products, Division of Union Carbide), and pyrographite (Supertemp Corporation). The specific gravity of the materials was 2.2 for pyrographite, and between 1.72 and 1.73 for the other graphites. At the different pressures and temperatures considered, methane and acetylene were assumed to be the predominant products. From previous studies, surface reaction mechanisms were assumed to be rate-controlling, and first order rate equations were postulated. They found that the acetylene producing reaction has an activation energy of 47.8 k cal/(g mole) while the methane producing reaction

has an activation energy of 24.2 k cal/(g mole). They compared their results with the activation energies obtained by Clarke and Fox.[65] The differences were thought to be due to the low pressures at which Clarke and Fox had done their experiments, leading to sublimation of the graphite and gaseous-phase reactions. Since the activation energies obtained by Clarke and Fox were larger than those of Chi and Landahl, the latter point out the possibility that the activation energy for the reactions in the gaseous phase are greater than those for the gas-solid reactions.

The reaction rate data of Chi and Landahl are difficult to apply to the case where the carbon is in the form of submicron sized particles. Perhaps the best indication of a discrepancy between the reaction rate predicted by their experiment and that observed with submicron sized particles, is the fact that at 11 atmospheres pressure they observed very little evidence of reaction below 1920°K, whereas Shenoy[12] observed a reduction in aerosol density which was attributed to a carbon reaction with hydrogen at temperatures above 922°K and one atmosphere pressure. Partain[13] verified that the reaction product was methane and that it reached a concentration of less than one mole percent for temperatures up to 1920°K.

Although the carbon-hydrogen reaction rate seems to rule out the use of carbon seed, this needs to be verified by using some of the carbon blacks (e.g. Sterling M.T.) that have average diameters of approximately 0.25 microns. To date the data have been taken using Carbolac 2 with an average diameter of 0.012 microns and Spheron 6 with an average diameter of 0.025 microns. The larger particles of Sterling M.T., which the electron micrographs show to be more nearly spherical than either the Carbolac 2

or the Spheron 6, may exhibit a much slower reaction rate.

After examining all of the chemical characteristics of potential seed materials, it appears the refractory metals are best suited.

Previous Experimental and Theoretical Research

In 1908 Mie[45] published a solution for Maxwell's equations describing the scattering and absorption of an electromagnetic wave by a homogeneous spherical particle in a homogeneous, transparent, nonmagnetic medium. Unfortunately the absorption and scattering cross sections were expressed in terms of an infinite series involving two scattering amplitude coefficients that were in turn complicated expressions involving Bessel and Hankel functions and their derivatives. Before the advent of electronic digital computers it was a long and tedious job to evaluate the coefficients and when the index of refraction is complex (inferring a particle with significant absorption) the task of evaluating the coefficients was almost impossible because no extensive tables were available for the Spherical Bessel functions of complex arguments. In 1951 Aden[52] published a solution of the Mie equations obtained by transforming the scattering amplitude coefficients to forms of logarithmic derivative functions. Aden's interest in the Mie theory was the result of an investigation he conducted into the reflection of microwave radar signals from rain drops.

Plass and Stull[67] developed a computer program for Mie calculations in 1960, and Plass[54] applied it to calculations of the scattering and absorption cross sections of radiant energy incident upon spherical particles of aluminum oxide and magnesium oxide. One of the principal

limitations was the lack of temperature dependent data for the complex
index of refraction. Plass was interested in the total emissivity of
flames from solid propellant rockets. The flames contained particles
of aluminum oxide and magnesium oxide. In 1966 Plass published an in-
vestigation[48] of the Mie scattering and absorption cross sections cal-
culated for spherical particles as a function of the complex index of
refraction, $n = n_1 - in_2$. The calculations were done for $n_1 = 1.01$,
1.33, 1.5, and 2 and for $n_2 = 10^{-4}$, 10^{-2}, 10^{-1}, 1, and 10. He also cal-
culated the variation of the scattered intensity with angle as n_2 is
varied for some typical cases. Kattawar and Plass continued this inves-
tigation in a paper published[49] in 1967. These two investigations are
very useful in gaining an appreciation for the way in which the complex
index of refraction influences the scattering and absorbing cross sec-
tions for different sized spherical particles at different incident
electromagnetic radiation frequencies. As was discussed in the Theory
Section the real and imaginary parts of the complex index of refraction
depend on rather predictable variations in the electrical conductivity,
the dielectric constant and the permeability. Thus intuitive insight
can be gained as to a material's ability to scatter and absorb radiant
energy if these physical properties are known.

Krascella,[68] using Aden's transformation, conducted a theoretical
investigation to determine the absorption, scattering and extinction
characteristics of small solid spherical particles that might be potential
seed materials. The calculations were made using the Mie theory to de-
termine the effect of particle size, wavelength, and particle temperature
on particle opacity in those regions of the ultraviolet, visible, and

infrared spectra for which complex index of refraction information was available. He considered the following materials: aluminum, carbon, cobalt, iridium, molybdenum, niobium, palladium, platinum, rhenium, rhodium, silicon, tantalum, titanium, tungsten, and vanadium. Not all of these were considered candidates for seed materials but were included to see if any general conclusions could be drawn as to the dependence of the scattering and absorption cross sections on the atomic weight. The main difficulty he experienced in his study was the lack of complex index of refraction data, especially values for the ultraviolet region, and also, values that were temperature dependent.

At the same time, Marteney,[58] also of United Aircraft, was making an experimental investigation of the absorption and scattering cross sections of carbon and tungsten particles using helium and nitrogen as the carrier gases. His experiments were carried out at room temperature, and indicated the importance of good dispersion of the seed material in order to reduce the size of the agglomerates. In addition, Marteney[69] measured the complex refractive indices of hafnium, molybdenum, nickel, and tungsten in the wavelength range between 0.2 and 0.7 microns using the ellipsometric technique. He observed from his own research and that of others, that the surface preparation of the sample (polished, etched, cleaved, etc.) could create up to 20 percent variations in the complex indices measured.

In 1967 Krascella[18] took the complex indices measured by Marteney and the most current values from the literature and performed a through theoretical investigation of materials for potential seeding particles. He calculated spectral extinction, absorption and scattering parameters using the Mie theory for a range of wavelengths and temperatures. In

addition, he calculated the spectral bulk absorption parameters for the different materials. The bulk absorption parameters apply to seeds in the form of thin plates and are generally higher than those for seeds in the form of spherical particles. Since tungsten appeared to be one of the more promising seed materials, he evaluated the spectral absorption coefficients and the Rosseland mean opacity of gaseous tungsten using a heavy-atom model.

Lanzo and Ragsdale of the NASA Lewis Research Center published a study[70] in 1962 of the spectral opacity characteristics of small solid carbon, hafnium carbide, aluminum oxide and tungsten particles dispersed in water. In 1964 they measured[71,72] the absorption of thermal radiation by suspended particles as a function of material, size, and concentration. This experiment involved radiating energy from an electric arc to air that contained submicron-sized refractory particles. Seeded air was introduced into an annular heat exchanger. The arc was initiated and the unseeded air temperature in the annulus reached 556°K. When carbon particles were added to the air stream, they absorbed radiant energy causing the outlet temperature to increase to 667°K, thus showing that particle-seeding will enhance radiant heat transfer to gases.

McAlister, Keng, and Orr[73,74] reported theoretical and experimental studies of radiant heat transfer from a heated tungsten cylindrical enclosure to a particle cloud within it. A transparent gas, helium, was passed through the tube and the tube dimensions and helium flow rate were selected to give a low thermal efficiency for forced convection heating. The addition of tungsten or carbon particles to render the gas opaque caused a significant increase in heat absorption.

The first measurements of the absorption of radiant energy by particle-seeded hydrogen at high temperatures were reported in 1967 by Burkig.[75] In this experiment, a cloud of particles in a gas was injected into a transparent quartz tube and exposed to a flash of a xenon flash tube. The temperature rise of the gas was inferred from the pressure rise measured with a fast response pressure transducer. The bulk of the work was with micron-sized particles of carbon, iron, and tantalum carbide. In general, initial pressures of two and five atmospheres were investigated for both helium and hydrogen. During the flash, as indicated by the pressure transducer, the temperature of the carbon aerosol rose to about $2500^\circ K$ or more for about one millisecond. They experienced difficulty in preventing the seed material from depositing on the walls of the quartz tube and were not able to achieve good particle dispersion with their equipment. The inability to achieve good seed material dispersion required them to increase their seed material to gas mass ratio to about 500 per cent, whereas a more realistic limit of the mass ratio for the gas core nuclear reactor is one per cent. A phenomenon that they observed was a sharp increase in the extinction parameter at high temperatures. Theorizing that this might be due to a cloud of electrons around the particle (due to thermionic emission) that effectively increased the size of the particle, they measured the electrical conductivity and found that the conductivity increased strongly during the period of time when the transmittance decreased.

In 1967 Williams[76] measured the extinction coefficient of carbon seed material dispersed in nitrogen as a function of temperature and wavelength of incident radiant energy. In this experiment the particle-

seeded gas was heated to temperatures up to $1100^\circ K$ in a furnace and a beam of radiant energy from a hydrogen capillary discharge lamp was passed through the heated aerosol. A spectrometer was used to separate the intensity of the transmitted light as a function of wavelength.

Shenoy[12] improved considerably on this experimental technique and was able to use an aerosol of particle-seeded hydrogen gas at much higher temperatures. He was able to measure the extinction parameter of carbon, tungsten, and silicon seed materials of varying size at temperatures up to $1915^\circ K$. He observed only a small wavelength dependence and very little temperature dependence. His work emphasized the importance of making the measurements in a hydrogen medium since chemical reactions between the hydrogen and the submicron-sized particles could be observed. As was mentioned in the Theory section the chemical behavior of colloidal particles is not necessarily the same as it is for bulk samples.

Klein[77] is conducting experiments at United Aircraft Laboratories which are designed to develop methods for injecting solid particle seeds into a simulated propellant stream to show that large amounts of radiant energy can be deposited in a particle seeded gas. The experiment consists of flowing carbon seeded argon past a plasma produced by a r-f induction heater and measuring the temperature rise of the aerosol. The aerosol is contained between the walls of two concentric fused silica tubes. There is some difficulty in preventing deposition on the walls of the tubes.

Since ultimately the scattering parameter and the scattering amplitude function must be known and used in conjunction with the extinction

parameter to provide the data required for a competent radiant heat transfer analysis, there has been some work in this area. Plass,[49] Marteney,[58] Love,[76] Williams,[79,80] and Jacobs[80] have contributed to this area. An up-to-date summary of the experimental theoretical investigations conducted at Georgia Tech that are related to this research are contained in a paper by Williams[81] presented at the AIAA 5th Thermophysics Conference.

CHAPTER III

INSTRUMENTATION AND EQUIPMENT

The experimental apparatus is designed to measure the transmission of light through a heated and pressurized aerosol and to measure simultaneously the particle density of the aerosol. The objective is to measure the extinction parameter of the aerosol as a function of wavelength of the incident radiant energy. This is accomplished by passing a beam of radiant energy through the furnace containing the hydrogen aerosol and using a monochromator to record the transmitted beam intensity as a function of wavelength. The transmitted intensity is first measured with only the hydrogen gas present and then measured again after a seed material has been introduced into the hydrogen at the same temperature and pressure. The ratio of the two measured intensities gives the attenuation. By measuring the density of the aerosol simultaneously with the intensity measurements the extinction parameter (in cm^2/gm) can be calculated.

The Monochromator Assembly

Figure 7 is a schematic of the apparatus through which the radiant energy beam traverses. The light source is a mercury arc lamp which produces a focused beam of ultraviolet and visible light which passes through the sight port of the furnace and through the aerosol column flowing up the center refractory tube in the furnace. The transmitted light leaves the furnace through the opposite sight port and is focused
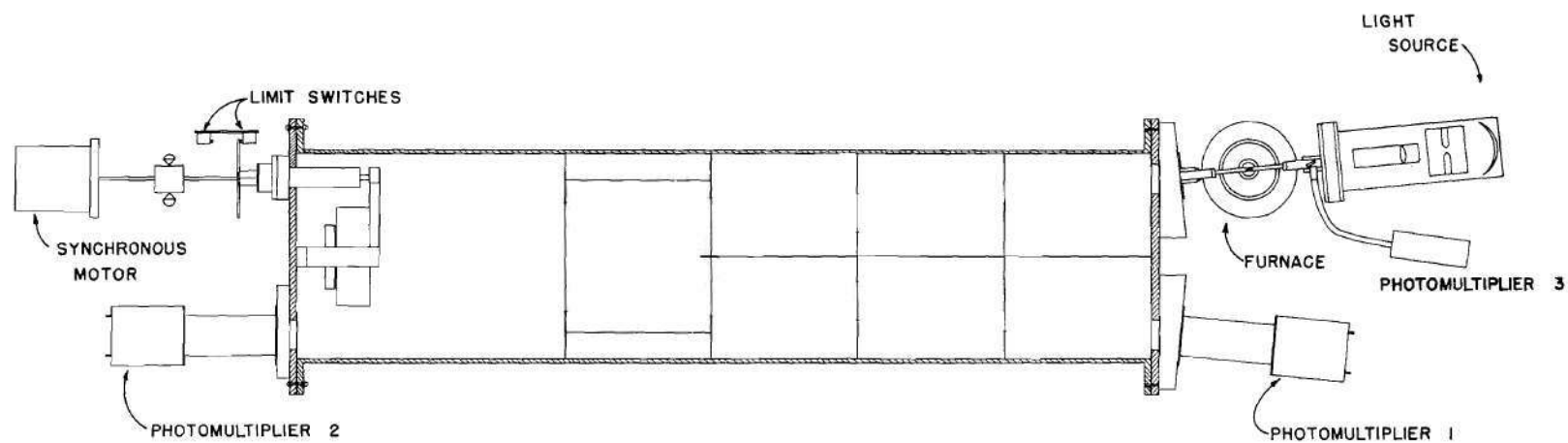
Figure 7.   Furnace and Monochromator Layout

by a lens through the diffusing screen and pinhole opening into the monochromator. Light passing through the pinhole strikes the diffraction grating assembly at the far end of the monochromator. The diffracted light of a selected wavelength is focused by the grating onto the slit, and the intensity of light passing through the slit is monitored by photomultiplier number 1. A system of four baffles in the monochromator prevents reflections from the incoming beam from interfering with the diffracted light. Part of the beam incident upon the diffraction grating strikes a set of mirrors which direct this portion of the beam to photomultiplier 2. The signal from photomultiplier 2 is used to normalize the effect of the varying aerosol density on the signal being recorded by photomultiplier 1. Photomultiplier 3 monitors a reflection of the incident beam of light from a quartz window placed at 45 degrees in the path of the beam. The signal from photomultiplier 3 is used to correct both the signal from photomultiplier 1 and photomultiplier 2 due to fluctuations in the light source intensity.

Figure 8 is an expanded view of the furnace end of the monochromator showing the light source, sight ports, and photomultipliers 1 and 3 in greater detail. The furnace is connected to the spectrometer at an angle of six degrees to the centerline axis of the monochromator. A quartz lens in the arc lamp focuses the beam of light down to approximately one-quarter inch diameter as it passes through the center of the furnace. Another quartz lens in the sight path on the other side of the furnace focuses the transmitted beam onto a diffusing screen and through a pinhole into the monochromator. The effect of this lens and diffusing
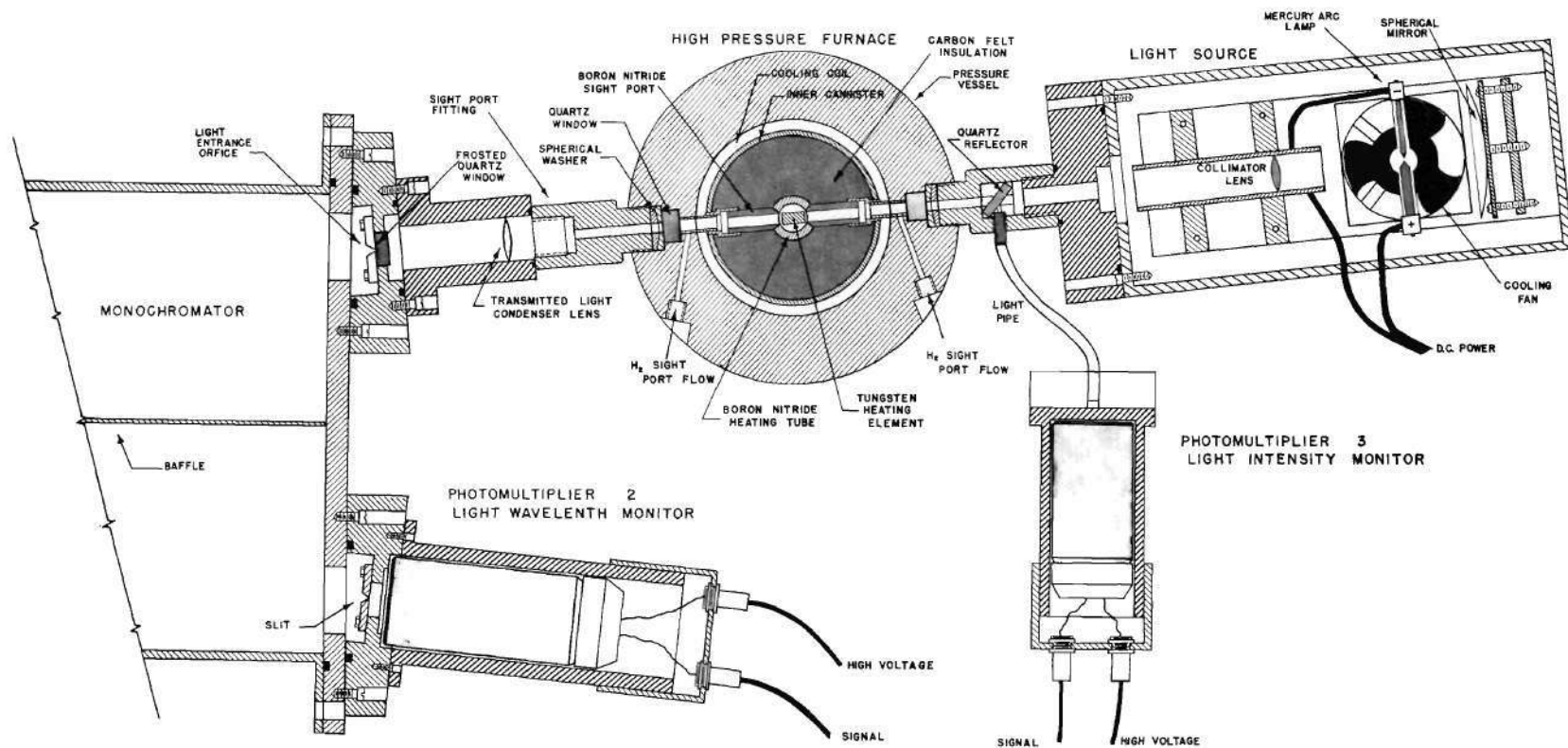
Figure 8.   Monochromator Assembly - Furnace End

screen is to optically integrate spatial intensity variations resulting from refraction by the dense, turbulent hydrogen. A light pipe is used to transmit the reflection from the 45 degree quartz window between the light source and the furnace to photomultiplier 3.

The monochromator shown in Figure 7 is a modified version of the one built by Dr. J. R. Stevenson, located in the Georgia Tech School of Physics. The monochromator tank is a stainless steel tube 10.75 inches in outside diameter with a wall thickness of 0.165 inch. It is 42 inches long and has one-half inch stainless steel plates bolted to each end and sealed with O-rings. A mechanical vacuum pump can evacuate the monochromator to a pressure of less than one micron of mercury. A meter on the control console indicates the monochromator pressure as measured by a thermocouple vacuum gauge.

Figure 9 shows the grating end of the monochromator in greater detail. The grating is a concave spherical replica grating with a 90 by 50 millimeters ruled area. The curvature is 998.8 mm and the groove spacing is 600 lines per millimeter with a $8°38'$ blaze angle. The grating drive mechanism is a fine-threaded precision screw which advances and pushes an arm attached to the aluminum grating mounting block. The grating mount pivots and sweeps the diffracted spectrum across the slit at the far end of the monochromator tank. The drive motor for the mechanized grating assembly is a reversible 75 rpm synchronous motor. The use of a synchronous motor permits time synchronization of the grating position with the chart recorder. A "START" button on the control panel actuates both the grating drive system and the oscillograph.

TO DRIVE
MOTOR

DRIVE MECHANISM

END PLATE

GRATING

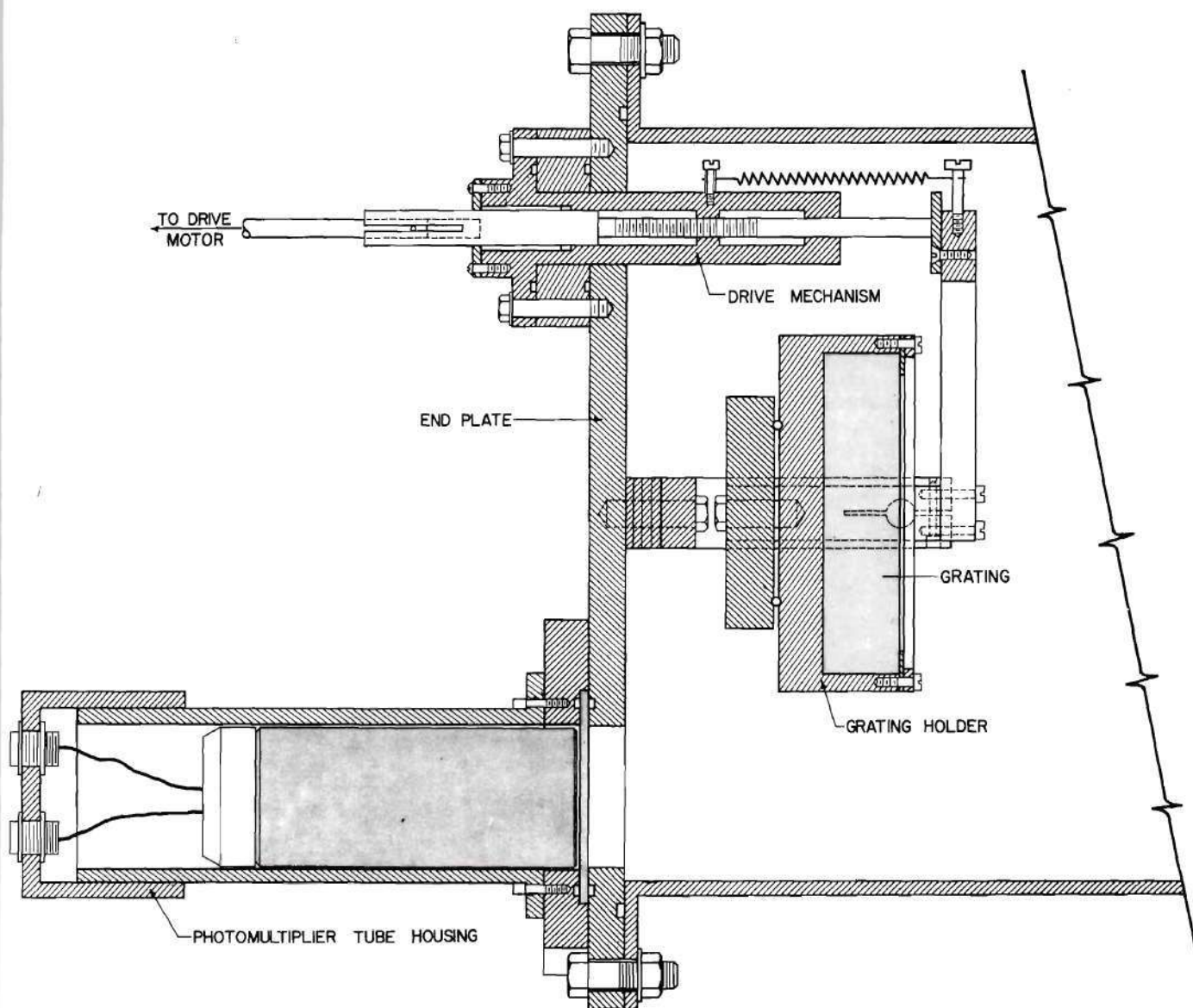GRATING HOLDER

PHOTOMULTIPLIER TUBE HOUSING

Figure 9.   Monochromator Assembly - Diffraction Grating

Limit switches reverse the drive motor at the end of the scan and drive
it back over the spectrum. This technique permits data to be recorded
at one amplification on the forward scan and another amplification on
the reverse scan. Accurate intensity measurements on spectrum peaks
that differ by more than an order of magnitude can be obtained by this
method.

High Pressure Furnace

The pressure chamber of the furnace is constructed from mild steel
tubing with a $7\frac{1}{2}$ inch outside diameter and a $4\frac{1}{2}$ inch inside diameter.
The interior length is $18\frac{1}{4}$ inches. Both ends are capped with two inch
thick steel plates secured by eight cap screws. The $1\frac{1}{2}$ inch wall thick-
ness far exceeded the strength needed for a 1500 psi working pressure
but was used for ease in designing and machining the through-the-wall
fittings.

Figure 10 is a drawing of the furnace assembly. Figure 11 is
enlarged for better detail of the upper portion of the furnace. At
the bottom of Figure 10 can be seen one of the water-cooled copper
power leads and its conical Teflon seal. The pressure inside the
chamber produces a leak-tight seal by acting on the conical base of the
power lead and its seal. The hydrogen aerosol enters a fitting at the
base of the furnace and splits into two streams as it passes through
the vee-shaped passages machined into the bottom plate of the
furnace. One of the two passages is shown in the figure. A hole in
each of the power leads is aligned with one of the inlet passages and
the aerosol passes into the boron nitride heating chamber. The heating

COOLING STACK

EXHAUST GAS
COOLING COIL

WATER INLET FOR
GAS COOLING COIL
TUNGSTEN SAMPLING TUBE
BN WASHER
THERMOCOUPLES
BN SIGHT PORT
HYDROGEN INLET FOR SIGHT
PORT PURGE
QUARTZ WINDOW

LIGHT PATH

CARBON FELT INSULATION
(NOT SHOWN)

PRESSURE CHAMBER

PRESSURE CHAMBER
COOLING COILS

INNER CANNISTER

BN HEATING CHAMBER

BN DIVIDER STRIP

TUNGSTEN HEATING ELEMENT

WATER COOLED ELECTRODE

HYDROGEN AEROSOL PASSAGE
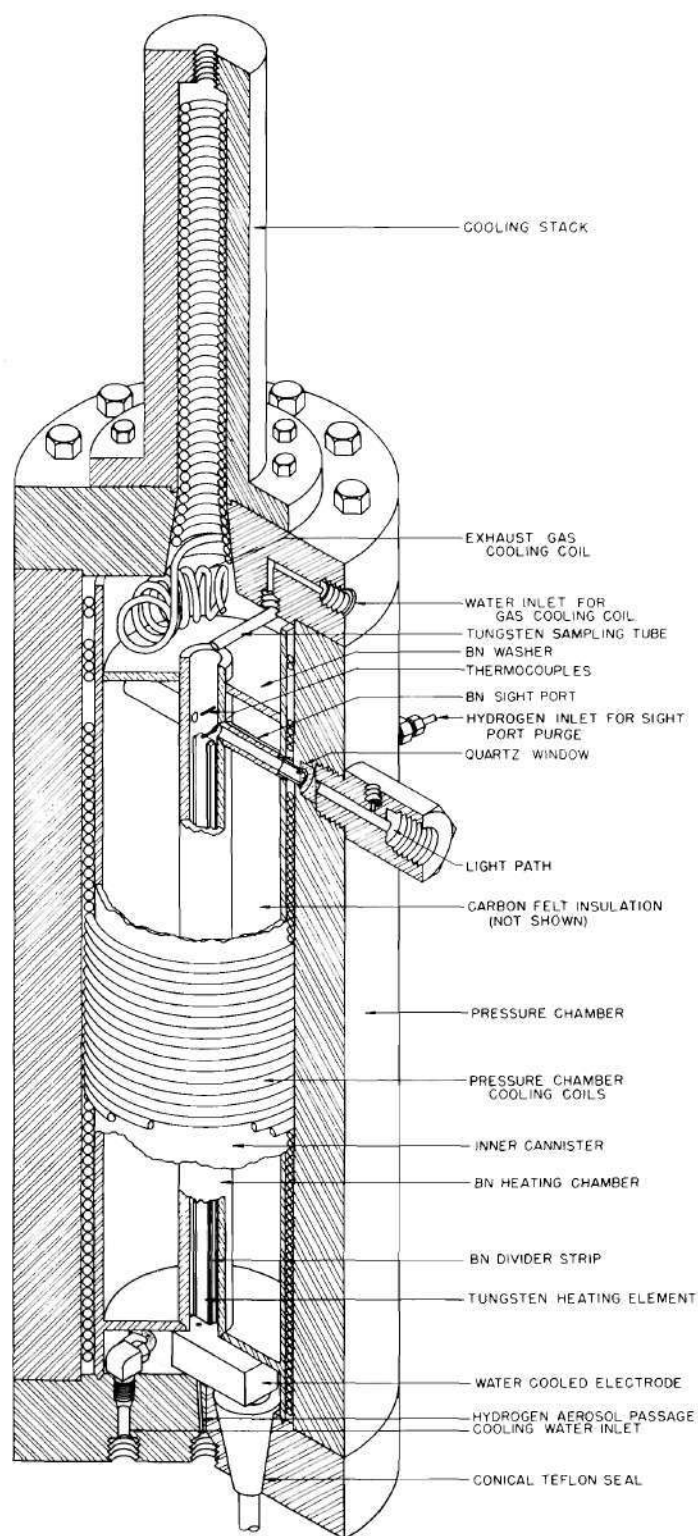COOLING WATER INLET

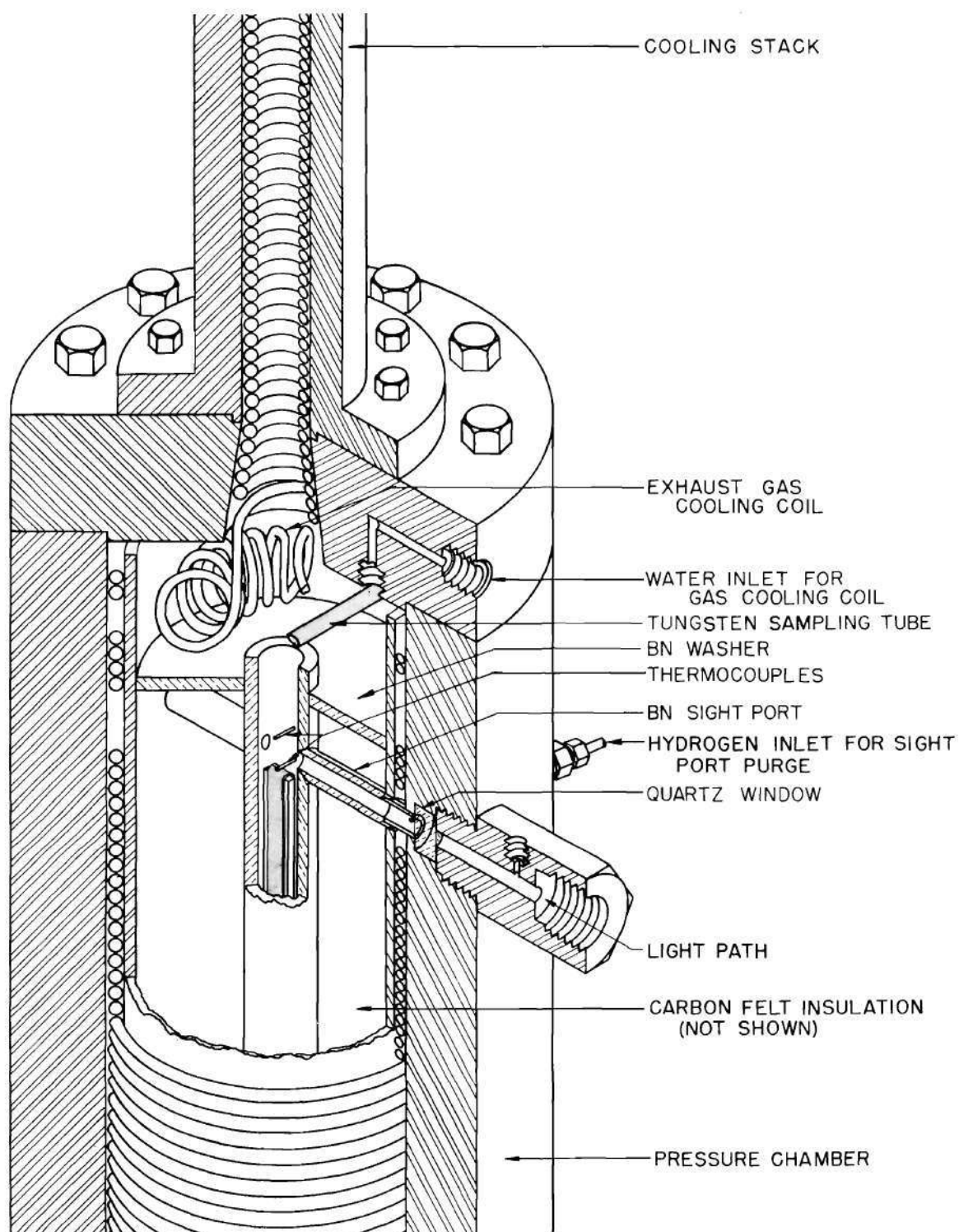CONICAL TEFLON SEAL

Figure 10.   High Pressure Furnace

Figure 11. High Pressure Furnace (Upper Detail)

chamber is a 15 inch tube with a one inch outside diameter and a five-eighths inch inside diameter. The heating element is a 28 inch long strip of tungsten which is separated by a one-eighth inch strip of boron nitride at the bottom. The tungsten strip is nominally 28 inches long, one-half inch wide and 50 mils thick. The boron nitride divider strip shown in Figure 10 has been modified so that it extends only half way up the tungsten strip, thereby improving flow conditions in the furnace. Just above the top of the sight path is a tungsten-five percent rhenium and tungsten-26 percent rhenium thermocouple in a boron nitride shield. At the top of the boron nitride heating chamber is located a boron nitride sampling tube through which a sample of the aerosol is withdrawn for density measurements. Above the sampling tube, the aerosol passes through 12 inches of copper cooling coils as it travels up the cooling stack. Figure 12 is a sketch of the effluent handling system. The gas is cooled as it travels up the cooling stack and then it goes to the seed filter where the seed material is recovered by passing the aerosol, still under pressure, through a 4.7 cm diameter fiberglass filter. The hydrogen passes through a backpressure regulator which holds the pressure in the furnace system to the desired operating pressure. A throttling valve is sometimes used in lieu of the backpressure regulator to prevent the pressure surges that sometimes occur with the backpressure regulator. The hydrogen leaving the throttling valve is passed through a flow meter and then exhausted to the atmosphere.

In Figure 11 the light path is shown in detail. Mating flanges screw into the external pressure fittings containing the windows in order

FIBERGLASS
FILTER ELEMENT

FURNACE
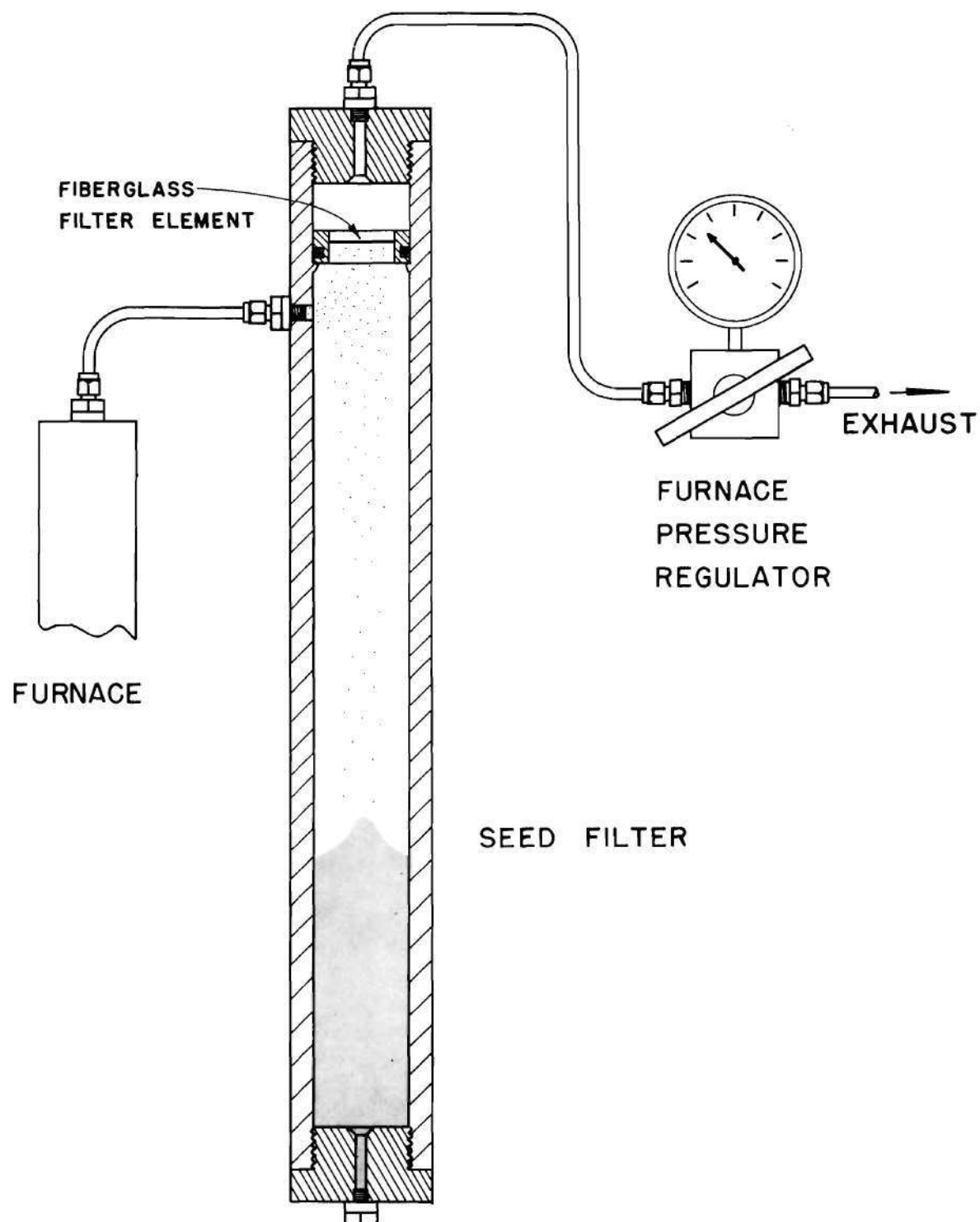
FURNACE
PRESSURE
REGULATOR

EXHAUST

SEED FILTER

Figure 12. High Pressure Seed Material Filter

to provide a connection for the monochromator assembly on one side and the arc lamp on the other. There is a backup quartz window, not shown, in case the primary quartz window, which is shown, should rupture. The primary quartz window is three-eighths of an inch thick and three-quarters of an inch in diameter. Teflon seals inside and outside the quartz window plus a spherical washer outside the window provide a stress free pressure seal. Just inside the quartz window is shown the metal sleeve and the inlet for the hydrogen purge gas flowing through the sight ports into the heating chamber. The amount of purge gas is a small percentage of the gas flowing in the main aerosol stream, but it serves to keep the sight ports free of seed material. The beam of radiant energy passes through the boron nitride heating chamber above the end of the tungsten heating strip.

The furnace is cooled by three cooling systems. One is for cooling the two copper power leads, which have cooling channels within them. The second is the main cooling coil which is adjacent to the pressure chamber wall to protect it from the high temperatures. The third system is a coil that cools the upper plate of the furnace and the gas as it passes up the cooling stack attached to the upper plate. Flow measurements have indicated that each of these coils can handle better than 10 kilowatts of power for normal water pressure.

The design and construction of the furnace were carried out with the goal of accurate alignment and ease of assembly. This led to the incorporation of an inner cannister made of stainless steel which contains the boron nitride heating chamber, tungsten filament, carbon

felt insulation around the heating chamber, thermocouple leads, and the boron nitride sight port tubes. These units, which represent the main alignment problem, can be lifted out of the furnace intact. In addition, a tungsten heating element can be replaced by merely releasing the gripping torque of the copper power leads, removing the top plate of the furnace, and interchanging heating elements. A modification has been made to the boron nitride heating tube that is not shown in Figure 10. The tube is supported from the top by being pinned to the boron nitride centering washer that is located above the sight port tubes. The lower end of the heating tube fits loosely in a copper sleeve at the bottom of the inner cannister. This method of support for the heating tube prevents a misalignment of the slight port tubes due to thermal expansion of the heating tube.

The furnace is mounted on a dolly adjacent to the table dolly on which the monochromator assembly is mounted. One-quarter inch copper tubes supply cooling water, and all gas connections are made with one-quarter inch outside diameter stainless steel, seamless tubing. The power supply for the furnace is rated for 20 kilowatts direct current.

Light Sources

Initially a McPherson Model 630 Hinterregger-type gas discharge lamp was used as the lamp source. This source provided a spectrum extending from the near infrared to below 1200 $\overset{\circ}{A}$ containing both continua and line spectra. There were several disadvantages to this light source. The usable portion of the light emitted was too weak to override the thermal background emitted from the hot furnace and the

data included a background run necessary to remove the influence of
the thermal background from the intensity measurements. The back-
ground run increased the time that pressure and temperature conditions
had to be held constant in the furnace and greatly complicated the
analysis of the recorded intensity data. In addition a high voltage,
high power source was required for the discharge lamp which could not
be sufficiently filtered to remove the 120 hz noise from the output of
the lamp. The windows in the high pressure furnace are made of quartz
because of its high strength as compared with LiF or MgF which transmit
wavelengths as short as 1100 Å. Since the quartz does not transmit
wavelengths below 1750 Å the discharge lamp did not offer a significant
advantage over the spectrum available from a quartz mercury arc lamp
which produces almost a point source of light that can be focused so as
to concentrate its intensity. A mercury arc light source was constructed
which utilizes a 100 watt PEK lamp powered by a well filtered PEK Model
401 A d.c. power supply. Figure 8 shows the construction of the light
source which includes a spherical front surface mirror to project an
image of the arc back onto the arc from the rear and the quartz conver-
ging lens used to project the light into a beam through the furnace. A
small blower is used to cool the lamp. Experience has shown that operat-
ing the arc at 75 watts instead of its 100 watt rating increases the
stability of the arc intensity. The intensity of the beam of light
transmitted through the furnace is two orders of magnitude greater than
the highest thermal emission from the hot furnace.

Aerosol Generators

Several aerosol generators have been developed in the course of this research. Their performance is related to the type of seed material being used and the pressure at which the aerosol is formed. Most of the high pressure attenuation measurements have been performed with tungsten aerosols since tungsten appears to be the best choice for a seed material in the gas core nuclear rocket concept. However, aerosols of carbon, silicon, silicon carbide, and tungsten carbide have also been generated. The silicon and silicon carbide powders disperse easily and are well suited for an aerosol generator that uses mixing blades to create a metallic aerosol in a container, from which it can be forced into the furnace as needed. Tungsten and tungsten carbide, on the other hand, are heavier and appear to settle faster. In addition, they form powder structures around the mixing blades and deposit on the walls of the container, thereby preventing the mixing blades from further agitating the powders.

Figure 13 is an illustration of an early high pressure aerosol generator developed for forming a tungsten aerosol. One of the principal problems was sealing the shafts to the auger and the high speed mixing motor. This is especially difficult with a powder aerosol generator since the powder forced into the seals by the pressure rapidly destroys them. There was also some difficulty in entraining the tungsten in the auger.

Figure 14 shows a high pressure aerosol generator that uses the motor and mixing blades from a commercial food blender. The problem of

POWDER RESERVOIR

GAS

AEROSOL

AUGER

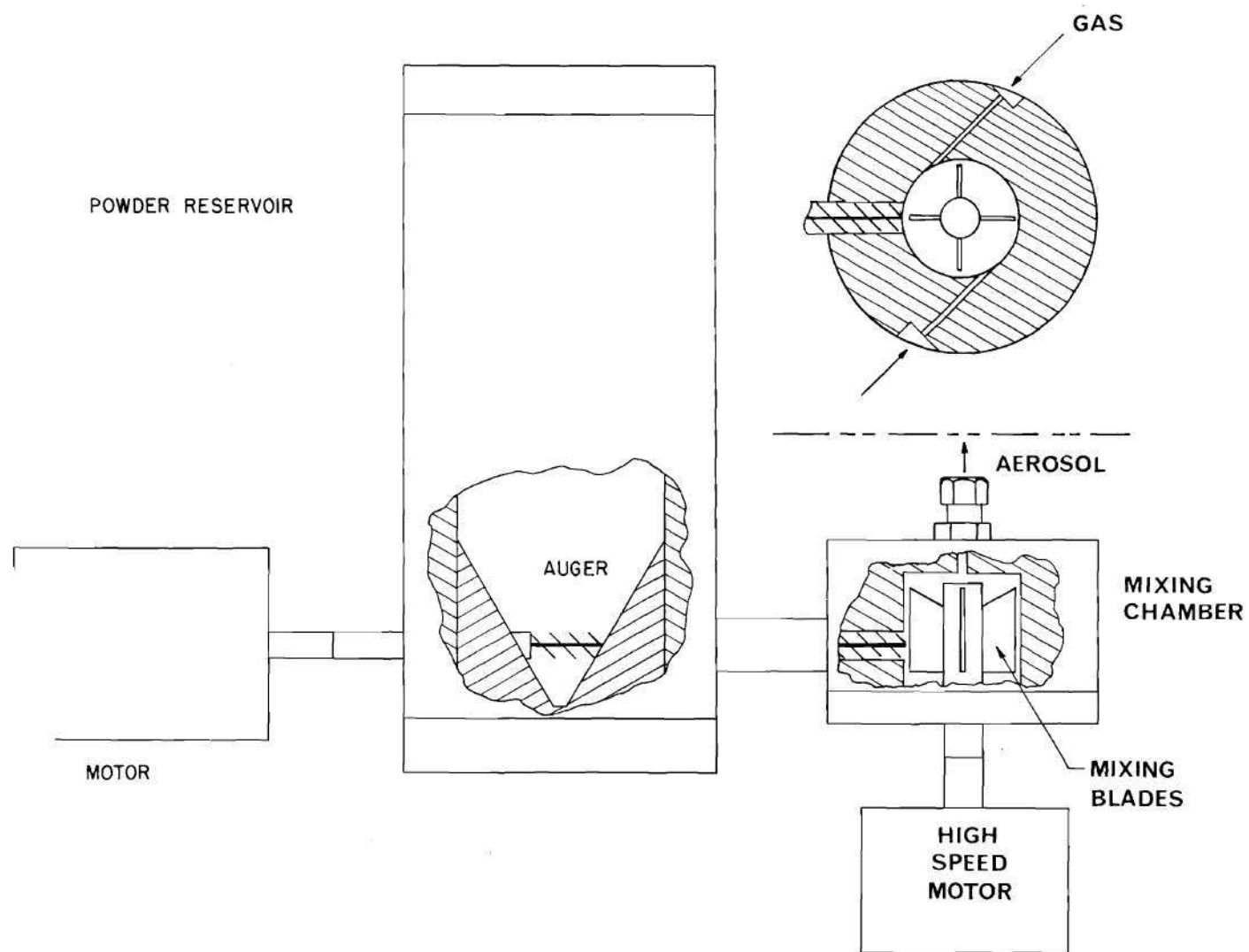MIXING CHAMBER

MIXING BLADES

MOTOR

HIGH SPEED MOTOR

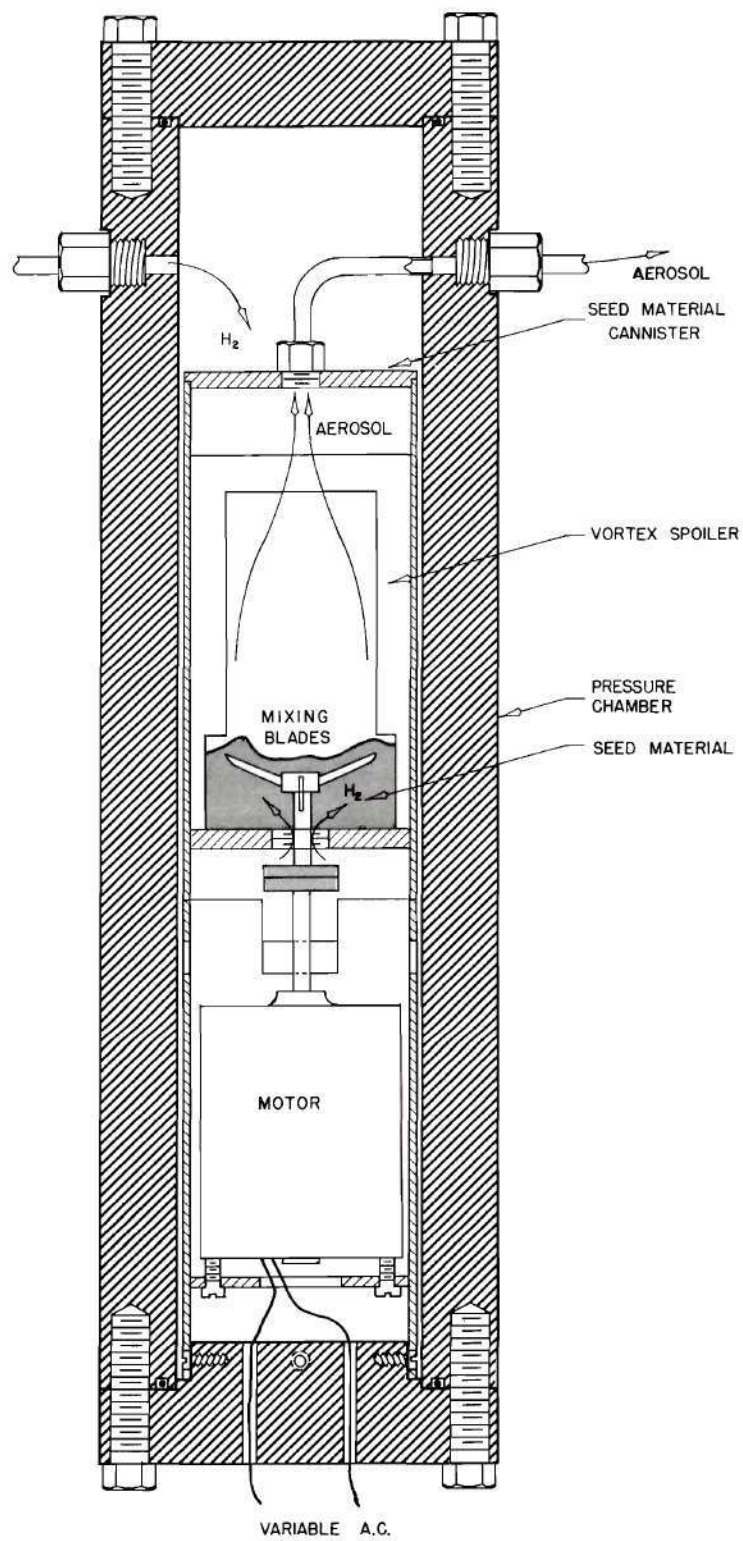Figure 13.   High Pressure Auger Aerosol Generator

Figure 14. High Pressure Blender Aerosol Generator

shaft seals was alleviated by placing the motor inside the pressure chamber and having the incoming gas "leak" through the mixing blade shaft into the inner chamber containing the seed material in contact with the mixing blades. The aerosol generated is then taken out through a fitting in the inner chamber through a pipe to the outside of the larger pressure chamber. This has worked satisfactorily with silicon and silicon carbide since they disperse easily and tend to remain in suspension. In general the aerosols produced by this device are thin. Since there is a practical limit on the mass flow rate of hydrogen that can be passed through the furnace at elevated temperatures the volume flow rate is much less at the higher pressures. This low volume flow rate further compounds the thin aerosol problem with this aerosol generator, since the dense aerosol near the mixing blades is not carried out of the inner chamber. For this reason, this aerosol generator was not used successfully at pressures above 300 psi. The blender high pressure aerosol generator did not work satisfactorily with tungsten since the tungsten powder would stick to the inner chamber walls and avoid extensive agitation. The large internal volume of this aerosol generator was also a liability since pressure surges between it and the furnace could cause operating conditions to vary significantly.

The aerosol generator that has been used to obtain the high pressure tungsten data is shown in Figure 15. The design is a modified version of the Wright Dust Feed Mechanism developed by Wright.[82] The scraper head is supported on a one-quarter inch OD pipe that is secured to the base and through which the aerosol is carried out. The gas
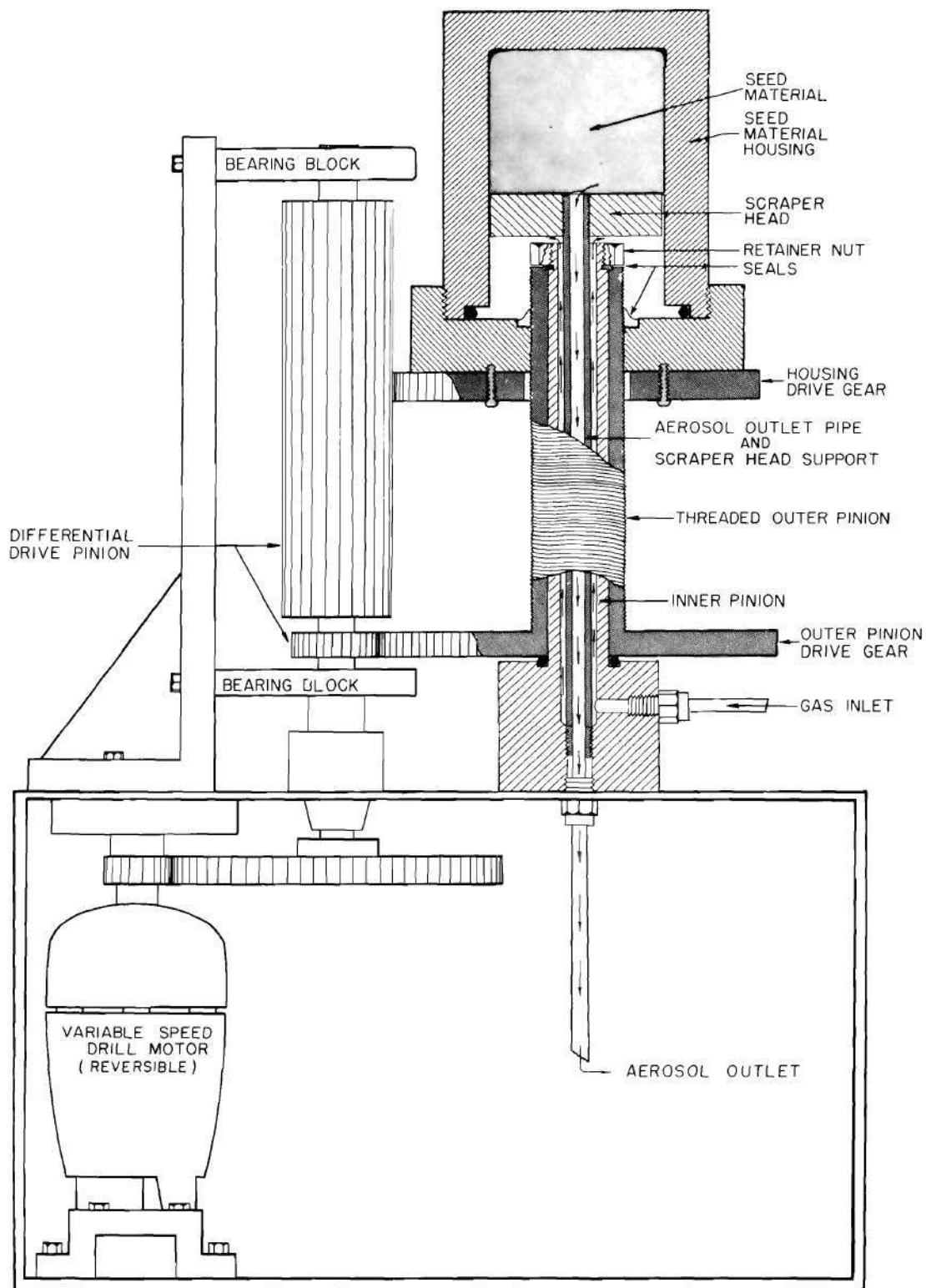
Figure 15. High Pressure Wright Dust Feed Aerosol Generator

enters through a hollow pinion shaft surrounding the outlet pipe. The hollow pinion shaft is labled "inner pinion" on the figure. The "outer pinion shaft", which is threaded, rides on the inner pinion shaft and a nut on the top of the inner pinion shaft prevents the pressure from lifting the outer pinion shaft up the inner pinion shaft. There is a Teflon seal between the nut and the outer pinion shaft to prevent the pressurized gas from leaking out between the two shafts. The base of the seed material chamber travels on the threaded outer pinion. Both the base of the seed chamber and the threaded outer pinion are gear driven, but gear ratios of the two are slightly different so that for approximately every five revolutions of the outer pinion and the seed material chamber, the seed material chamber has advanced one thread down on the threaded outer pinion. This slow advance of the seed material in the chamber onto the fixed scraper head while the two are rotating with respect to each other provides a gradual scraping of the seed material which is carried away by the gas passing up through the inner pinion, over the scraper head and down through the scraper head support pipe. The seed material must be packed so that it will remain in an inverted position until scraped off. Tungsten is ideal in this respect. One difficulty in using this device at high pressure, expecially with hydrogen gas, is the seal between the seed material chamber and the outer threaded pinion. A "shrunk" Teflon collar was not sufficient but a small layer of very viscous oil in the base of the seed material chamber acts as an excellent seal. Some care was taken that the oil did not contaminate the seed material but this proved to be no problem. The

real advantage of this aerosol generator is the positive entrainment of seed material in the aerosol lines even at low volume flow rates. Plus, the device can be operated at variable speeds to provide the desired seed density.

All these aerosol generators produce more highly dispersed aerosols if the aerosol is passed through a nozzle after it has been generated. A nozzle is the best way to direct the required forces on the small aggregate of submicron-sized particles to shear them apart. A pressure upstream of twice that downstream is needed to insure maximum shear pressures on the aerosol. This is difficult to achieve at the higher working pressures because of the limited supply pressure available. The fact that the pressure drop through the furnace, especially severe when a nozzle is used, is not the same as the pressure drop through the bypass line, makes it difficult to hold a constant pressure and temperature in the furnace during the "before aerosol" measurement and the "after aerosol" measurement. These problems prevented the use of a nozzle at high pressures.

Aerosol Density Sampling Apparatus

Figure 16 shows the layout of the aerosol density sampling apparatus. There are two sampling points. One is at the bottom of the furnace before the aerosol enters the furnace. The upper sampling point is located near the top of the furnace pressure vessel which is connected to the boron nitride sampling tube inside the furnace. There are four sample holders at both the top and bottom sampling points. Each filter holder is a two piece stainless steel holder three inches long and one
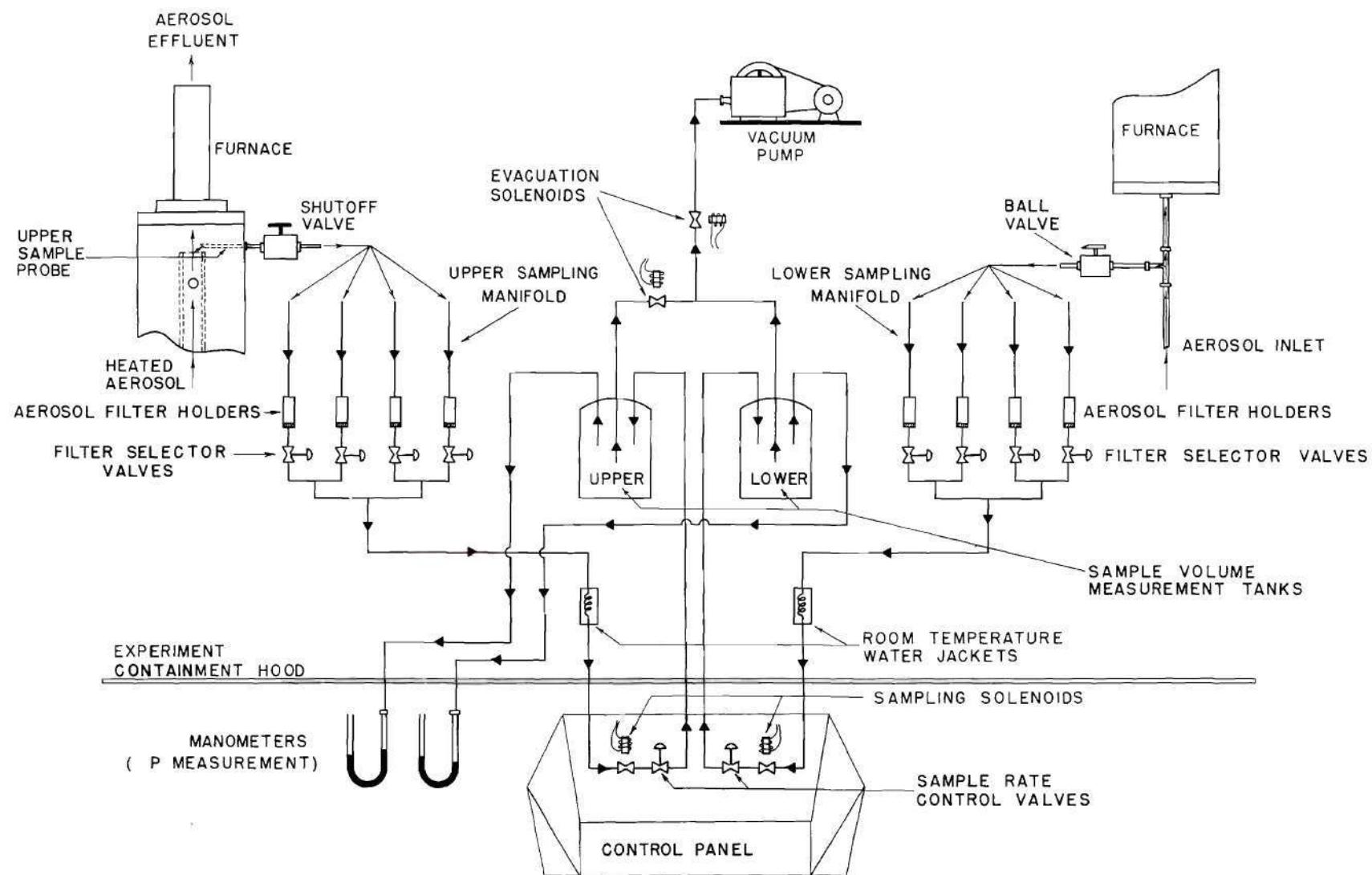
Figure 16. Aerosol Density Sampling Apparatus

and one-half inches in outside diameter. A fiberglass filter on cotton backing is clamped between the two pieces of the filter holder that screw together and are sealed by an O-ring. A ball valve is located on the sampling fitting at the bottom of the furnace to allow the filters to be interchanged. A double packing stainless steel valve is used at the top where the sampled aerosol is very hot. The small cutoff valve at the bottom of each filter holder line provides a means of rapidly inter-changing filters so that only one fitting has to be disconnected. The filters are all assembled and pressure tested to the working pressure before the actual data collection begins. Just before a sample is to be taken the furnace isolation valve is opened and the pressurized gas tra-vels through the filter that is attached and up the line to the solenoid valve indicated on the control panel. This is done before aerosol is introduced into the furnace. A sampling throttling valve is also located in the line at the control panel and this has been preset for the pro-per sampling rate at the chosen operating pressure. The sample volume measurement tanks with an average capacity of six liters are evacuated by means of the vacuum pump shown and the evacuation solenoid valves reset to their closed positions. The pressure in the tanks is read from the two manometers mounted beside the control panel. When the aerosol is introduced into the furnace and a density measurement is desired, the sample solenoid is activated which allows the high pressure gas to move to the throttling valve where it is metered at the desired rate into the sample gas volume tanks. After the aerosol sample has been drawn the sampling solenoid is shut off and the pressure in the

sample volume tanks is read again. After this the sample volume tanks can again be evacuated, the furnace isolation valve closed, and a new filter connected into place. In the lines going to the sample solenoid valve is located a cannister filled with water at room temperature which contains several coils of the line carrying the sampled gas. Its purpose is to insure that the sampled gas is at ambient temperature inside the sample volume tanks when the pressure is recorded.

The Particle Sampling Apparatus

The radiant energy extinction cross section that is measured is relevant only if the aerosol which produced this value can be accurately described. The seed materials used consisted of submicron-sized particles, but the degree of dispersion obtained by the aerosol generator greatly affects the particle size distribution. The particle size distributions of the aerosols used in this research were evaluated by collecting representative samples on electron microscope grids and making electron micrographs. The method by which the sample is collected is important. Just passing an electron microscope grid mounted on a slide holder in front of a stream of aerosol produces a sample on the grid which is not truly representative of the aerosol since the larger particles are most likely to impinge on the grid and stick, while the smaller particles may be carried around the electron microscope grid by the gas stream. Another approach would be to collect some of the aerosol in a settling chamber where it could settle on electron microscope grids placed at the bottom, but it was felt that the particles might tend to agglomerate extensively before settling to the bottom of the container.

The sampling scheme used to study aerosols employed an electro-static precipatator. The apparatus used to collect the samples for the electron micrographs of tungsten is shown in Figure 17. It consists of a plexiglass box, approximately two inches by two inches by four inches long, with a grounded metal side to which the electron microscope grids were taped. Protruding into the box through the other side was a three inch needle which was in turn touched to a 75 kV Van de Graaff generator to provide the electrostatic potential and electron beam required to charge the particles and then force them onto the grounded plate. Several grids were located parallel to the flow and a sample taken. Since there was no appreciable difference in the particle size distribution observed on the electron microscope grids located at different points on the grounded plate, it was concluded that gravity-induced precipitation and preferential settling according to particle size along the axis of the box were not factors in the sampling scheme. It should be mentioned that a similar device is sometimes used to obtain particles which are preci-pitated along the axis of flow according to size, but this required charging the particles before they arrive in the precipitation container and providing a turbulent free flow zone and parallel electrical poten-tial plates. Due to the geometry of the sampling apparatus where both the charging and the field establishment is done by a sharp needle there is no observable tendency to preferential precipitation.

Electron micrographs of tungsten particles from the aerosol are shown in Figure 18.

ELECTROSTATIC FILTER

TO VACUUM PUMP

FURNACE

COOLING JACKET

FILTER
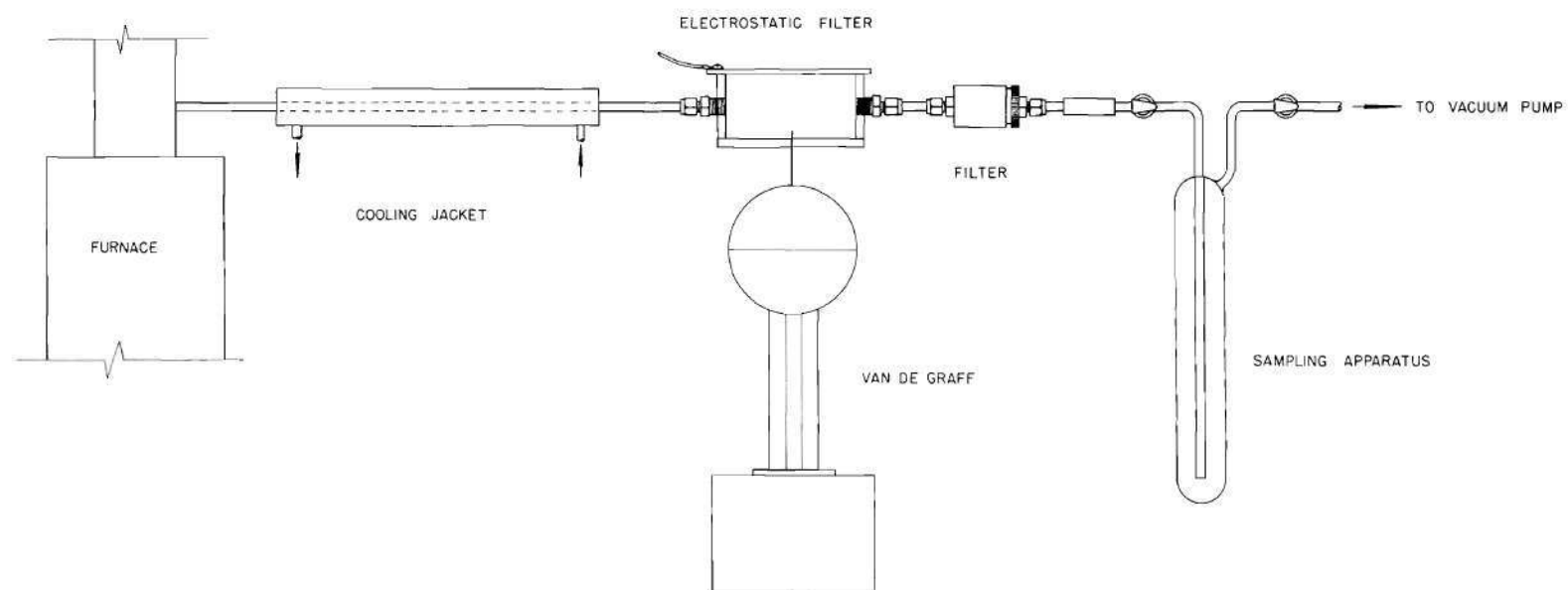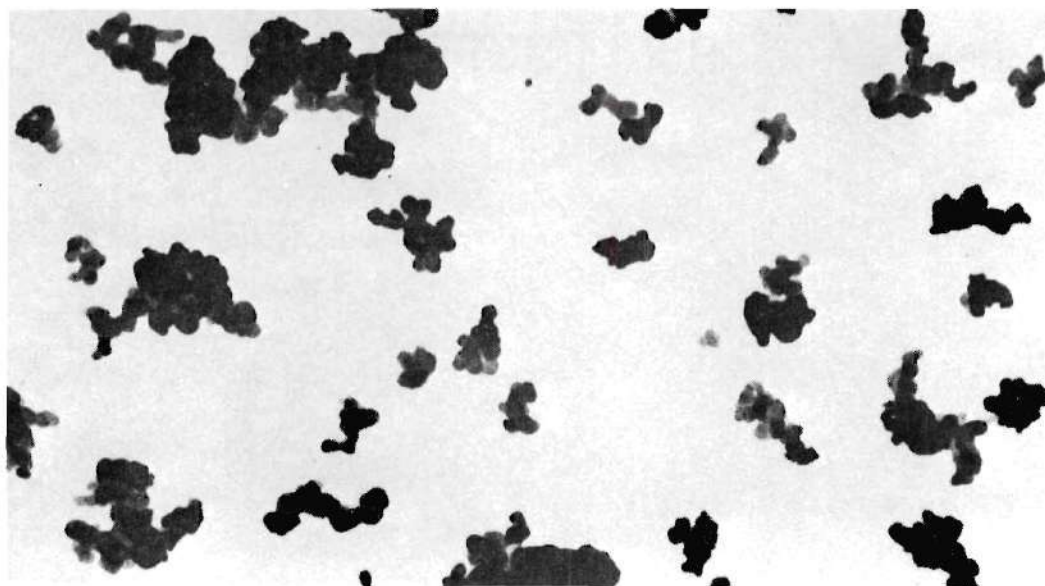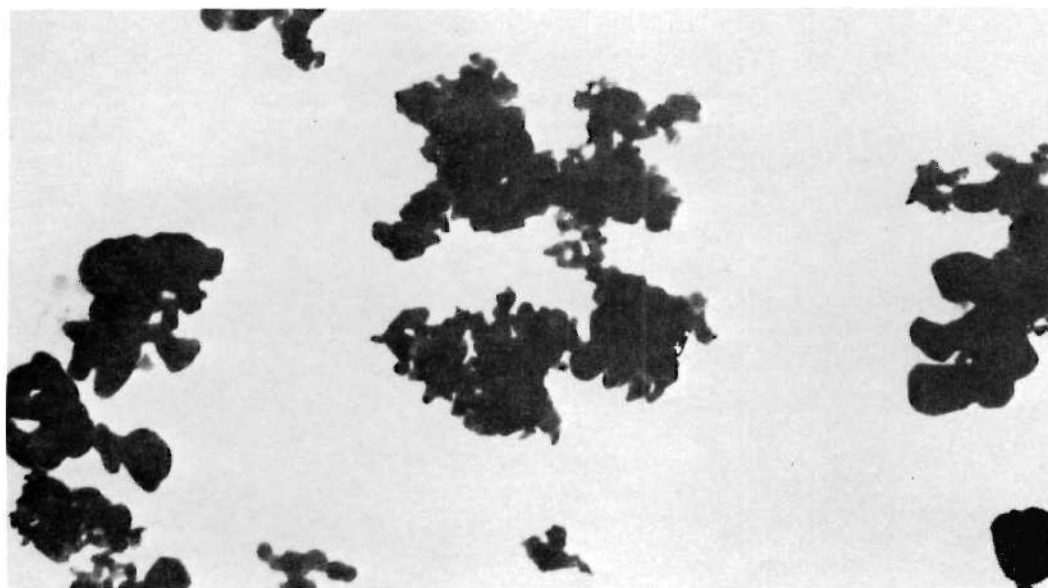
VAN DE GRAFF

SAMPLING APPARATUS

Figure 17. Electrostatic Particle Sampling Apparatus

With Nozzle Dispersion

1.0 Micron

Without Nozzle Dispersion

Figure 18.   Electron Micrographs of Tungsten Particles
with and without Nozzle Dispersion

Aerosol Effluent Sampling Apparatus

On two occasions the effluent from the furnace was sampled to determine if a chemical reaction of the seed material and the hydrogen gas was occurring and, if so, to what extent. Vacuum sampling tubes with vacuum sealed stopcocks at either end were evacuated and then attached to a line which sampled the furnace effluent after it had passed through the seed filter. This sampling could have been accomplished through the density sampling tube had it been desirable to quench quickly the hot effluent to prevent a reverse reaction, but this was not done.   The gas samples were taken to the Georgia Tech Chemistry Department where Mr. George Turner analyzed them on the mass spectrometer. This technique was used to determine the presence of methane in the effluent when a carbon aerosol was heated in the furnace.

Gas Flow Control System

The hydrogen gas and the nitrogen gas required to flush all air from the system are purchased in bottles containing 225 cubic feet at 2200 psi. Since one bottle does not last very long when supplying gas at the higher operating pressures it was necessary to build a manifold. The complete gas supply and control system are illustrated by Figure 19. The gas storage area is located outside the building. There is a foot wide space between the top of the walls and the roof of the 12 by 20 foot area which provides natural ventilation. Approximately 150 bottles can be stored in the area at one time. The manifold consists of six groups of four bottles each. Three of the groups are designed to handle hydrogen tanks and the other groups are for nitrogen although the ratio
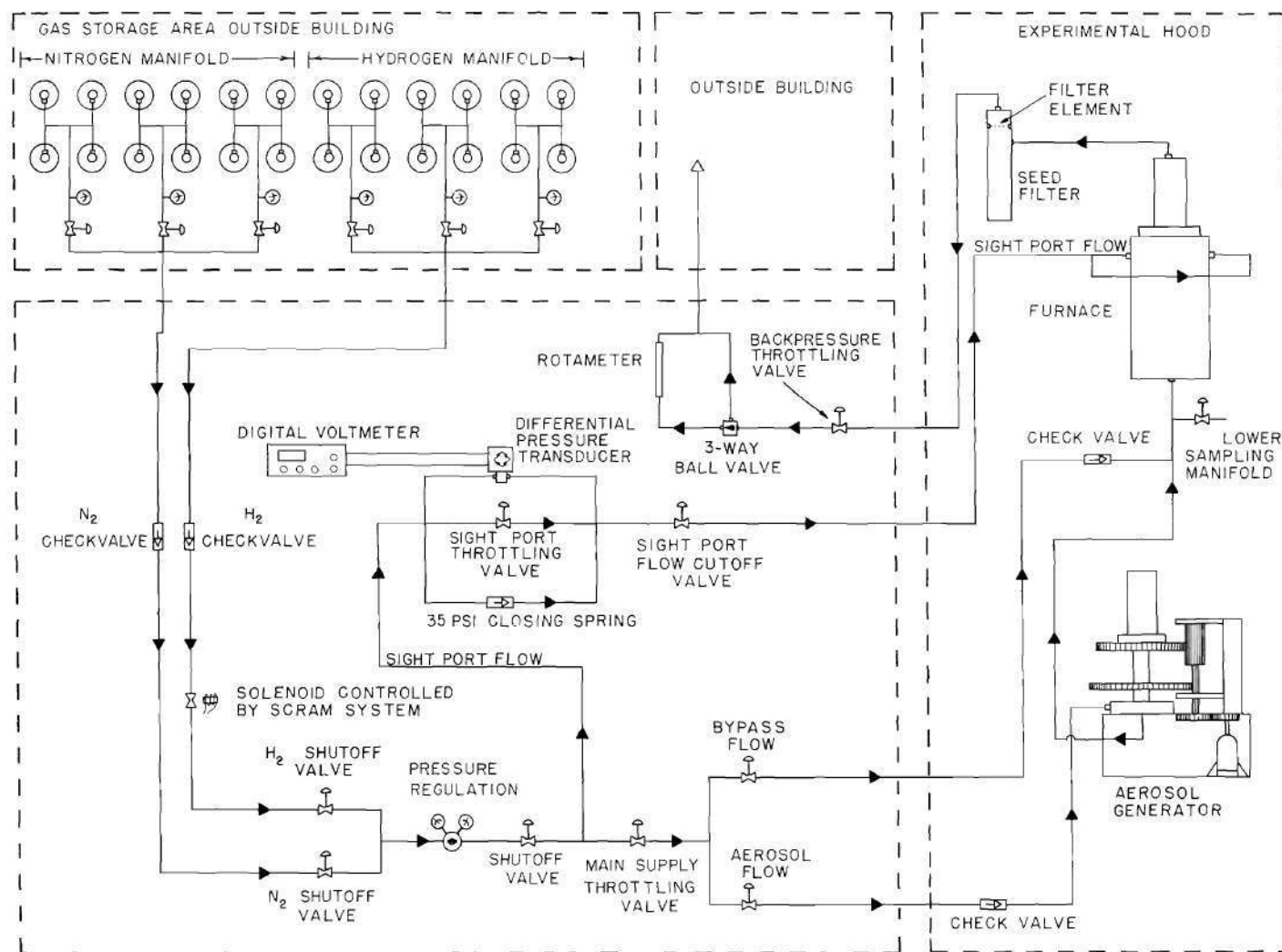
Figure 19.   Gas Supply and Flow Control System

can easily be changed by changing a few connections. Each of the groups

containing four tanks has a pressure gauge and a cutoff valve. This

permits partially empty tanks to be replaced while other tanks are

supplying gas to the experimental equipment. Two three-eighths inch steel

lines carry the hydrogen and the nitrogen into the laboratory. Check

valves are located immediately inside the laboratory so that the two

gases cannot become mixed in the tanks by backfeeding. A solenoid

valve located in the hydrogen line is connected to the safety "SCRAM"

system. This will automatically interrupt the flow of hydrogen should

some malfunction activate the "SCRAM" system. There are two cutoff

valves in the two lines just before they join together into a tee and

enter the single regulator that controls both gases as selected. The

regulator is set to the pressure that is desired in the furnace. The

backpressure throttling valve in the effluent line is adjusted to give

the flow rate desired. Immediately beyond the supply regulator there is

a tap for the sight port flow and then a supply throttling valve for the

main flow to the furnace. After the desired flow rate has been obtained

this supply throttling valve is adjusted to give approximately a five

psi drop across it. This supplies the pressure differential necessary

to drive the sight port flow. This adjustment is made with the sight

port flow throttling valve closed so that the differential pressure

transducer connected across it indicates the pressure differential that

exists across the supply throttling valve. This is possible since there

is no pressure drop across the aerosol generator or the entrance to the

furnace. After these adjustments have been completed the sight port

throttling valve can be opened slightly until the differential pressure transducer indicates a slight decrease in the pressure drop across it, assuring a small flow is present. There is a tee after the supply throttling valve which allows the main flow to go through the bypass line straight to the base of the furnace or, alternatively, through the aerosol generator and then to the base of the furnace. Check valves are located at the base of the furnace in the bypass line and immediately before the aerosol generator in the aerosol supply line. These are in the system to prevent the gas in the furnace from backflowing into the control area in the event there were a line break at the control panel. Another check valve is connected across the differential pressure transducer, but it is placed in the line backwards and fitted with a 35 psi closing spring so that it will act as a safety device to protect the transducer from experiencing an over-pressure if the sight port throttling valve were inadvertently closed when the furnace depressurized.

The effluent gas leaves the cooling tower on the furnace through a line which carries it to the seed filter. The seed filter is approximately 30 inches long with a 2 inch ID and 3 inch OD. The filter is a 4.7 centimeter fiberglass filter with a wire gauze backing. The gas enters the side of the chamber and the filter is placed at the top so the seed material can settle to the bottom without being picked up by large flow rates through the filter when the furnace is being depressurized. After leaving the seed filter the effluent line returns to the control panel where it passes through the furnace backpressure throttling valve and then to a three-way ball valve which directs it either through a

flow meter or directly to the one-half inch pipe that exhausts the
effluent to the atmosphere. The equipment is usually operated with the
flow being monitored in the flow meter, but the flow meter bypass is
available in case the furnace needs to be depressurized very rapidly.

The pressure in the furnace is displayed by four gauges connected
in parallel and mounted on the control panel. Four different ranges are
used for accurate readings at all pressures. There are valves on the
three lower pressure gauges to isolate them when the system pressure
exceeds their range.

Data Recording Instrumentation

Three light intensity signals must be recorded. EMI photomulti-
plier tubes are used to monitor these signals. Photomultiplier tube 3
(used to record the wavelength dependent signal) is an EMI Model 9558QC
tube with a response range of 1750 Å to 8000 Å. Each photomultiplier
signal goes to a picoammeter. The signal monitoring the light source
intensity and the signal monitoring the aerosol density variations do not
vary more than an order of magnitude so linear picoammeters are used to
amplify these signals. The wavelength dependent signal can very many
orders of magnitude and therefore it is amplified by an automatic ranging
picoammeter which automatically measures current from 10^{-13} ampere to
10^{-2} ampere. Most of the time, however, this was operated in the manual
mode and changed by one order of magnitude amplification during the reverse
scan of the spectrum. This allowed spectrum peaks differing by one order
of magnitude to be accurately recorded. The automatic ranging feature
works best when a continuum spectrum is present since the rapid range

changes when scanning a line spectrum are confusing. A block diagram of the data collection system is shown in Figure 20.

The output signals from the picoammeters are fed into a junction box where a set of interconnecting cables lead to the oscillograph. The oscillograph is a mirror galvanometer device which records the signals on light sensitive chart paper. Another set of parallel interconnection cables from the signal junction box lead to the instrumentation tape recorder which can record four channels of information on normal one-quarter inch recording tape. The information can be recorded directly as voltages or encoded as a frequency modulated signal. The frequency modulation mode is used since the direct current portions in the signals that would not be picked up in the direct record mode. The signal junction box also has a set of signal taps that are used when the signal amplitudes are adjusted on the Ampex tape recorder for optimum performance.

The three intensity signals are recorded simultaneously by the oscillograph and the tape recorder. The output from the thermocouple in the furnace is displayed by a digital voltmeter and is recorded manually in the data log. The pressure in the furnace, and the pressure changes in the density volume measurement tanks, as indicated by the manometers, are also recorded manually.

The light intensity data can be analyzed manually from the oscillograph chart trace or, optionally, the data tape from the Ampex tape recorder can be carried to the Georgie Tech Rich Electronic Computer Center where it is fed into an analog-to-digital converter unit which
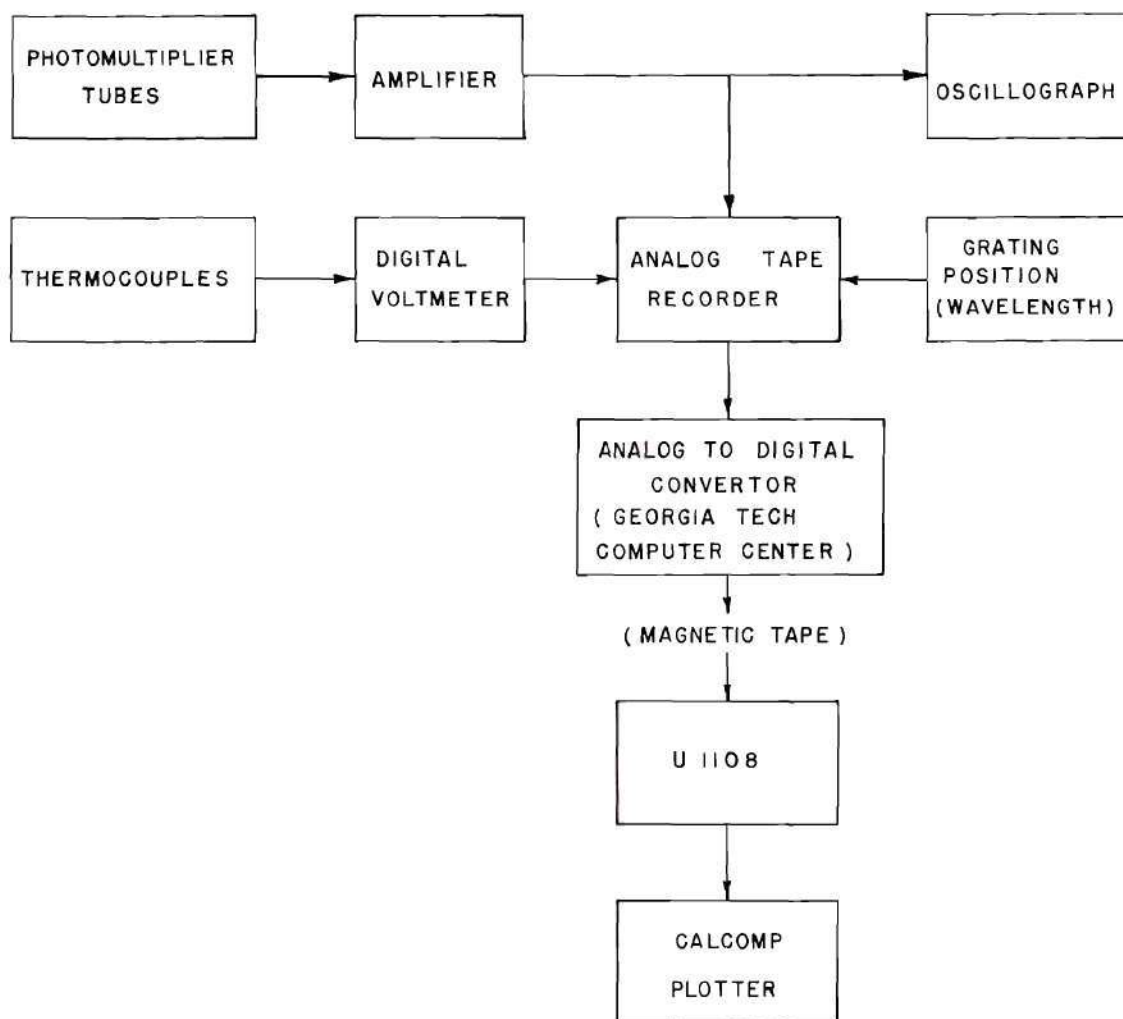
Figure 20. Block Diagram of Data Handling System

digitizes the data and records it on digital computer compatable magnetic tape. A data reduction program analyzes the signals and prints out the results. The use of the CALCOMP Plotter to present directly the results in graphical form is feasible and is shown on Figure 20 but was not used in this research.

The Safety System

Figures 21 and 22 are renderings of the laboratory layout. A double wall aluminum hood with a double wall plexiglass window divides the room. The experiment hood is capped with a plexiglass cover to catch any rising hydrogen. Since the experiment involves the use of hydrogen at high pressure and high temperature, all the equipment design and layout was done with safe operation in mind. The experimental apparatus is located in the hood while the remote control console and the data recording instrumentation are on the other side of the hood.

A high volume exhaust fan is mounted at the top of the experiment hood and continually exhausts the air from the experiment hood. This prevents a buildup of hydrogen in the laboratory should a leak be present. In addition an explosimeter is located at the control console with a sampling line leading to the experiment hood where samples are taken to check for any trace of a hydrogen leak. Check valves are located on the main gas flow lines leading to the furnace so that a break in the gas supply lines at the control panel would not allow the gas in the furnace to backflow into that area.

When the experiment was designed it was done so with the philosophy that all operations could be carried out from a control console
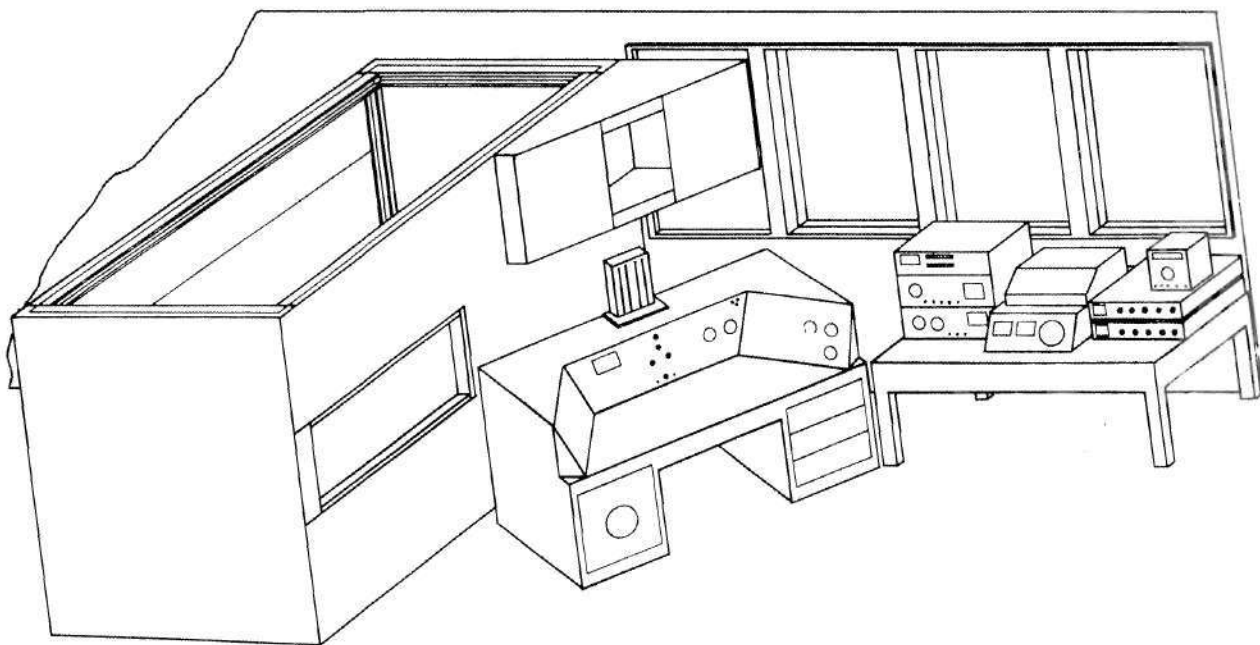
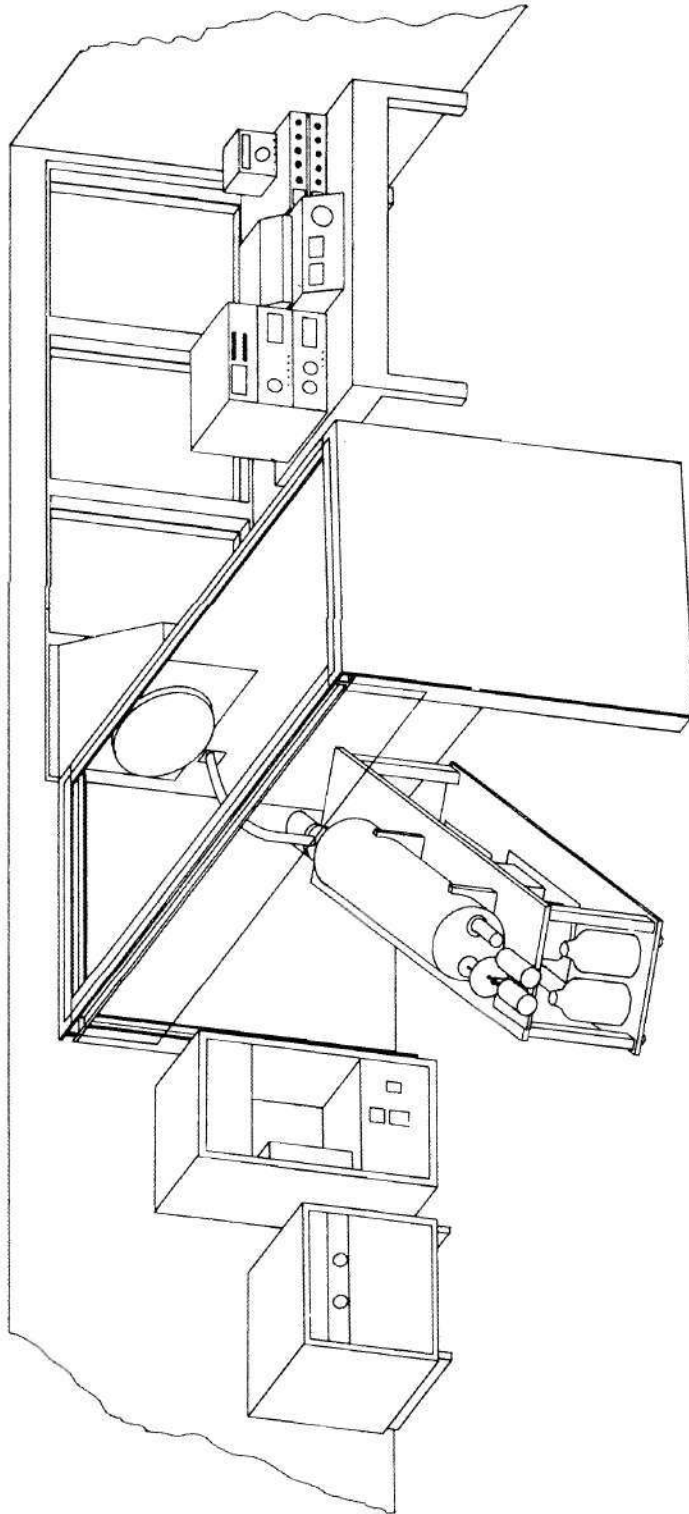Figure 21. Laboratory Layout Viewed From Control Panel

Figure 22. Laboratory Layout Viewed From Equipment Area

so that the operating personnel would not be required to enter the experiment hood while the furnace was pressurized with hydrogen. This was accomplished with one exception. An economically feasible plan for changing the aerosol density samples remotely was never found. Other than this exception all equipment and power supplies can be operated from the control console as can all gas supply controls.

It was decided that the operator should have a convenient means of quickly shutting down the experiment in the case of an emergency. This in addition to the desirability of having the equipment remain off in the case of a power failure led to a centrally controlled electrical distribution system and a "scram" system. The electrical power is brought to the control panel where it is passed through relays in the Scram box (Figure 23). A Scram button on the control panel operates these relays and removes electrical power from all the power supplies and instruments including the furnace power supply. The solenoid in the hydrogen supply line is also connected to this system and will automatically close when the Scram system is deactivated. For further protection some of the safety features of the experiment such as the hood exhaust blower serve as interlocks in the Scram system preventing the experimental apparatus from being turned on until the exhaust fan is turned on. A reset button must be pushed once the Scram system has been deactivated. This prevents an unexpected equipment start up after a power failure.

The d.c. power supply for the furnace requires 220 VAC three-phase power. A fused control box supplies power to a three-phase Variac which varies the a.c. voltage level input to the 20 kilowatt d.c. power supply,
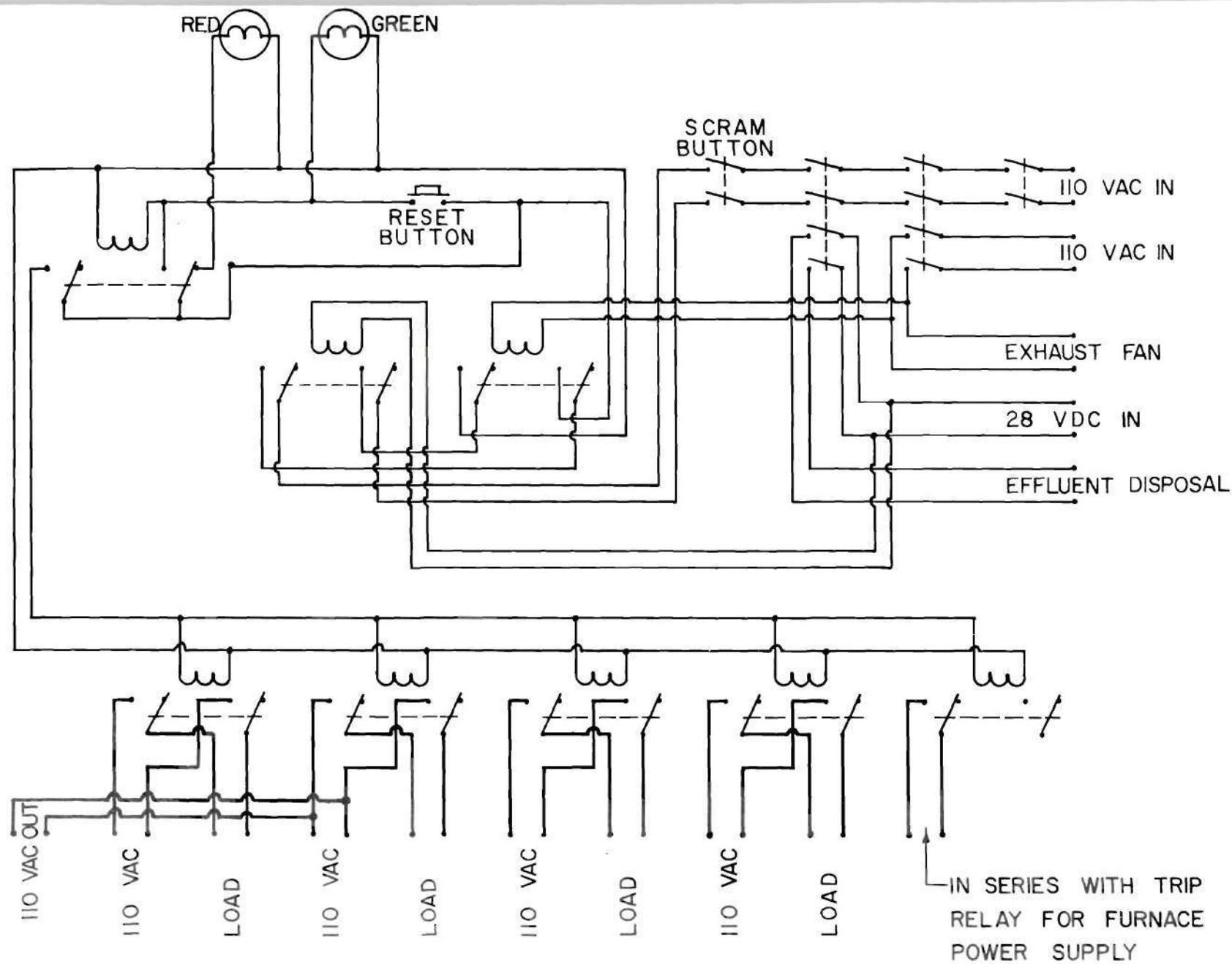
Figure 23. SCRAM System

thereby varying the d.c. output voltage. A voltage and current meter mounted on the control panel indicate the amount of power being fed to the tungsten heater strip.

CHAPTER IV

EXPERIMENTAL PROCEDURE

Operational Steps

The detailed steps necessary to conduct an experimental measure-
ment, usually referred to as an experimental run, are listed in Appendix
A. This chapter outlines the overall preparation and technique involved
in collecting data.

One of the aerosol generators described in Chapter III is chosen
by taking into consideration the seed material that will be used and the
pressure at which the measurement is to be made. The aerosol is removed
from the vacuum drying oven immediately prior to placing it in the aerosol
generator. Then the furnace, aerosol generator, and aerosol sampling
system is pressure tested with nitrogen gas to a pressure higher than
the pressure at which the measurement is to be made. The pre-weighed
filter papers have been placed in the filter holders by this time and
are pressure tested along with the rest of the equipment to insure that
no leaks are present. After determining that no leaks are present in
the system the pressure is reduced and nitrogen gas is allowed to flow
through the system for several minutes to insure all the air has been
purged from the system. Hydrogen is then introduced into the system and
allowed to flow for several minutes in order to flush out the nitrogen
gas. This step is necessary since the nitrogen gas appears to react
either with the tungsten or the boron nitride when it is heated. After

flushing the system with hydrogen the backpresure throttling valve is closed and the furnace is slowly pressurized to the desired operating pressure. After checking again for leaks in the system the cooling water to the furnace is turned on and the aerosol density volume tanks are evacuated. The calibration of all of the electronic data recording instrumentation is checked while the furnace is being pressurized. The explosimeter is calibrated before hydrogen is introduced into the system and is periodically turned on for any indication of hydrogen in the experimental hood.

Since prolonged operation of the mercury arc lamp can lead to instability of the arc, it is not turned on until this point in the sequence. The power to the 20 kw d.c. power supply is fed to the Variac and the power to the heating element is slowly increased. In order to have an accurate measure of the temperature while the furnace is heating, the backpressure throttling valve is opened slightly and a small flow of hydrogen through the system is permitted. The flow is increased by a factor of five to ten when data are being collected but to maintain this flow during the warm up period would unnecessarily waste the gas. When the desired operating temperature is approached the gas flow is increased according to the operating pressure. Approximately one cubic foot per minute (s.t.p.) is used near atmospheric pressure while a ten cubic feet per minute (s.t.p.) flow is used at 100 atmospheres pressure. The higher flow rate at the increased pressure is necessary in order to provide sufficient volumetric flow through the aerosol generator to carry the seed particles through the system to the furnace.

After the main flow rate has been established and the sight port flow adjusted as described in the Gas Control Section of Chapter III, the temperature and pressure in the furnace are allowed to stabilize. Operating conditions are then recorded and the equipment start button is pushed which automatically starts the oscillograph and the diffraction grating drive motor. When the direction of the grating drive motor reverses, the amplication factor on the picoammeter recording the intensity of the wavelength dependent signal is changed by an order of magnitude so that more peaks in the mercury spectrum are available for accurate intensity measurements. After completing the scan without the particles in the hydrogen, the gas flow is sent through the aerosol generator which is then turned on. Within ten to fifteen seconds there is an indication on the background monitoring photomultiplier tube that the aerosol has reached the furnace. Upon seeing this indication the START button is again depressed and simultaneously the sampling solenoid is opened. After the diffraction grating has scanned in both forward and reverse directions the sampling solenoid is closed and the pressure difference in the aerosol density volume measurement tanks is recorded. This completes an experimental run for a given pressure and temperature operating point. A new filter is connected in place, the main flow is diverted through the by-pass line, and the furnace is set to a new operating condition in preparation for the next experimental run.

Light Intensity Measurements

The mercury arc lamp generates a usable spectrum between 2500 and 6000 Å. The intensity measurements are made on the peaks in the spectrum.

The peaks are broadened by using a larger pinhole entrance to the mono-chromator assembly thereby providing an optical integration over a short real time operating interval. This desensitizes the intensity measurements to instrument noise and very abrupt instantaneous aerosol fluctuations which can occur if a single large agglomerate passes in front of the sight ports.

There are three signals that are recorded by the oscillograph. The primary signal is the wavelength dependent signal from which the attenuation measurements are made. However fluctuations in either the lamp source or the aerosol density would create an erroneous attenuation measurement if this were the only signal taken into consideration. In order to measure the aerosol fluctuations and use the measurement so that the wavelength dependent signal can be corrected for aerosol fluctuations, a second photomultiplier tube is mounted at the diffraction grating end of the monochromator. This photomultiplier tube has a near ultraviolet filter in front so that it detects a narrow bandwidth of the spectrum. Since for a particular wavelength the change in the intensity of the signal is related exponentially to a change in the aerosol density it is possible to combine the information from this signal with the average density given by the sample which was drawn from the aerosol during the experimental run and thereby calculate the aerosol density at every wavelength corresponding to each time during which the data are recorded. This procedure is explained in detail in Chapter V.

At this time all of the intensity variations with the exception of the light source intensity have been taken into account. Since a variation in the light source strength would affect both the wavelength

dependent signal and aerosol density monitor signal it is necessary to monitor the intensity of the light source with a third photomultiplier tube which is located in the beam between the light source and the sight port entrance to the furnace. In the sequence of data reduction which is covered more completely in Chapter V the light source strength correction is applied to both the measurement of the wavelength dependent signal and the aerosol density monitor signal. The aerosol density monitor signal is used to calculate an effective density at each wavelength which in turn is used in the final calculation of the extinction coefficient at each wavelength.

Aerosol Density Measurement

The aerosol density sampling system, which is illustrated and described in Chapter III, obtains a representative aerosol density sample at the points of interest without disturbing the furnace operating conditions. This means that only a small percentage of the total flow can be sampled. With such a small flow rate in the sample system it is imperative that the sample holder be located as close as possible to the point to be sampled to that loss of seed material due to settling in the lines is minimized.

There is an upper and a lower sampling manifold to allow the density of the aerosol entering the furnace to be compared with the density of the aerosol after it has been heated. This is useful in determining if there is a decrease in the density of the aerosol due to a reaction with hydrogen such as occurs with 0.012 micron diameter carbon particles.

The filter papers are weighed and numbered before they are placed

in the filter holders and then are weighed along with the deposit on them after the sample has been drawn. The volume of gas that was drawn is measured by allowing it to flow into a tank of known volume and measuring the pressure in the tank before and after the addition of the sampled gas. The volume of gas at standard temperature and pressure is converted to the volume that it would have occupied in the furnace at the operating pressure and temperature and then the density of the aerosol in grams per cubic centimeter is calculated as the average density.

CHAPTER V

DATA REDUCTION AND ANALYSIS

Calculation of Linear Attenuation Coefficient

The beam of light from the mercury arc passes through the 1.587 cm inside diameter heating chamber containing the hot, pressurized hydrogen aerosol, and then into the monochromator. The intensity of the transmitted beam is recorded as a function of wavelength. Figure 24 illustrates the recorded intensities as they appear on the oscillograph trace. The upper trace illustrates a spectrum scan with only the heated pressurized hydrogen present in the furnace. The lower trace was taken after aerosol was introduced into the furnace. Both traces illustrate two scans of the spectrum. Since the grating must be driven back to its original position, both the forward and the reverse scan of the spectrum is recorded. However, on the reverse scan the amplification on the picoammeter monitoring the wavelength dependent signal is changed by a factor of ten so that more peaks in the mercury spectrum can be analyzed. The grating scans the mercury arc spectrum from 2000 Å to 7500 Å, but, since the last major peak is 5800 Å, the extended scan permits the recording of second-order reflections of several of the strongest mercury peaks. The second-order peaks are less intense than the primary peaks.

Three signals are recorded by the oscillograph. The first is the intensity, I_L, of the focused beam of light from the mercury arc.
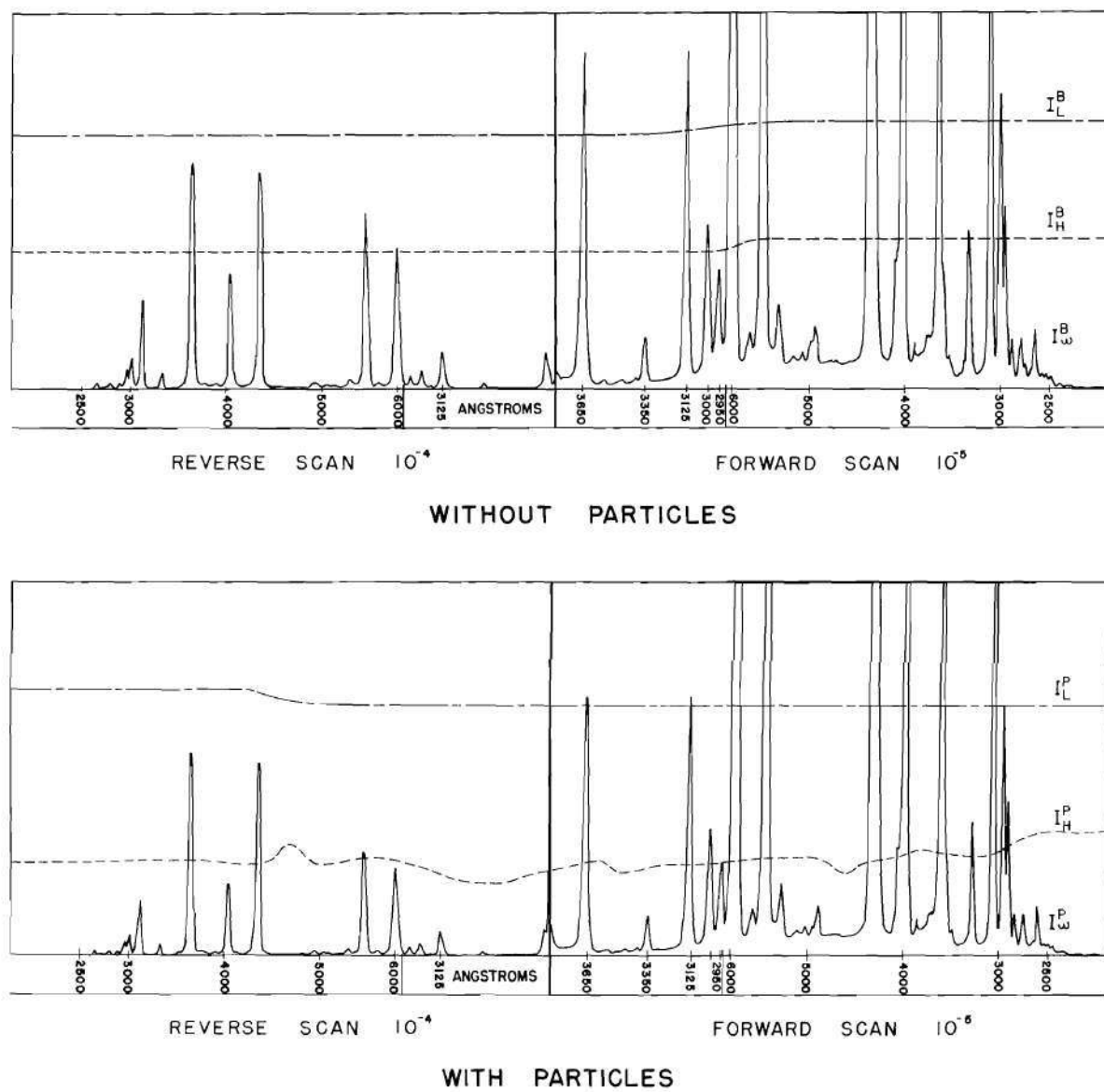
Figure 24. Intensity Traces from Oscillograph

The second intensity recorded, I_H, is a very narrow portion of the ultra-violet monitored after the beam of light has passed through the furnace. This is necessary in order to be able to detect variations in the aerosol density. The third signal is the wavelength dependent signal, I_ω. A superscript $\underline{B}$ is added to denote that the intensity was measured without aerosol in the furnace and the superscript $\underline{P}$ is added when the signal was measured with aerosol present.

The following is a summary of the notation to be used in the analysis (refer to Figure 7 for photomultiplier designations):

I_ω^B = Signal from photomultiplier 1 without aerosol present

I_H^B = Signal from photomultiplier 2 without aerosol present

I_L^B = Signal from photomultiplier 3 without aerosol present

I_ω^B corr = I_ω^B corrected for variations in light source intensity

I_H^B corr = I_H^B corrected for variations in light source intensity

I_ω^P = Signal from photomultiplier 1 with aerosol present

I_H^P = Signal from photomultiplier 2 with aerosol present

I_L^P = Signal from photomultiplier 3 with aerosol present

I_ω^P corr = I_ω^P corrected for variations in light source intensity

I_H^P corr = I_H^P corrected for variations in light source intensity

The density of the aerosol changes with time while the intensity of the signal depends on the wavelength. Since the grating is motor driven

at a constant speed, it is convenient to use wavelength as the independent variable for the changing aerosol density.

The extinction parameter $\mu(\lambda)$ is given by

$$\mu(\lambda) = \frac{K(\lambda)}{\rho(\lambda)} \tag{1}$$

where $K(\lambda)$ is the linear attenuation parameter and $\rho(\lambda)$ is the density of the aerosol correlated to the wavelength. The calculation of $\mu(\lambda)$ involves two separate calculations. One is the calculation of $K(\lambda)$ and the other is the calculation of $\rho(\lambda)$. $K(\lambda)$ is given by the expression

$$K(\lambda) = \frac{1}{X} \ln \left[\frac{I_\omega^{B \ corr}}{I_\omega^{P \ corr}} \right] \tag{2}$$

where X = aerosol path length.

The variations in signal strength due to fluctuations in the light source strength are normalized by

$$I_\omega^{B \ corr} = I_\omega^{B} \times \frac{1}{I_L^{B}} \tag{3}$$

$$I_H^{B \ corr} = I_H^{B} \times \frac{1}{I_L^{B}}$$

$$I_\omega^{P \ corr} = I_\omega^{P} \times \frac{1}{I_L^{P}}$$

$$I_H^{P \ corr} = I_H^{P} \times \frac{1}{I_L^{P}}$$

Calculation of Aerosol Density

The average density, ρ, is obtained by drawing a sample of the aerosol at a constant rate during the spectrum scan. The instantaneous aerosol density, $\rho(t)$, is calculated from the signal, I_H. This signal has no wavelength dependence since it is obtained by monitoring a small bandwidth of the ultraviolet spectrum.

The average density, ρ, of the aerosol is given by

$$\rho = \frac{1}{T} \int_0^T \rho(t)\, dt \tag{4}$$

where T = sampling time. When $\rho(t)$ does not change rapidly with time, this integration can be expressed

$$\rho = \frac{1}{T} \sum_{i=1}^N \rho(t_i)\, \Delta t_i \tag{5}$$

where

$$T = \sum_{i=1}^N \Delta t_i$$

Δt_i = time interval short compared to aerosol fluctuations

Since the wavelength is proportional to time as a result of the constant speed grating drive, it is convenient to use wavelength as the independent variable. Therefore,

$$\rho = \frac{1}{L} \sum_{i=1}^N \rho(\lambda_i)\, \Delta \lambda_i \tag{6}$$

where $L = \sum\limits_{i=1}^{N} \Delta \lambda_i$

The relationship of I_H to the instantaneous aerosol density $\rho(\lambda_i)$ is given by

$$\frac{I_H^{B\ corr}}{I_H^{P\ corr}(\lambda_i)} = e^{\mu X \rho(\lambda_i)} \tag{7}$$

where μ is not a function of wavelength since I_H represents only a narrow bandwidth of wavelengths in the spectrum.

Rewriting the expression in terms of $\rho(\lambda_i)$

$$\rho(\lambda_i) = \frac{1}{\mu X} \ln \left[\frac{I_H^{B\ corr}}{I_H^{P\ corr}(\lambda_i)} \right] \tag{8}$$

Substituting equation (8) into (6)

$$\rho = \frac{1}{\mu XL} \sum_{i=1}^{N} \left(\ln \left[\frac{I_H^{B\ corr}}{I_H^{P\ corr}(\lambda_i)} \right] \right) \Delta \lambda_i \tag{9}$$

Up to this point the independent variable λ_i has been used instead of time since the $\Delta \lambda_i$ are chosen small enough to preclude a significant change in aerosol density. The index $\underline{i}$ to λ_i indicates that a finite number of intervals are chosen in order to compute the sum given by equation (9). Now the independent variable λ is introduced as a correlation between wavelength in the spectrum and time dependent aerosol density.

For any wavelength λ

$$\frac{I_H^{B\ corr}}{I_H^{P}(\lambda)^{corr}} = e^{\mu X \rho(\lambda)} \qquad (10)$$

Therefore,

$$\rho(\lambda) = \frac{1}{\mu X} \ln \left[\frac{I_H^{B\ corr}}{I_H^{P}(\lambda)^{corr}} \right] \qquad (11)$$

substituting $\frac{1}{\mu X}$ from equation (9)

$$\rho(\lambda) = \frac{\rho L}{\sum\limits_{i=1}^{N} \left(\ln \left[\frac{I_H^{B\ corr}}{I_H^{P}(\lambda_i)^{corr}} \right] \Delta\lambda_i \right)} \cdot \ln \left[\frac{I_H^{B\ corr}}{I_H^{P}(\lambda)^{corr}} \right] \qquad (12)$$

A constant is defined

$$R = \frac{\rho L}{\sum\limits_{i=1}^{N} \left(\ln \left[\frac{I_H^{B\ corr}}{I_H^{P}(\lambda_i)^{corr}} \right] \Delta\lambda_i \right)} \qquad (13)$$

The aerosol density at any wavelength λ is calculated from

$$\rho(\lambda) = R \ln \left[\frac{I_H^{B\ corr}}{I_H^{P}(\lambda)^{corr}} \right] \qquad (14)$$

Error Analysis

The percentage of uncertainty in the measurements of I_{ω}, I_H, I_L and ρ are estimated. The error in the light intensity measurements are due, principally, to the accuracy to which the intensity levels can be measured from the oscillograph recording. The estimated error in ρ reflects the accuracy with which a sample of aerosol can be collected and weighed.

The uncertainties in the determinations of these measurements are propagated through the calculations necessary to obtain the extinction parameter and determine the uncertainty for the value calculated. The manner in which these uncertainties are propagated is shown by considering a function, M, of several independent variables.

$$M = f(x,y,z)$$

The error ΔM in M is calculated by

$$\Delta M = \Delta x \left(\frac{\partial M}{\partial x}\right)_{y_o z_o} + \Delta y \left(\frac{\partial M}{\partial y}\right)_{x_o z_o} + \Delta z \left(\frac{\partial M}{\partial z}\right)_{x_o y_o}$$

If the uncertainties in x, y, and z are not related, there will be no cross correlation terms and the expression for ΔM can be simplified to

$$\left(\frac{\Delta M}{M}\right)^2 = \frac{\left(\frac{\partial M}{\partial x}\Delta x\right)^2 + \left(\frac{\partial M}{\partial y}\Delta y\right)^2 + \left(\frac{\partial M}{\partial z}\Delta z\right)^2}{M^2}$$

Therefore the error in the extinction coefficient is calculated as follows:

From equation (1)

$$\mu(\lambda) = \frac{K(\lambda)}{\rho(\lambda)}$$

so

$$\left(\frac{\Delta\mu(\lambda)}{\mu(\lambda)}\right)^2 = \left(\frac{\Delta K(\lambda)}{K(\lambda)}\right)^2 + \left(\frac{\Delta\rho(\lambda)}{\rho(\lambda)}\right)^2 \tag{15}$$

From equation (2)

$$K(\lambda) = \frac{1}{X} \ln\left[\frac{I_\omega^B(\lambda)^{corr}}{I_\omega^P(\lambda)^{corr}}\right]$$

therefore

$$\left(\frac{\Delta K(\lambda)}{K(\lambda)}\right)^2 = \frac{1}{\left(\ln\left[\frac{I_\omega^B(\lambda)^{corr}}{I_\omega^P(\lambda)^{corr}}\right]\right)^2} \cdot \left\{\left(\frac{\Delta I_\omega^B(\lambda)^{corr}}{I_\omega^B(\lambda)^{corr}}\right)^2 + \left(\frac{\Delta I_\omega^P(\lambda)^{corr}}{I_\omega^P(\lambda)^{corr}}\right)^2\right\} + \left(\frac{\Delta x}{x}\right)^2 \tag{16}$$

From equation (3)

$$I_\omega^B(\lambda)^{corr} = \frac{I_\omega^B(\lambda)}{I_K^B(\lambda)}$$

and

$$I_\omega^P(\lambda)^{corr} = \frac{I_\omega^P(\lambda)}{I_L^P(\lambda)}$$

so,

$$\left(\frac{\Delta I_{\omega}^{B}(\lambda)^{corr}}{I_{\omega}^{B}(\lambda)^{corr}} \right)^{2} = \left(\frac{\Delta I_{\omega}^{B}(\lambda)}{I_{\omega}^{B}(\lambda)} \right)^{2} + \left(\frac{\Delta I_{L}^{B}(\lambda)}{I_{L}^{P}(\lambda)} \right)^{2}$$

and

$$\left(\frac{\Delta I_{\omega}^{P}(\lambda)^{corr}}{I_{\omega}^{P}(\lambda)^{corr}} \right)^{2} = \left(\frac{\Delta I_{\omega}^{P}(\lambda)}{I_{\omega}^{P}(\lambda)} \right)^{2} + \left(\frac{\Delta I_{L}^{P}(\lambda)}{I_{L}^{P}(\lambda)} \right)^{2}$$

From equation (14)

$$\rho(\lambda) = R \ln \left[\frac{I_{H}^{B \ corr}}{I_{H}^{P}(\lambda)^{corr}} \right]$$

so

$$\left(\frac{\Delta\rho(\lambda)}{\rho(\lambda)} \right) = \left(\frac{\Delta R}{R} \right) + \frac{1}{\left(\ln \left[\frac{I_{H}^{B \ corr}}{I_{H}^{P}(\lambda)^{corr}} \right] \right)^{2}} \left\{ \left(\frac{\Delta I_{H}^{B \ corr}}{I_{H}^{B \ corr}} \right)^{2} + \left(\frac{\Delta I_{H}^{P}(\lambda)^{corr}}{I_{H}^{P}(\lambda)^{corr}} \right)^{2} \right\} \qquad (18)$$

where from equation (3)

$$I_{H}^{B \ corr} = \frac{I_{H}^{B}}{I_{L}^{B}}$$

and

$$I_{H}^{P}(\lambda)^{corr} = \frac{I_{H}^{P}(\lambda)}{I_{L}^{P}(\lambda)}$$

therefore

$$\left(\frac{\Delta I_H^{B\ corr}}{I_H^{B\ corr}} \right)^2 = \left(\frac{\Delta I_H^{B}}{I_H^{B}} \right)^2 + \left(\frac{\Delta I_L^{B}}{I_L^{B}} \right)^2 \qquad (19)$$

and

$$\left(\frac{\Delta I_H^{P}(\lambda)^{corr}}{I_H^{P}(\lambda)^{corr}} \right)^2 = \left(\frac{\Delta I_H^{P}(\lambda)}{I_H^{P}(\lambda)} \right)^2 + \left(\frac{\Delta I_L^{P}(\lambda)}{I_L^{P}(\lambda)} \right)^2 \qquad (20)$$

From equation (13)

$$R = \frac{\rho L}{\sum\limits_{i=1}^{N} \left(\ln\left[\frac{I_H^{B\ corr}}{I_H^{P\ corr}(\lambda_i)} \right] \Delta\lambda_i \right)}$$

Therefore,

$$R = \frac{\Delta\rho L}{\sum\limits_{i=1}^{N} \left(\ln\left[\frac{I_H^{B\ corr}}{I_H^{P\ corr}(\lambda_i)} \right] \Delta\lambda_i \right)} + \frac{\rho\Delta L}{\sum\limits_{i=1}^{N} \left(\ln\left[\frac{I_H^{B\ corr}}{I_H^{P\ corr}(\lambda_i)} \right] \Delta\lambda_i \right)}$$

$$- \frac{\rho L \Delta \sum}{\left\{ \sum\limits_{i=1}^{N} \left(\ln\left[\frac{I_H^{B\ corr}}{I_H^{P\ corr}(\lambda_i)} \right] \Delta\lambda_i \right) \right\}^2} \qquad (21)$$

where

$$\Delta \sum = \sum_{i=1}^{N} \left[\ln \left[\frac{I_H^{B\ corr}}{I_H^{P\ corr}(\lambda_i)} \right] \Delta(\Delta\lambda_i) + \Delta\lambda_i \left(\frac{\Delta I_H^{B\ corr}}{I_H^{B\ corr}} - \frac{\Delta I_H^{P\ corr}(\lambda_i)}{I_H^{P\ corr}(\lambda_i)} \right) \right] \tag{22}$$

The error in the extinction parameter can be calculated from the above set of equations when $\frac{\Delta I}{I}$ for all of the signals, and $\frac{\Delta\rho}{\rho}$ are estimated.

CHAPTER VI

EXPERIMENTAL RESULTS

Summary

Measurements of the extinction parameter for tungsten-hydrogen aerosols were made at pressures to 115 atmospheres, temperatures to 2500°K, and for radiant energy wavelengths of 2500 Å to 5800 Å. The value of the extinction parameter was found to increase with temperature and to increase with pressure at high temperatures.

Tungsten-Hydrogen Aerosols

The tungsten seed material was a powder of submicron-sized particles. The electron micrographs in Figure 18 illustrate the sizes and shapes of these particles as they were collected from the aerosol. The top electron micrograph was taken of an aerosol that had been formed by passing it through a nozzle. The bottom electron micrograph was formed without using a nozzle and exhibits less dispersion. The average diameter of the particles in the well-dispersed aerosol lies between 0.1 and 0.2 micron while the average diameter in the less-dispersed aerosol lies between 0.2 and 0.5 micron. The well-dispersed aerosol was used in measuring the extinction parameter to 12.5 atmospheres pressure. The data at higher pressures were measurements of an aerosol formed without a nozzle, so the particle agglomerates were similar to those in the lower electron micrograph. The difference in average particle sizes produced

a corresponding difference in the measured extinction parameters as predicted by Mie theory. This is described in more detail in the following section.

The difficulty in using a nozzle in the aerosol generator at high pressures was discussed in the Aerosol Generator section of Chapter III.

The principal sources of error in the data were dilute aerosols and the difficulty in obtaining an accurate sample density. The scatter in the values of the extinction parameter at different wavelengths, during the same operating conditions, was always related to a very dilute aerosol as determined by the aerosol density sample. The fact that the extinction parameter varied as much as 20 percent for several measurements at the same operating conditions was attributed to the error in the aerosol sample density. The inherent difficulties in obtaining an accurate sample density are due to, first, the disturbance to the flow pattern in the heating chamber caused by sampling, and, second, the deposition of the seed material on the sampling tube walls as the result of coagulation, thermal precipitation, and gravity induced precipitation. An increased sampling rate would tend to reduce the precipitation rate but it increases the disturbance to the aerosol flow pattern in the heating chamber. Therefore an optimum sampling rate is a compromise to minimize the sum of the two effects.

No chemical reaction between the hydrogen and the tungsten was expected or observed. One of the beneficial effects of using hydrogen as the carrier gas in the tungsten aerosol was more efficient heat transfer from the heating element to the hydrogen, and in turn, to the particles.

When the heating element was above approximately 1500°K, the temperature would increase about five percent when particles were added to the gas, indicating that the particles were aiding the heat transfer process by absorbing the radiant energy and further heating the hydrogen.

Extinction Parameter Measurements

The extinction parameters of tungsten-hydrogen aerosols were measured over a range of temperatures in five pressure regimes: 12, 45, 70, 100, and 115 atmospheres. In addition, the extinction parameter data for tungsten-hydrogen aerosols at one atmosphere from reference 12 are used in showing trends due to pressure.

Figures 25 through 38 are plots of the extinction parameter data as a function of wavelength for various operating points. As a comparison, the theoretical values of the extinction parameter calculated from Mie theory are plotted for four particle diameters (0.02, 0.1, 0.2, and 0.5 micron). The data exhibiting a great deal of scatter in the values of the extinction parameter for different wavelengths are characteristic of measurements made with a dilute aerosol. The spectrum averaged value of the extinction parameter for room temperature data at 12.5 atmospheres is about 20,000 cm^2/gm. Since these data are for a nozzle-dispersed tungsten aerosol, they represent the extinction parameter for tungsten particles in the size range 0.1 to 0.2 micron discussed in the previous section. This average value compares closely with the average value for a similar aerosol at one atmosphere as measured by Shenoy.[12] The room temperature data for higher pressure tungsten-hydrogen aerosols were not generated with a nozzle. The spectrum averaged value of the
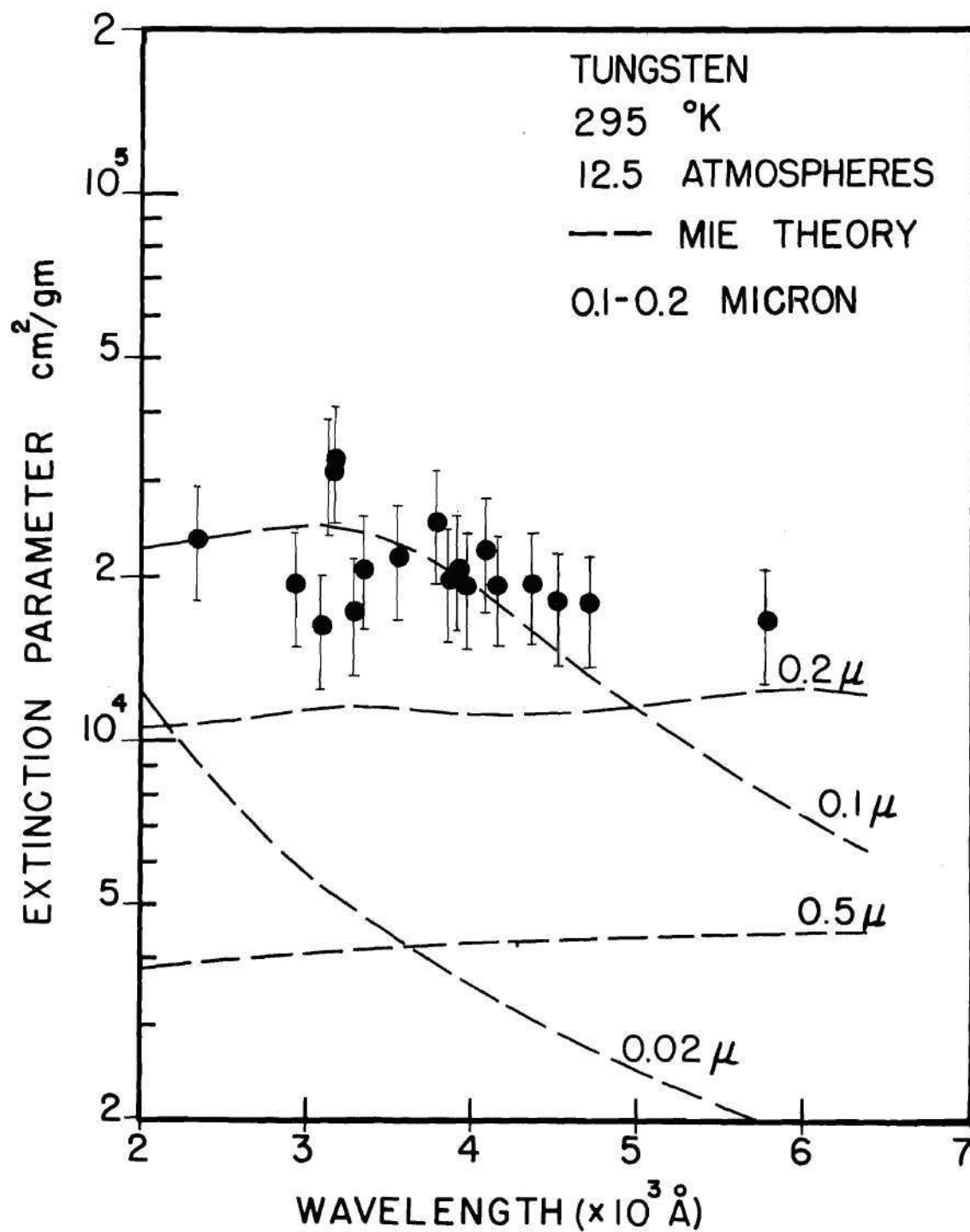
Figure 25. Extinction Parameter of Tungsten-Hydrogen Aerosol at 295°K and 12.5 Atmospheres
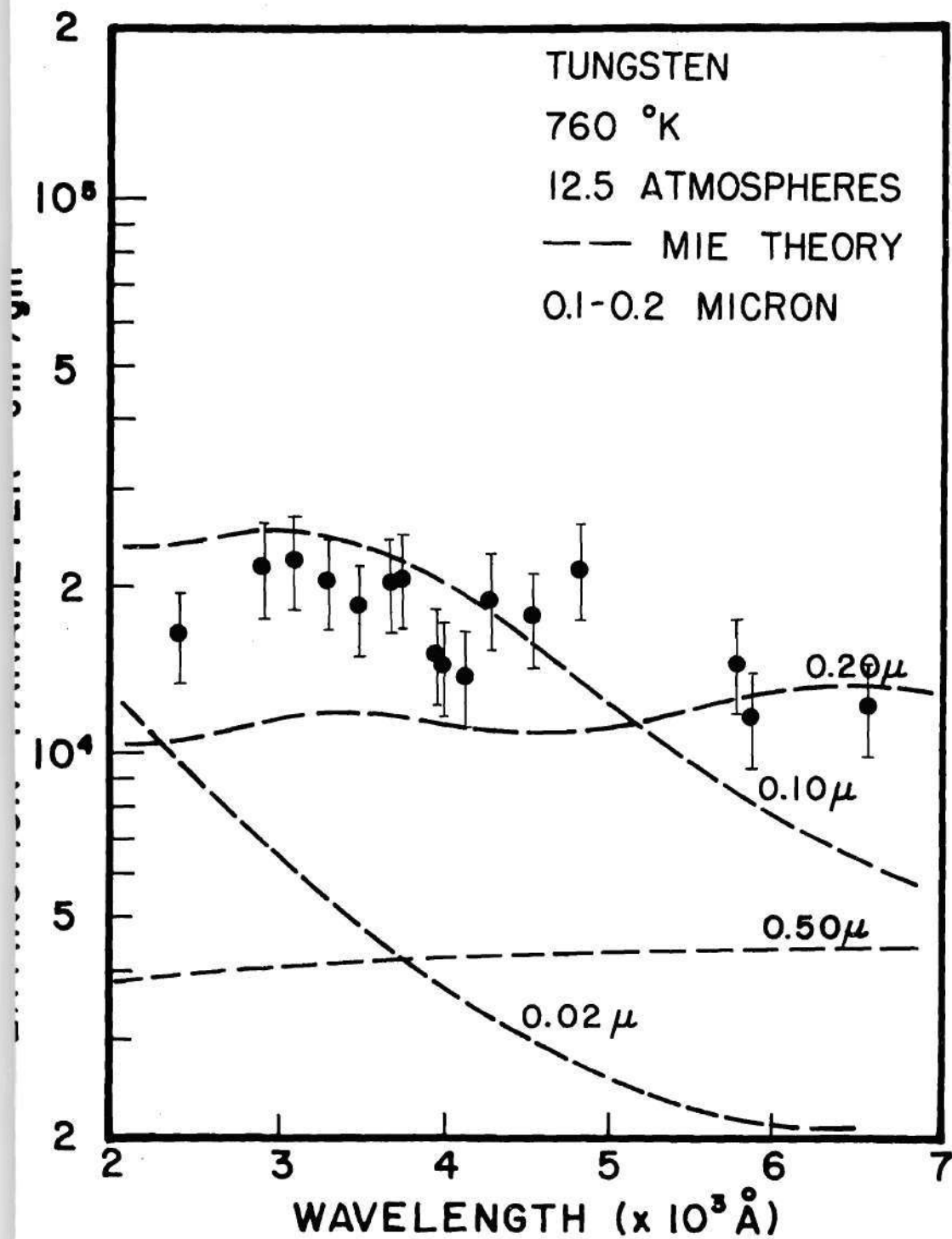
Figure 26. Extinction Parameter of Tungsten-Hydrogen Aerosol
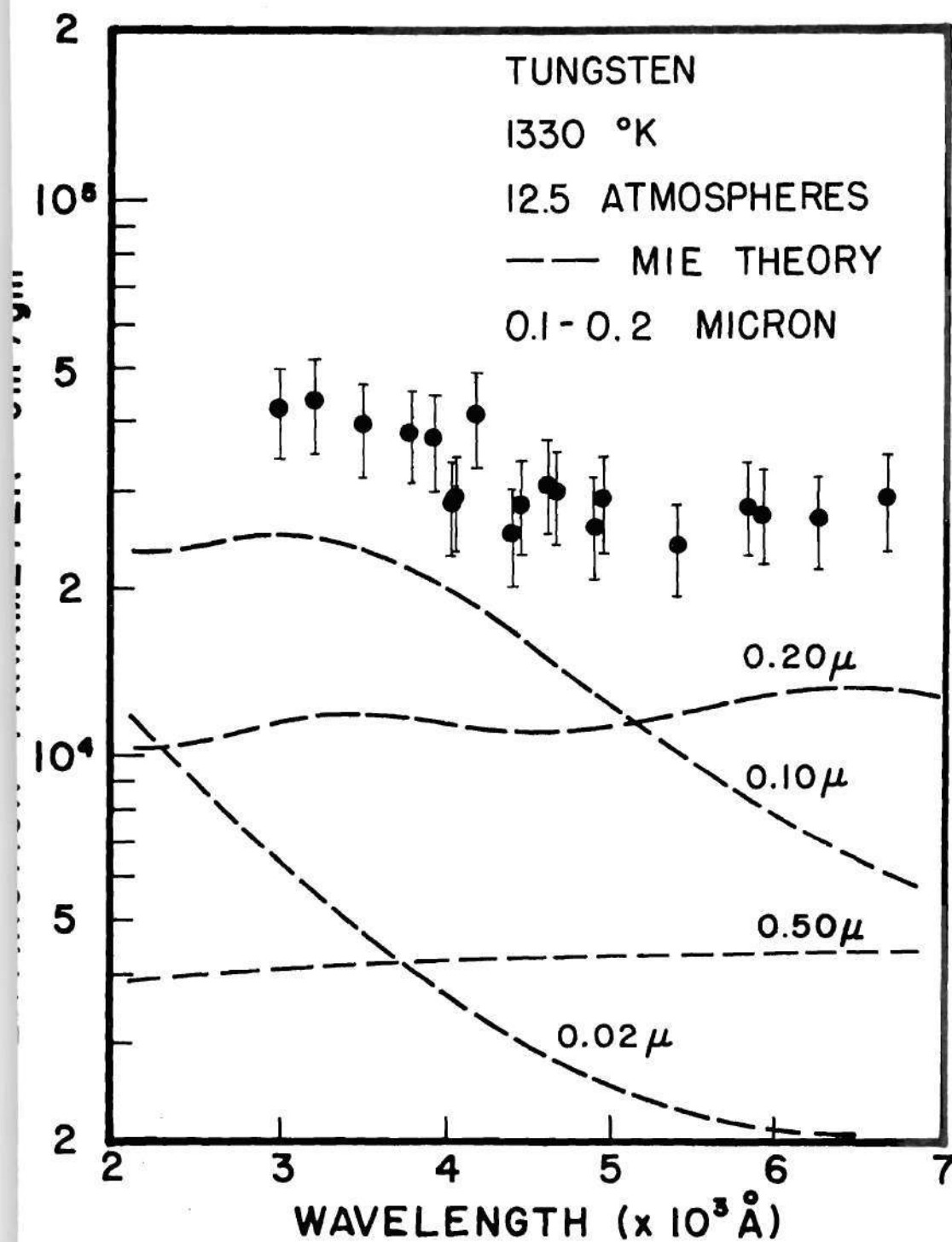at 760°K and 12.5 Atmospheres

Figure 27. Extinction Parameter of Tungsten-Hydrogen Aerosol at 1330°K and 12.5 Atmospheres
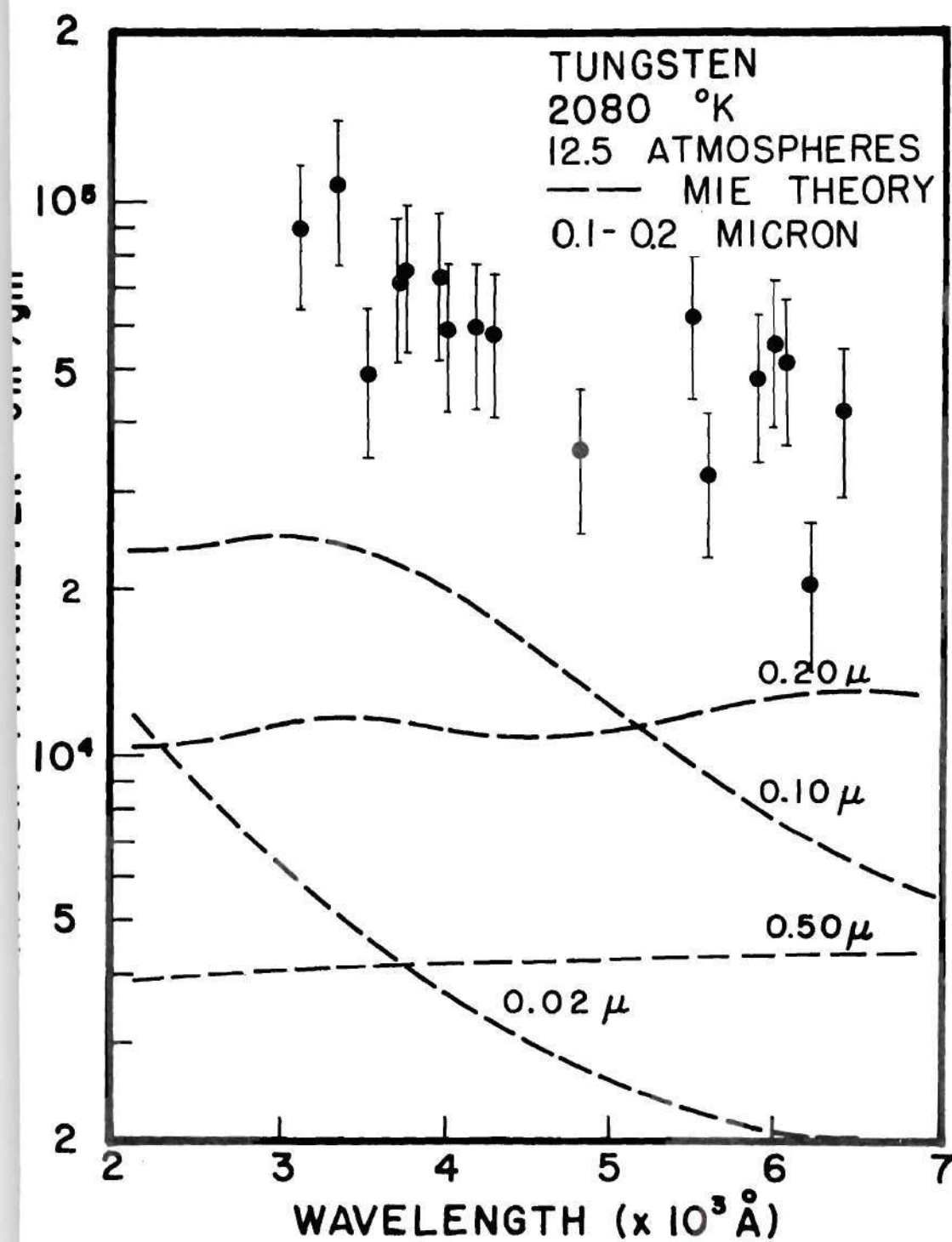
Figure 28. Extinction Parameter of Tungsten-Hydrogen Aerosol at 2080°K and 12.5 Atmospheres
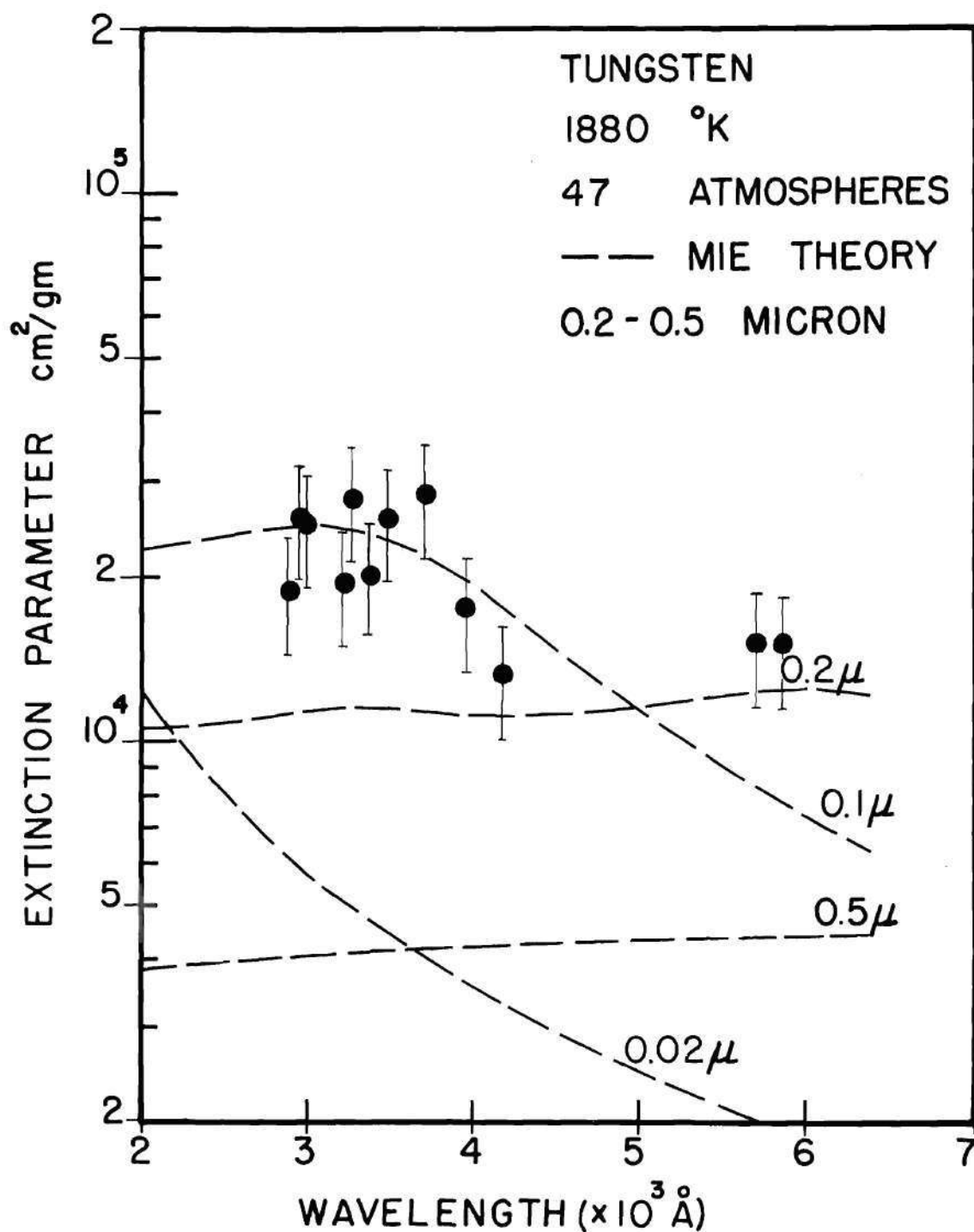
Figure 29. Extinction Parameter of Tungsten-Hydrogen Aerosol at 1880°K and 47 Atmospheres

Figure 30. Extinction Parameter of Tungsten-Hydrogen Aerosol at 2220°K and 42 Atmospheres

Figure 31. Extinction Parameter of Tungsten-Hydrogen Aerosol at 2550°K and 70 Atmospheres

Figure 32. Extinction Parameter of Tungsten-Hydrogen Aerosol at 295°K and 100 Atmospheres

Figure 33. Extinction Parameter of Tungsten-Hydrogen Aerosol at 410°K and 100 Atmospheres

Figure 34.   Extinction Parameter of Tungsten-Hydrogen Aerosol at 1180°K
and 100 Atmospheres

Figure 35. Extinction Parameter of Tungsten-Hydrogen Aerosol at 1520°K and 100 Atmospheres
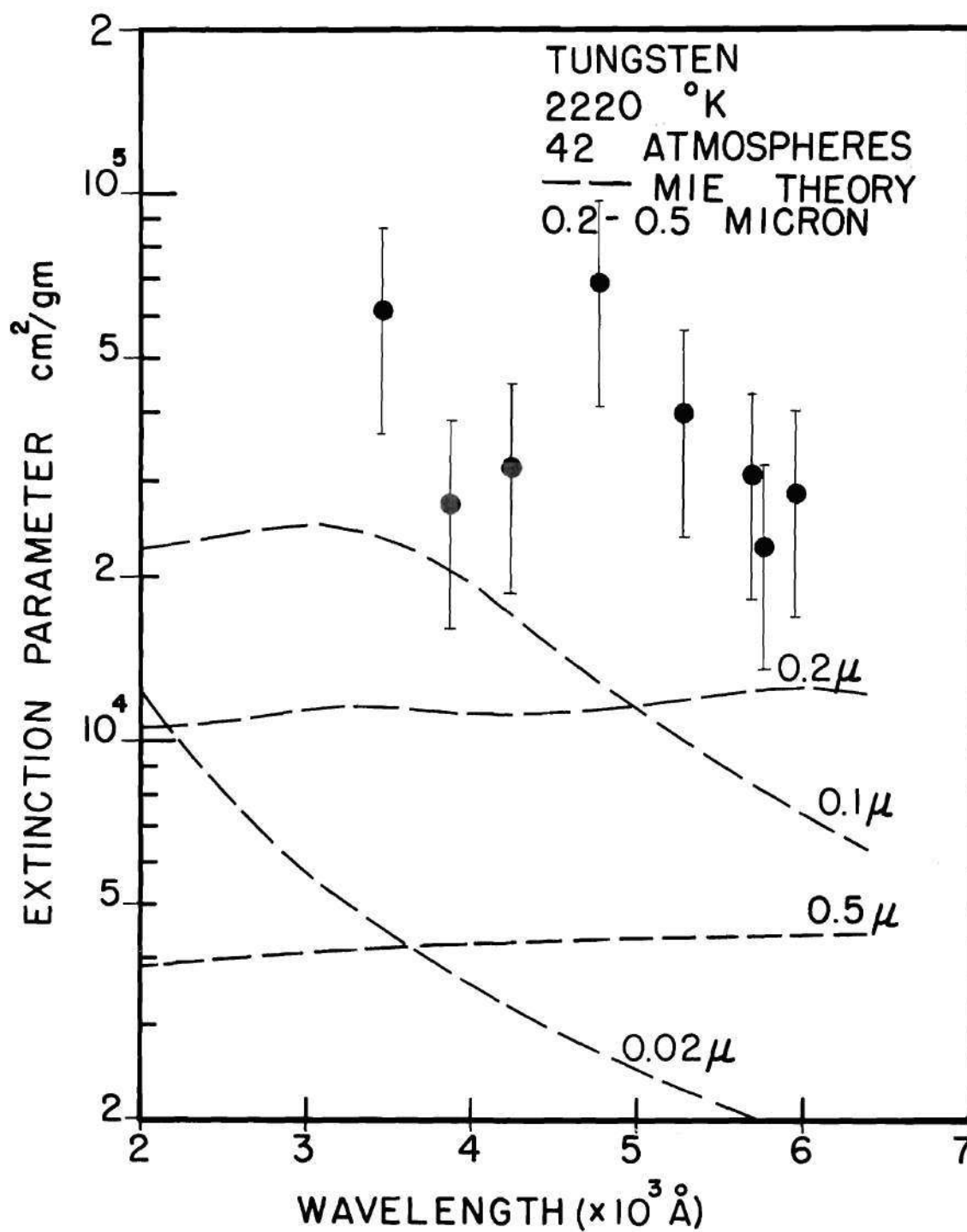
Figure 36. Extinction Parameter of Tungsten-Hydrogen Aerosol at 295°K and 115 Atmospheres
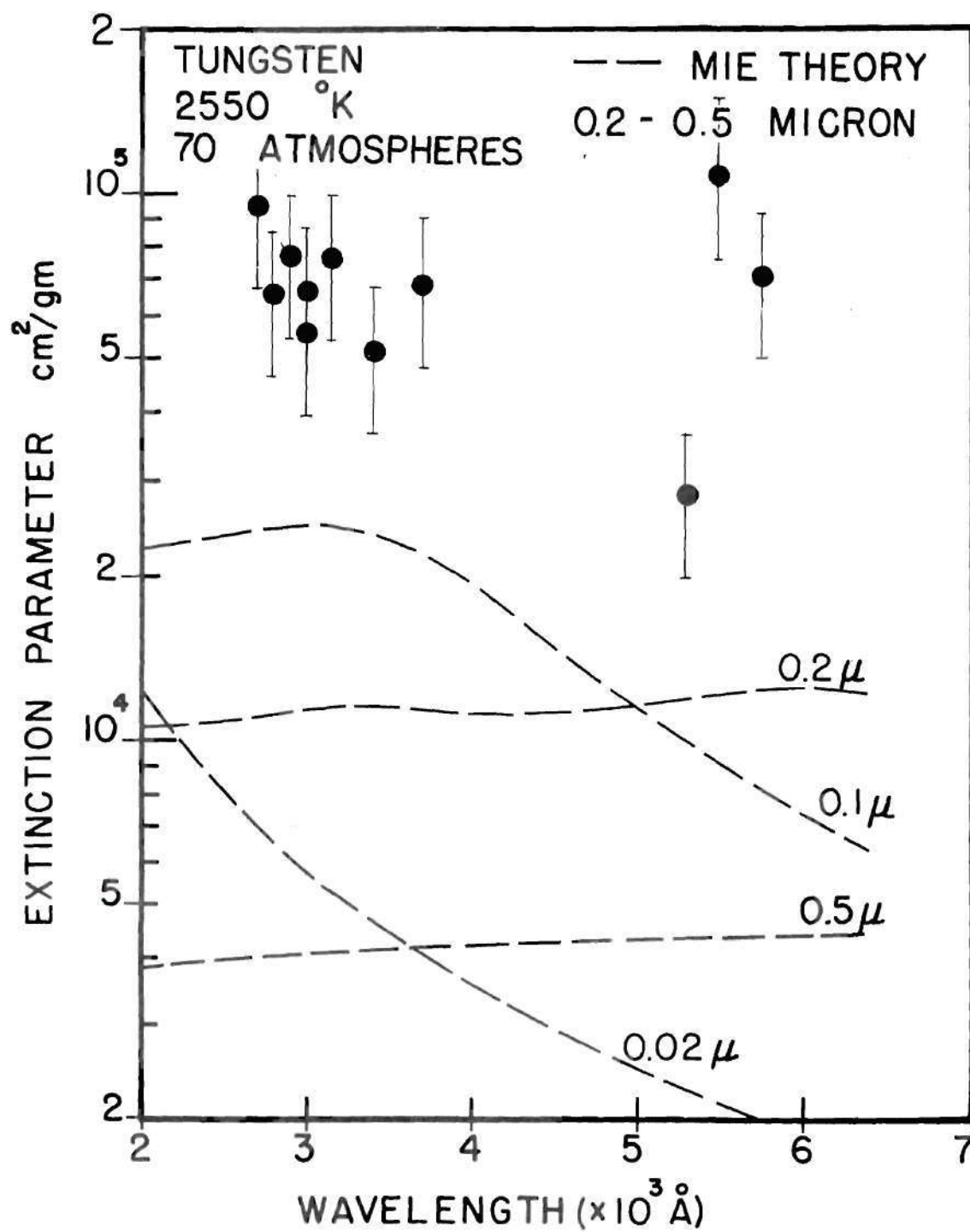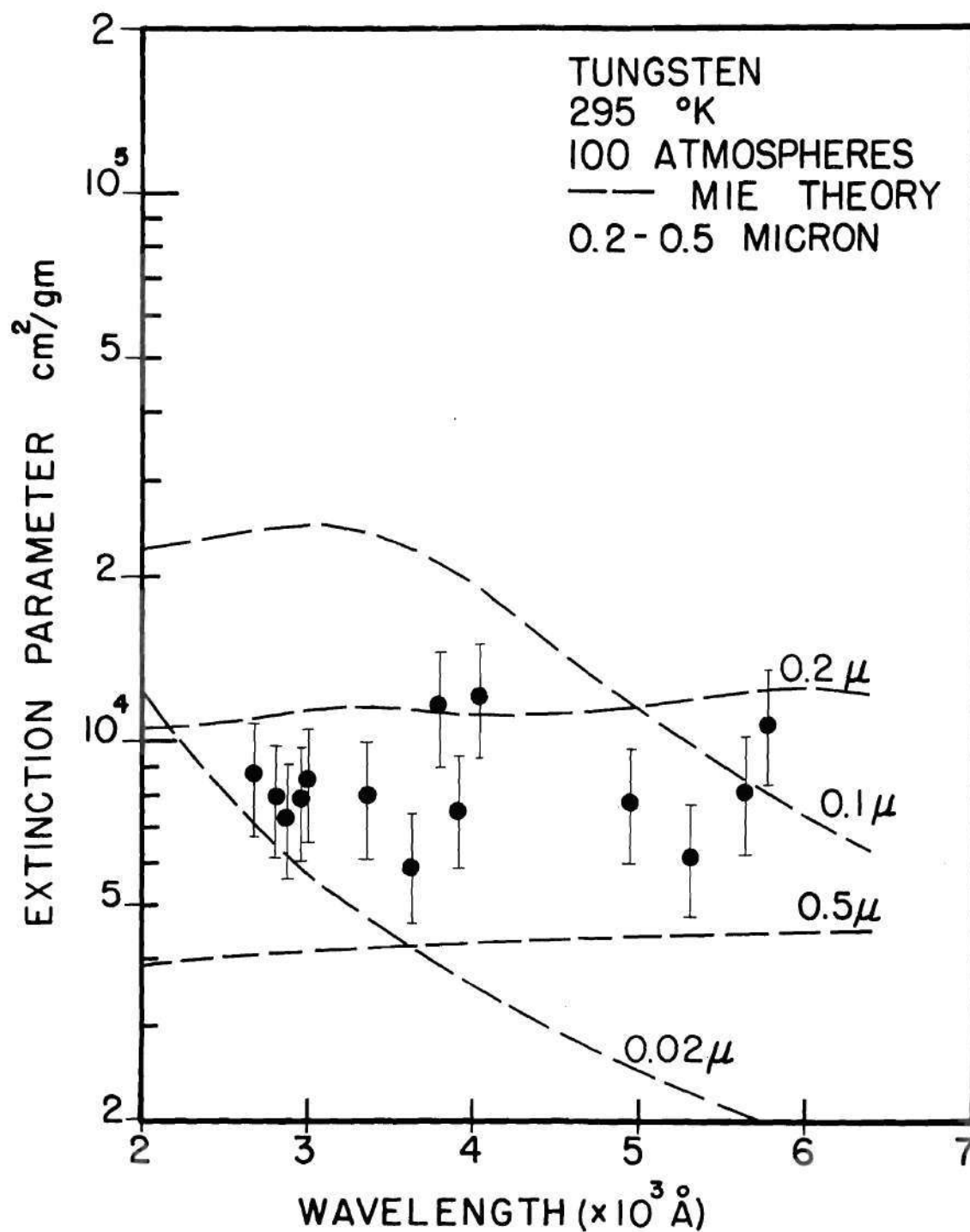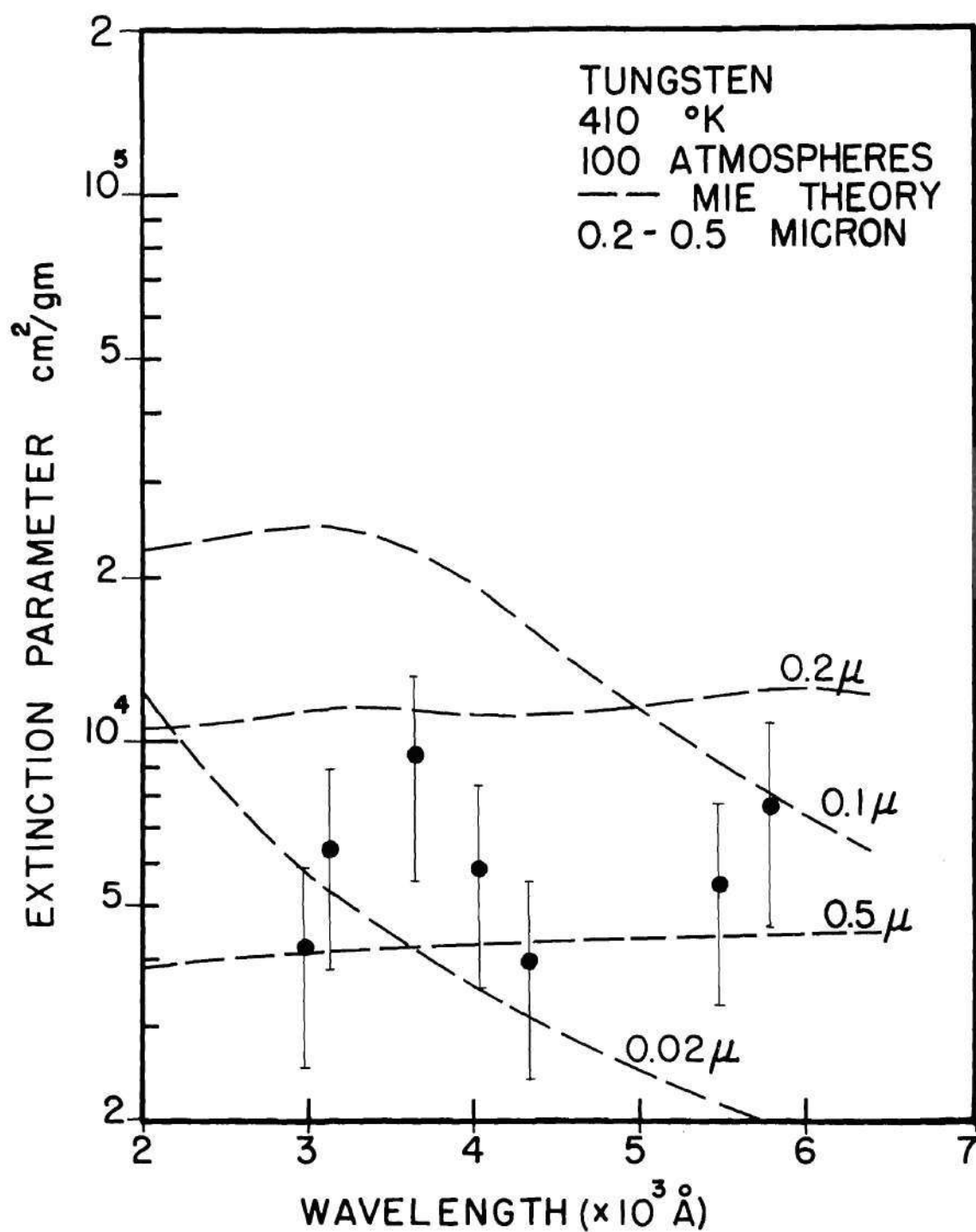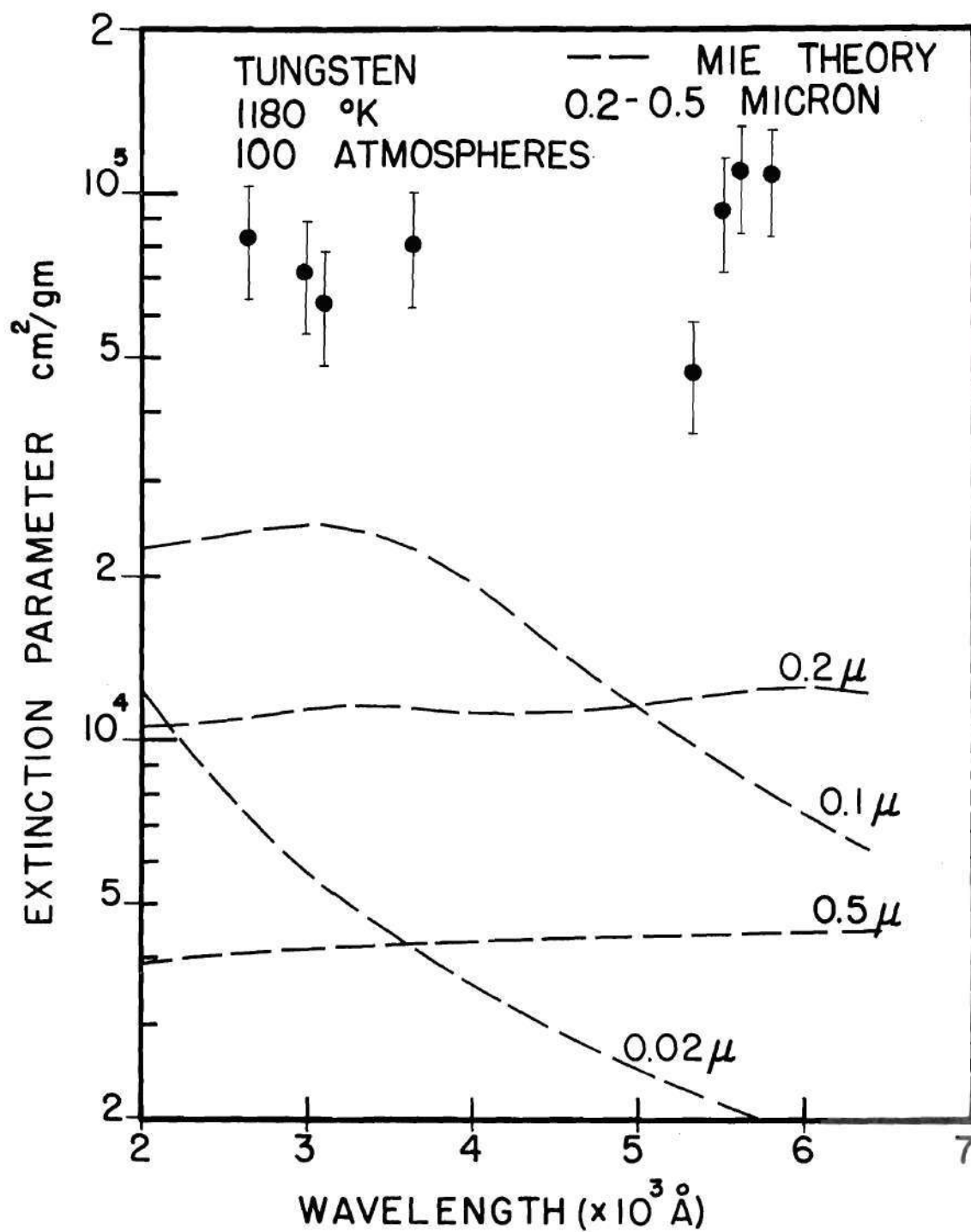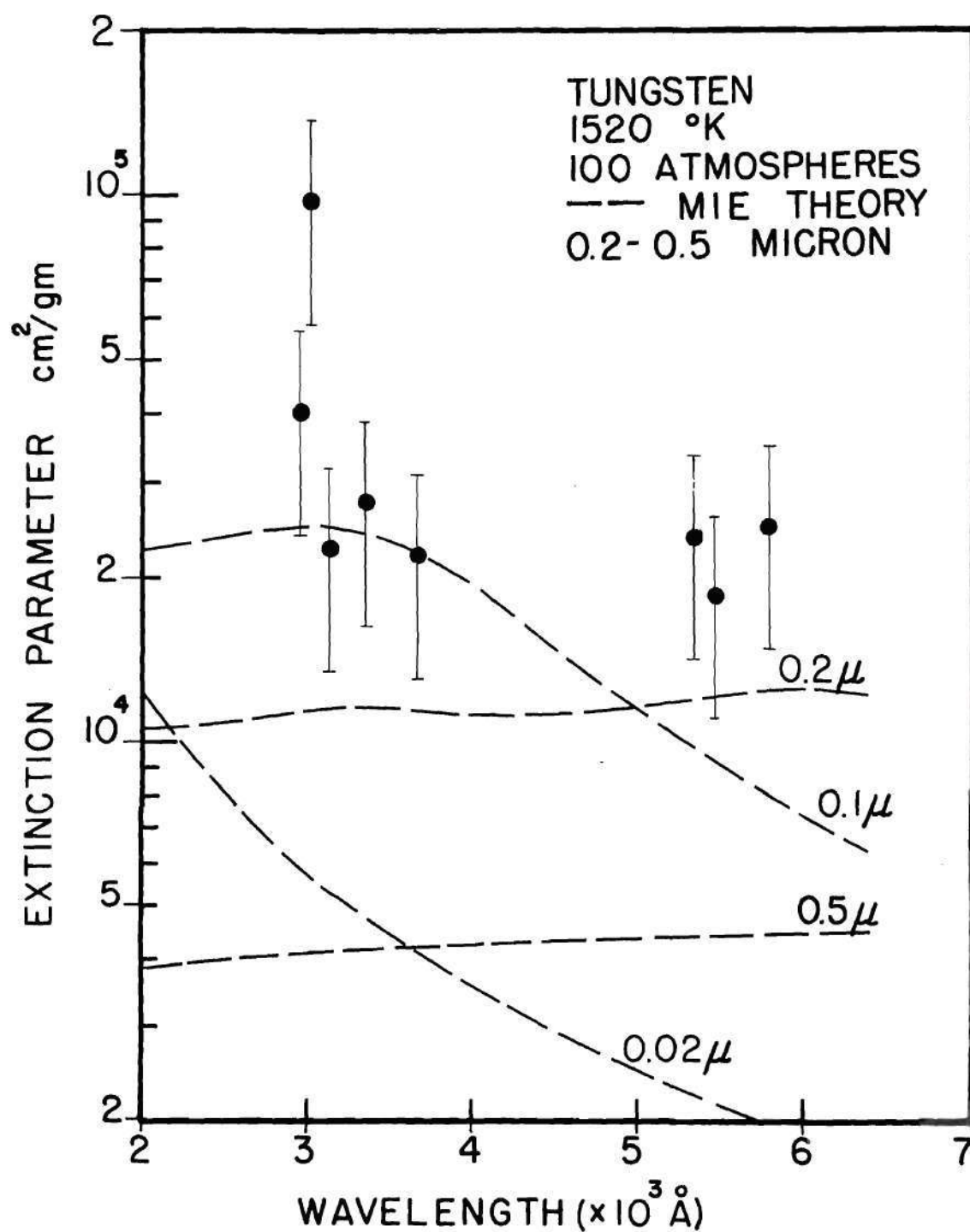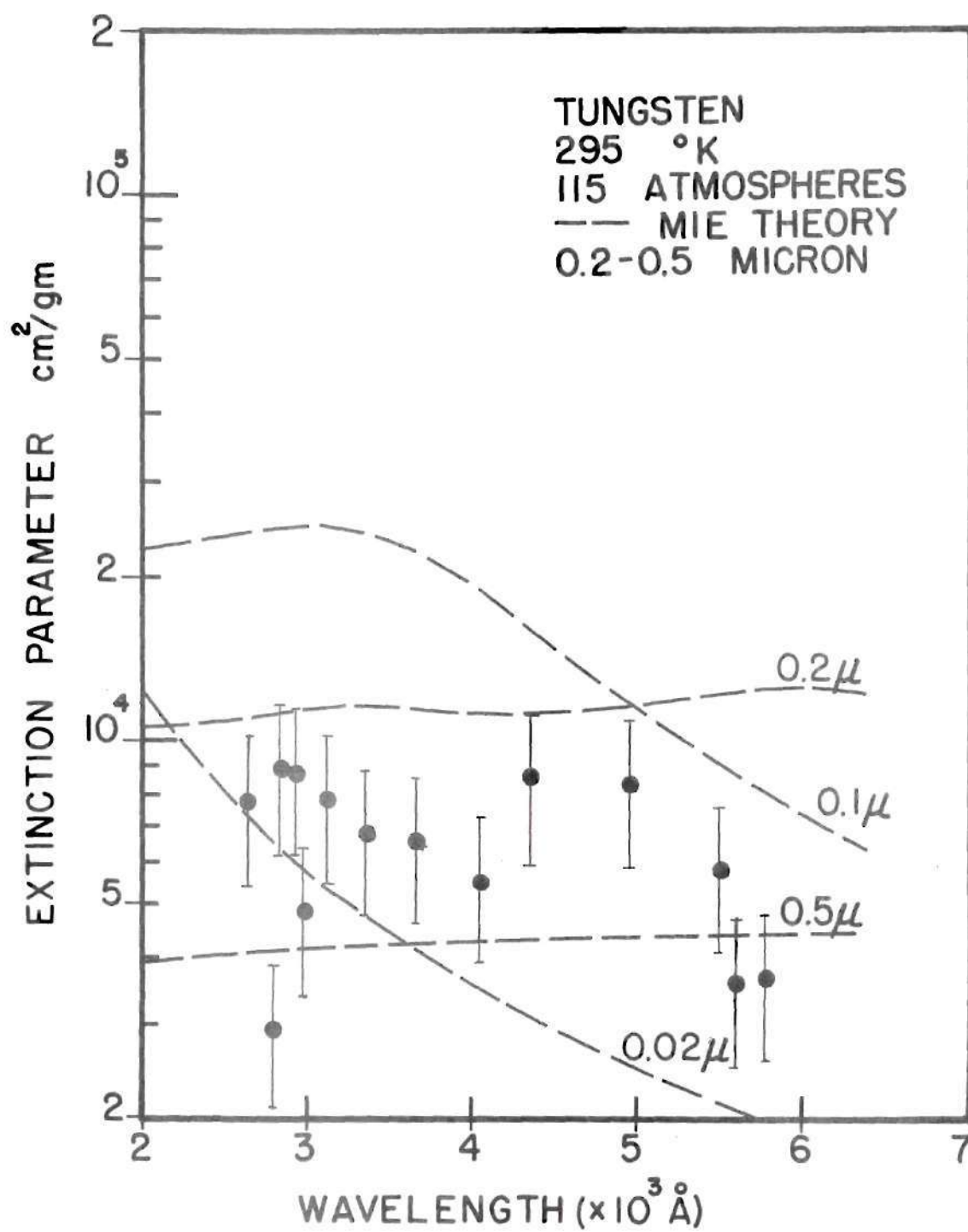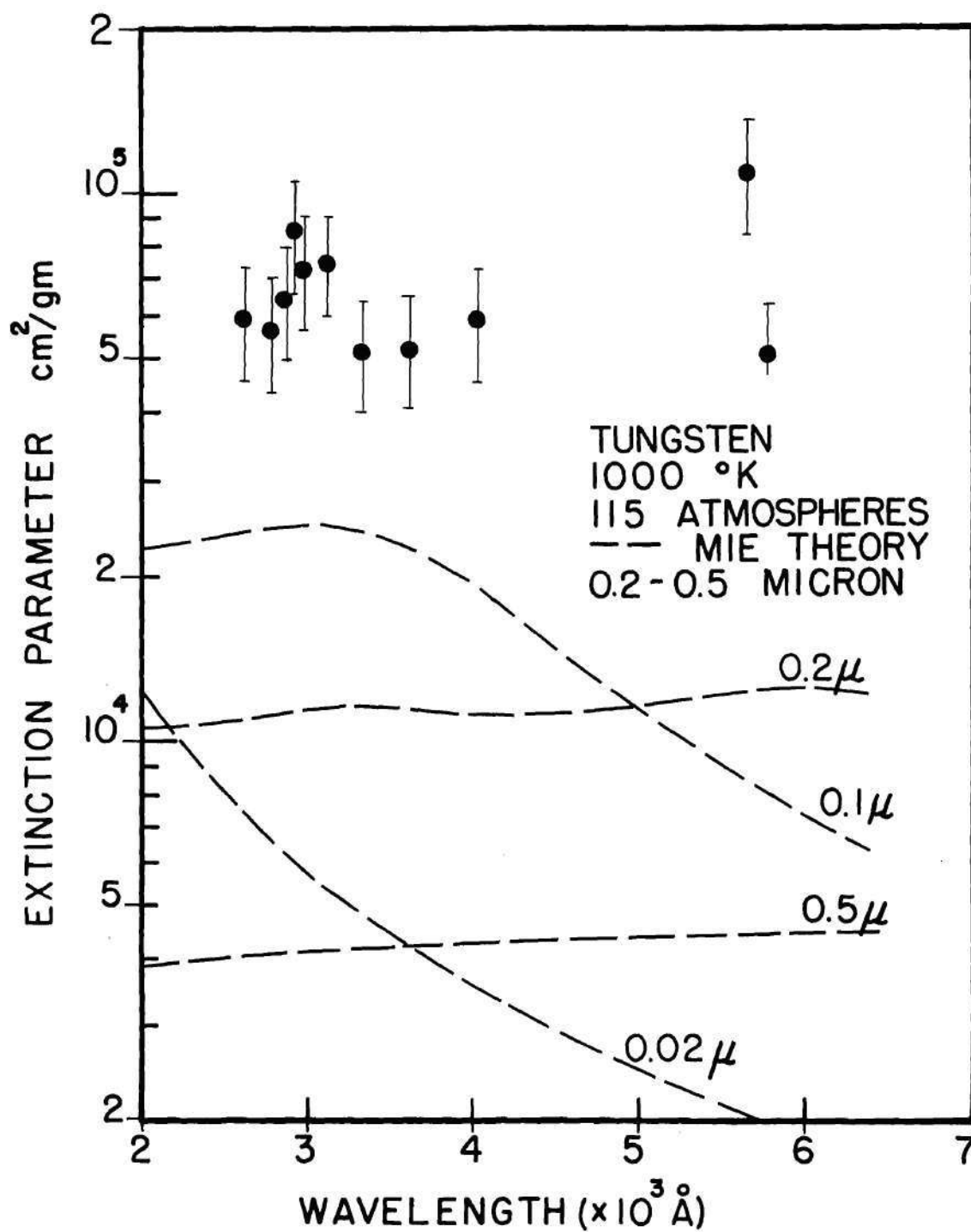
Figure 37. Extinction Parameter of Tungsten-Hydrogen Aerosol at 1000°K and 115 Atmospheres
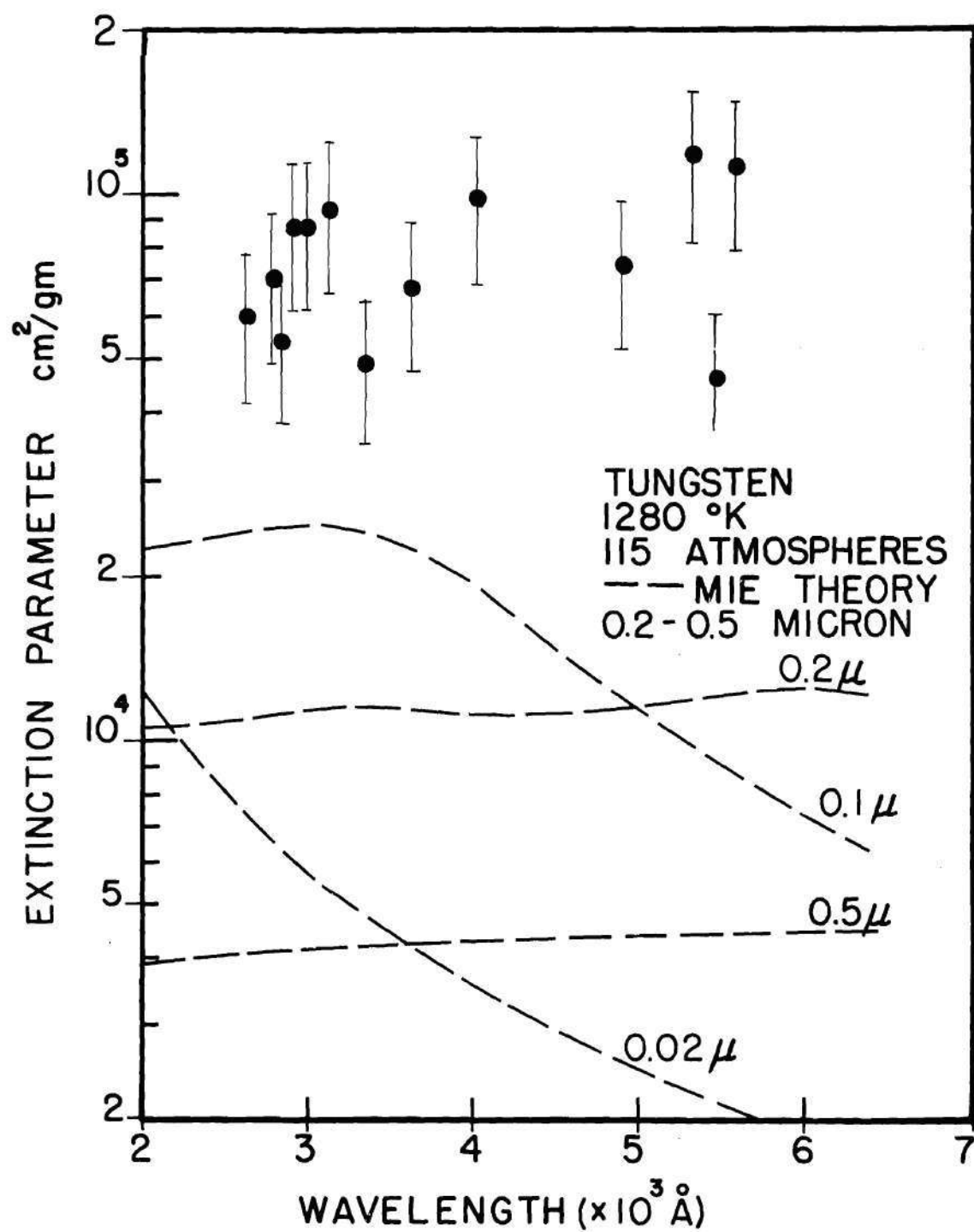
Figure 38. Extinction Parameter of Tungsten-Hydrogen Aerosol at 1280°K and 115 Atmospheres

room temperature extinction parameter at high pressures is about 8,000 cm^2/gm. This is approximately two-fifths the value obtained for the nozzle-dispersed aerosols measured at one and 12 atmospheres. An examination of the electron micrographs of Figure 18 indicates that the average particle diameter for well-dispersed aerosols is approximately 2.5 times smaller than for aerosols formed without using a dispersion nozzle. This is significant in that the room temperature values of the extinction parameter of the well-dispersed aerosols are about 2.5 times greater than for the less-dispersed aerosols, as is predicted by the Mie theory (Figure 5). Since the difference in room temperature extinction parameter data at low and high pressures can be accounted for by the change in the average particle diameter, there is no observed pressure dependence of the extinction parameter at room temperature.

Examination of Figures 25-38 indicates that there is a slight wavelength dependence in that the values for the extinction parameter are generally higher in the ultraviolet region than in the green to yellow portion of the spectrum. In order to examine the dependence, the spectrum over which the measurements were made, 2500 Å to 5800 Å, was divided into three sections and the extinction parameter values for the individual wavelengths in each section were averaged. The three sections were chosen as follows: 2500 Å to 4000 Å (ultraviolet), 4000 Å to 4912 Å (blue and violet), and 4912 Å to 5850 Å (green and yellow). The average values obtained were plotted as a function of temperature for different pressure regimes in Figures 39-44. The wavelength dependence is apparent since the ultraviolet and blue-violet averaged values are usually higher

Figure 39. Spectrum Averaged Values of the Extinction Parameters for Tungsten-Hydrogen Aerosols at 1 Atmosphere (Data from Reference 12)

Figure 40. Spectrum Averaged Values of the Extinction Parameters
for Tungsten-Hydrogen Aerosols at 12.5 Atmospheres

Figure 41. Spectrum Averaged Values of the Extinction Parameters
for Tungsten-Hydrogen Aerosols at 42 and 47 Atmospheres

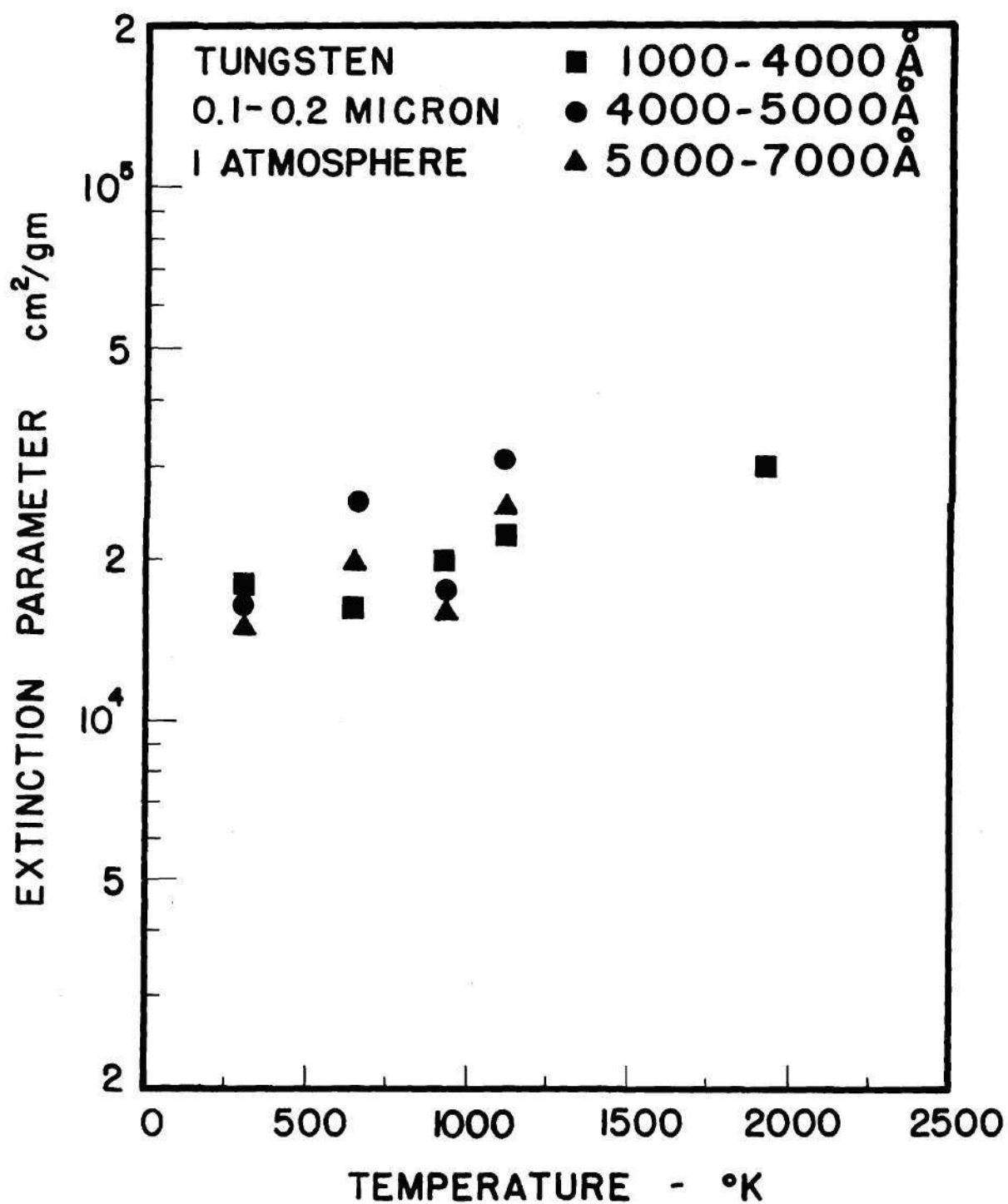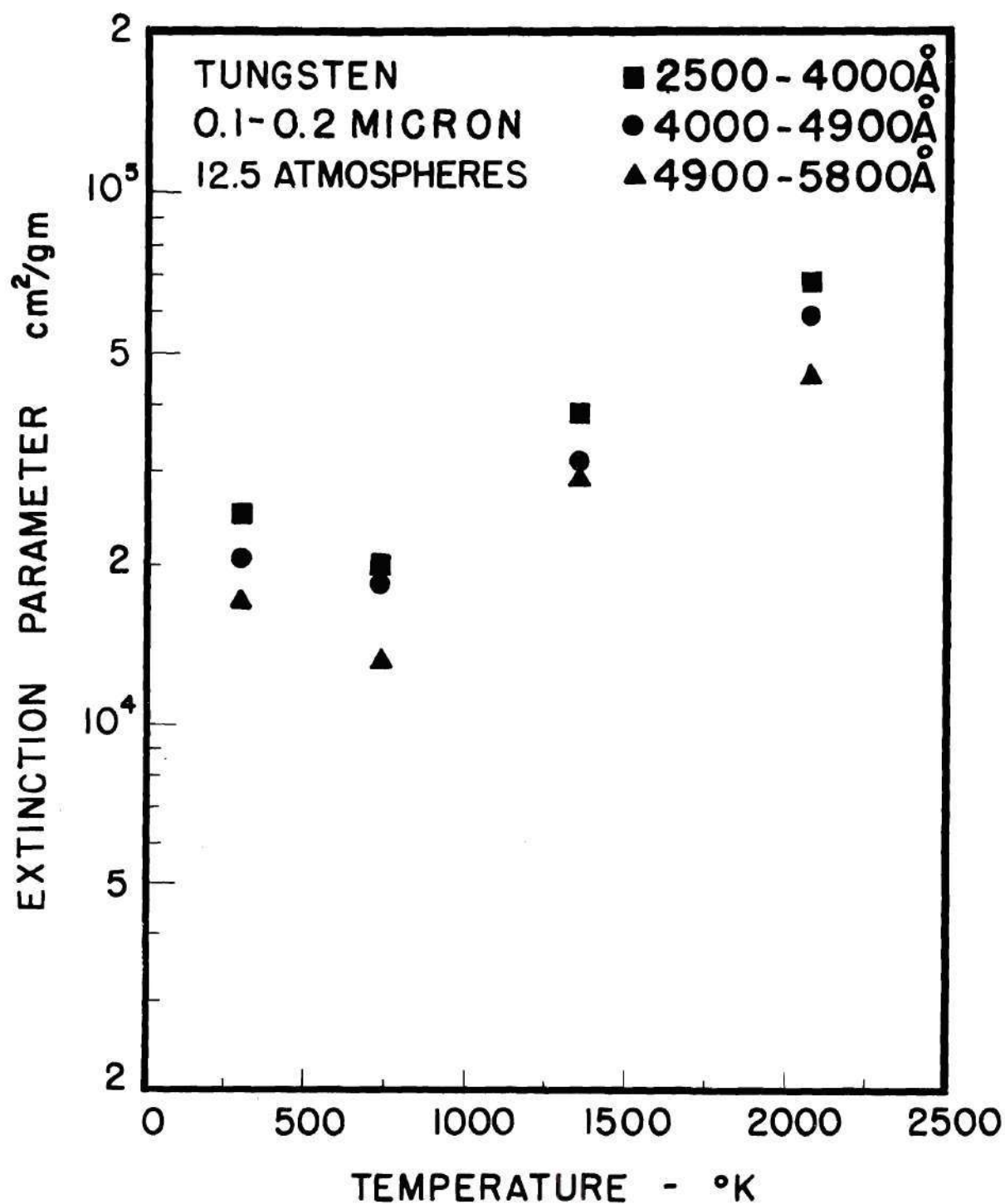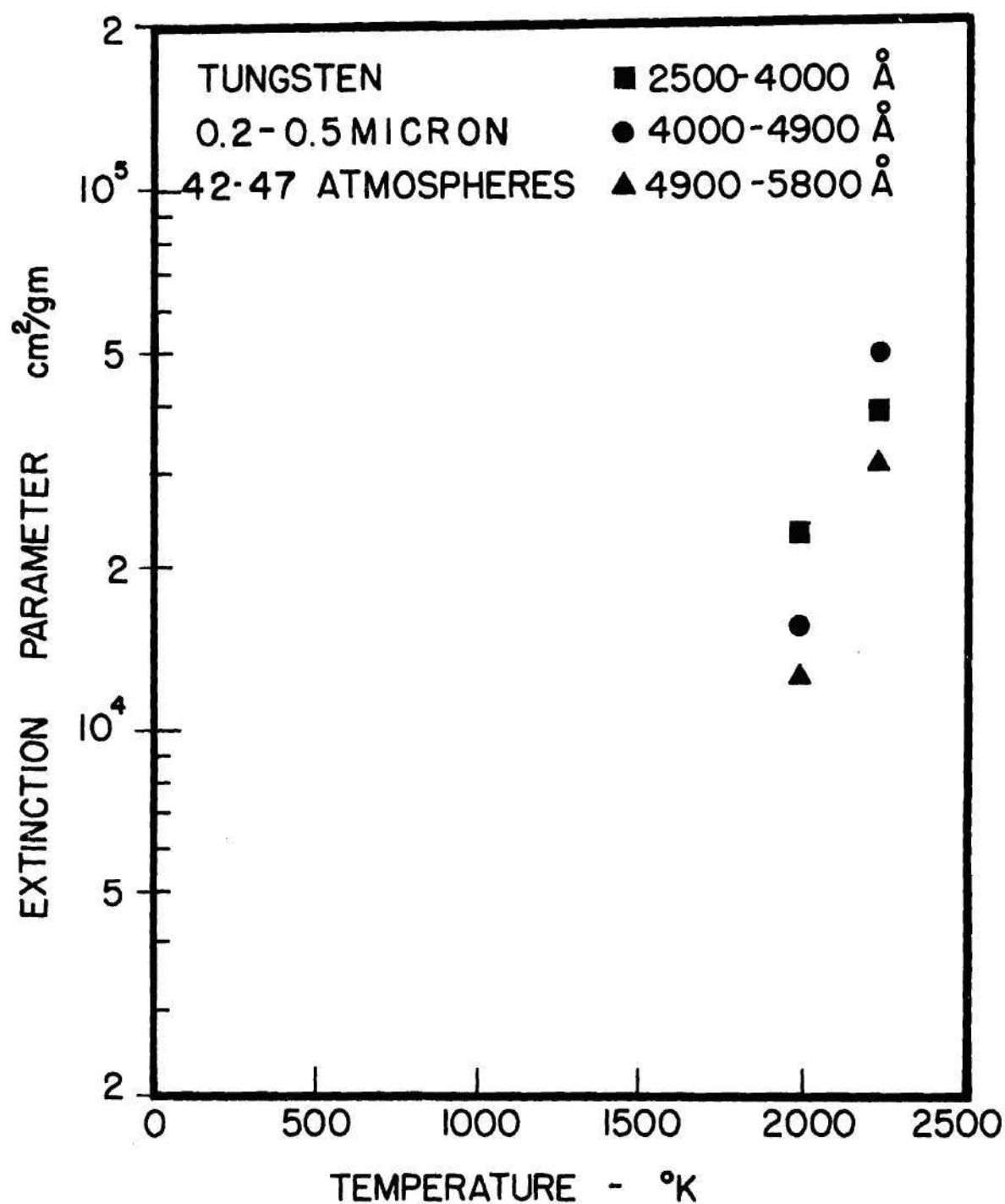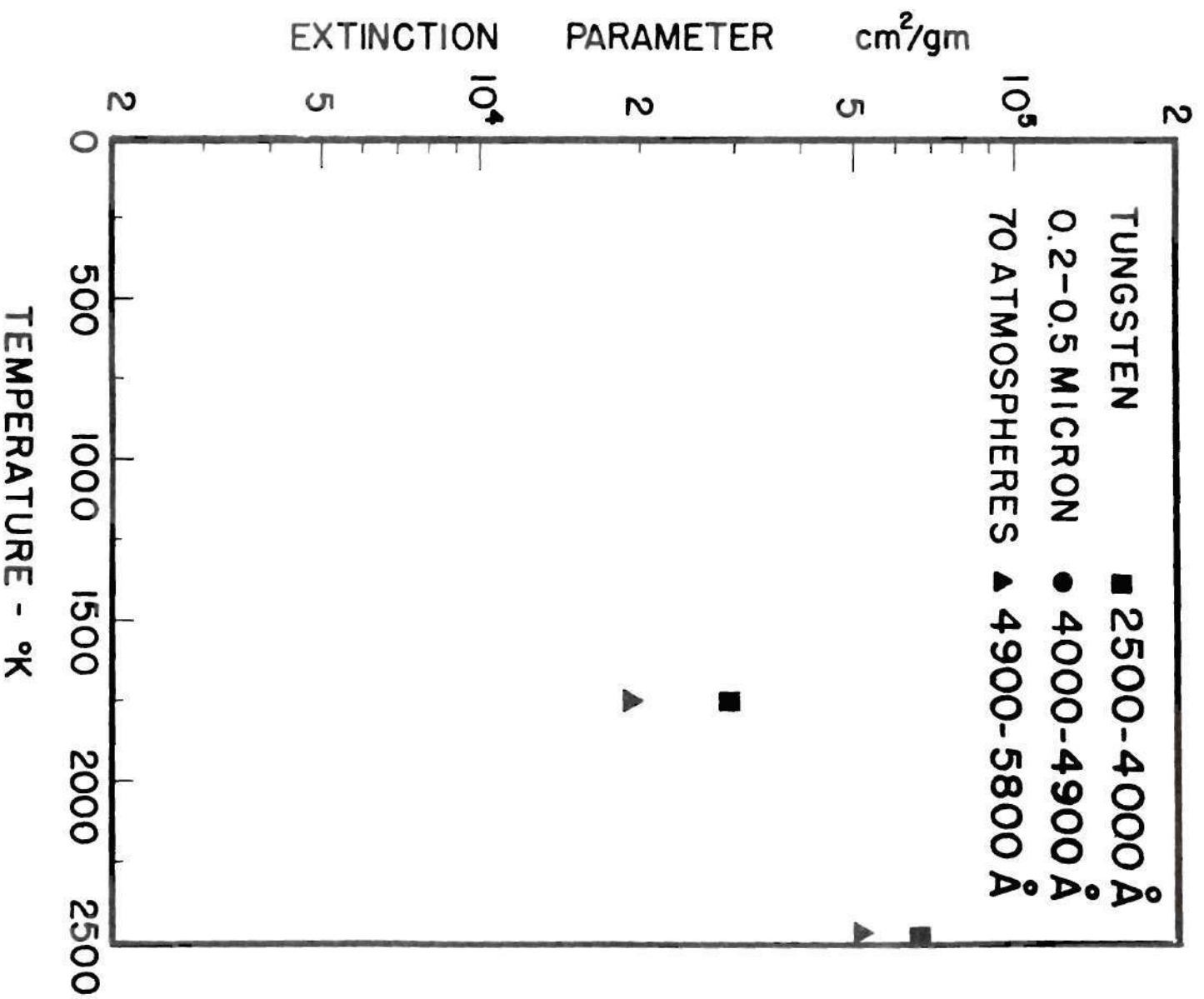Figure 42. Spectrum Averaged Values of the Extinction Parameters for Tungsten-Hydrogen Aerosols at 70 Atmospheres
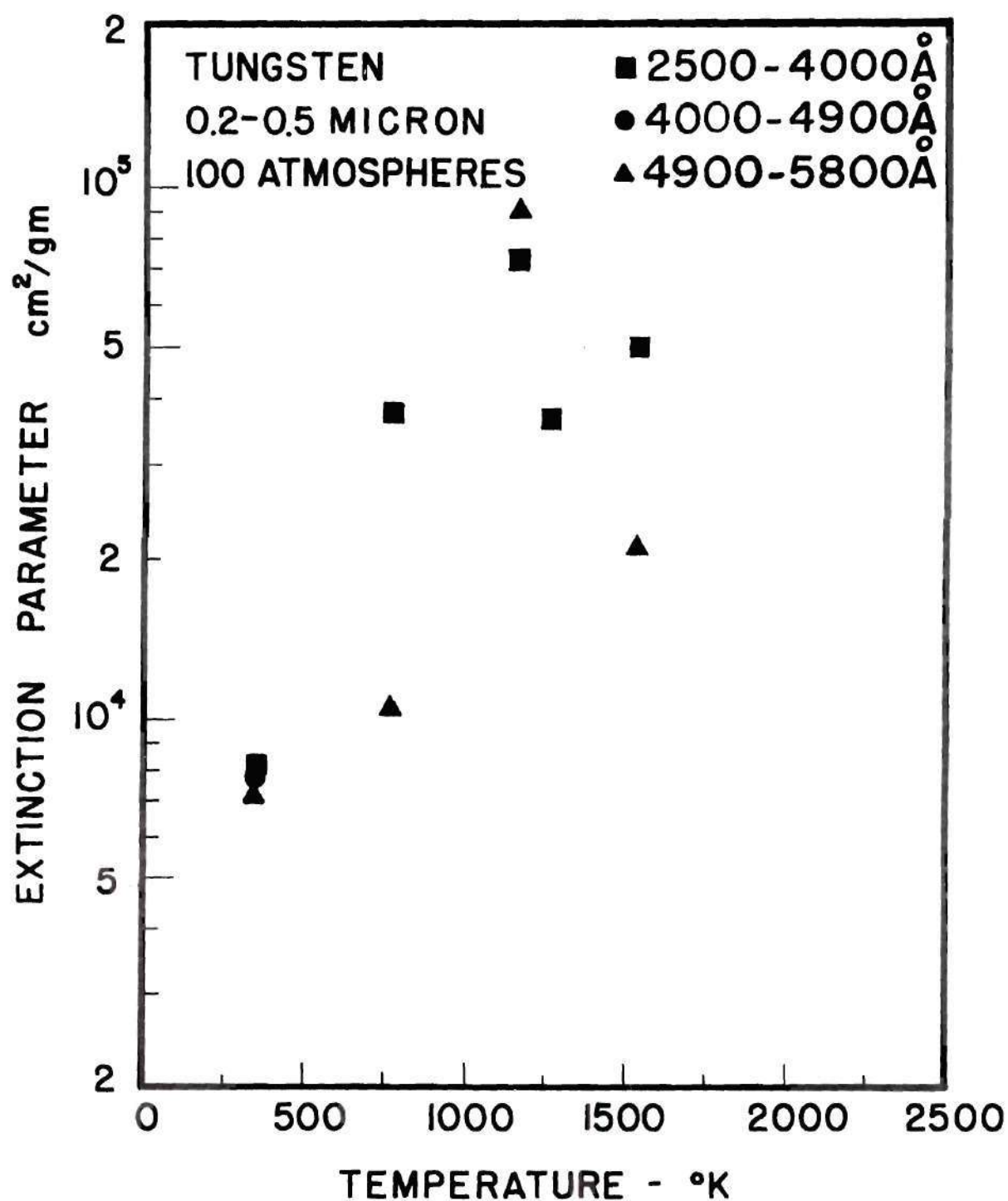
Figure 43. Spectrum Averaged Values of the Extinction Parameters for Tungsten-Hydrogen Aerosols at 100 Atmospheres
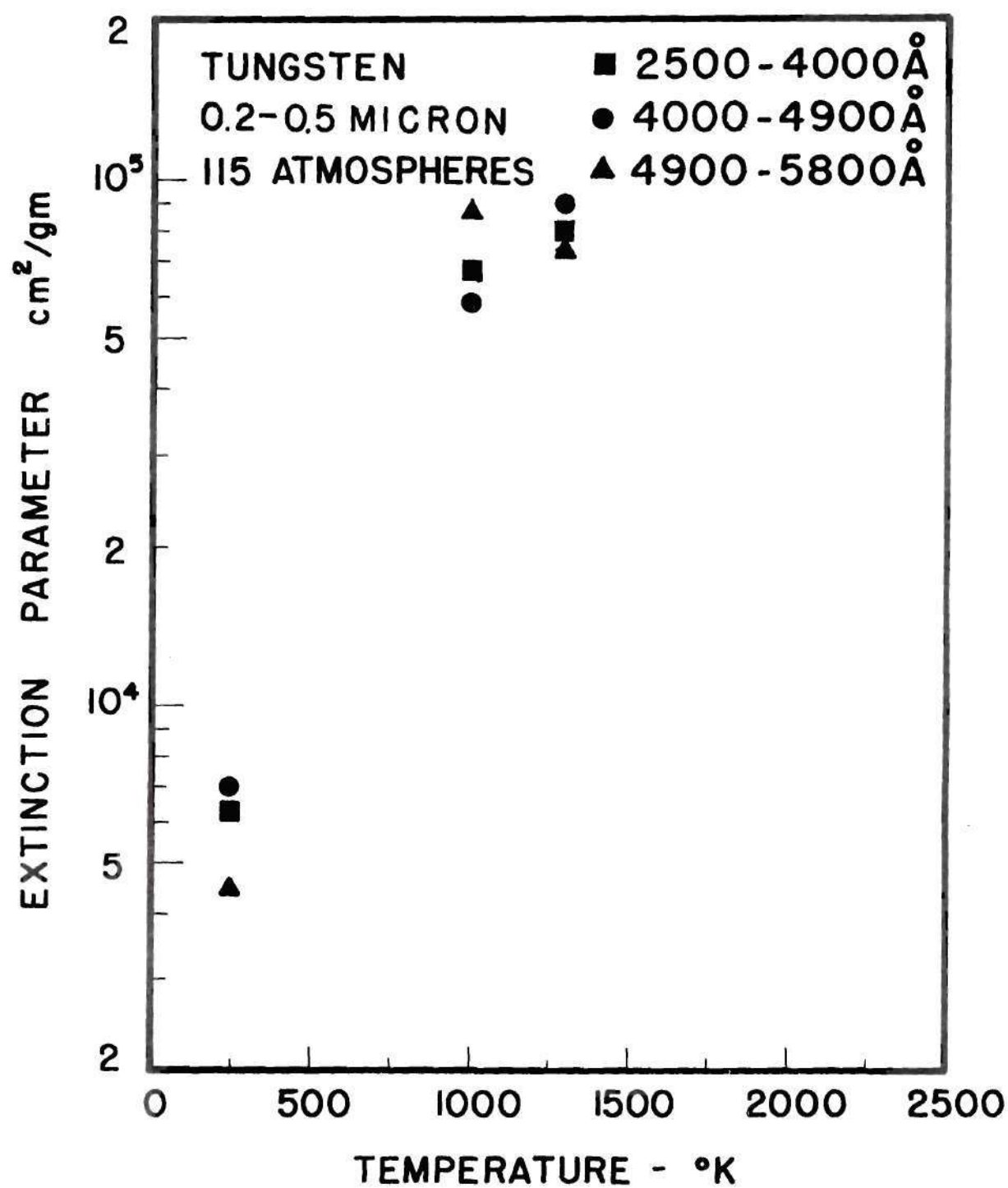
Figure 44. Spectrum Averaged Values of the Extinction Parameters for Tungsten-Hydrogen Aerosols at 115 Atmospheres

than the green-yellow averaged values.

Other trends become apparent in the data plots of Figures 39-44. The values of the extinction parameter increase with temperature and the rate of increase appears to be pressure dependent. Figure 39 is a temperature dependent plot of spectrum averaged data for one atmosphere aerosol taken from experimental measurements by Shenoy.[12] He concluded that the tungsten-hydrogen aerosol was not temperature dependent since the variation in magnitude of the extinction parameter as a function of temperature only slightly exceeded the estimated error associated with the measurements. Reviewing the one atmosphere data of tungsten-hydrogen aerosols for a correlation with the high pressure, high temperature data, a slight increase with temperature can be observed.

The rate at which the extinction parameter increases with temperature becomes larger as the pressure increases as shown in Figures 39-44. The extinction parameter at room temperature is about 2.5 times smaller at 40 to 115 atmospheres than it is at one and 12.5 atmospheres. This difference is explained in the previous section as being the result of the decreased tungsten particle size when the dispersion nozzle is used at the lower pressures. As the temperature of the high pressure aerosol approaches $1000°K$ a significant increase in the extinction parameter is observed and at 100 atmospheres and $1400°K$ the extinction parameter has increased approximately an order of magnitude over its value at room temperature. A potential explanation for this phenomenon is a reduction in the size of the agglomerated particles. It is probable that agglomerated particles could receive enough energy from particle-to-particle and gas-to-particle collisions to cause partial fragmentation. Inspection of

the tungsten particles in the electron micrographs of Figure 18, indicates that the particles are really agglomerates which may consist of individual particles as small as 0.01 micron in diameter. However, the optimum particle size for the radiant energy used in the experiment is between 0.1 and 0.2 micron diameter. The Mie theory predicts that a further reduction in the particle size would result in a decrease in the extinction parameter (the theoretical extinction parameter for a 0.02 micron diameter tungsten particle at 2400 Å wavelength is 10,000 cm^2/gm--see Figure 5).

Even if the optimum particle size were being formed, there still exists a factor of four increase in the extinction parameter that is not explained by the Mie theory.

Cory and Bennett[82] observed a decrease in the light transmitted through a refractory particle cloud at high temperatures and moderate pressures. The decrease in transmitted light was more significant as the pressure was raised. Their experiment consisted of heating a tantalum carbide-hydrogen aerosol in a quartz tube by exposing the tube to the focused light from a xenon flashlamp. As a result, the temperatures and pressures obtained were very transient conditions, lasting a few milliseconds. Cory and Bennett suspected that thermionic emission from the particles produced a positively charged particle surrounded by a cloud of electrons that were trapped by the potential well of the positively charged particle. The increased absorption by this system was thought to be an inverse bremsstrahlung effect whereby the electrons could capture and emit photons by momentum exchange with the electric field. In order to verify the existence of the electrons they measured

the conductivity of the aerosol and found that it increased to approximately 20 mho/cm at the maximum flash power point.

The literature[83-85] cited by Cory and Bennett does not provide a conclusive description of this process. The concept of inverse bremsstrahlung was used by Visvanathan[83] in describing free carrier absorption in semiconductors. The description of the electron cloud generated by thermionic emission and held in place by the resultant positive charge on a particle is given by Soo.[84] He describes some assumptions that are required before the electron cloud model can be established. First is the consideration of a single particle in a finite volume in order to equate the thermionic current density to the current density of electrons in the cavity. Second, the gas in the cavity is considered only in regard to its first ionizational potential and not with respect to the effects of gas molecule-particle collisions. Soo also states that as much as 80 percent of the potential bound electrons can be set free by turbulence in the gas, indicating that a hot aerosol of metallic particles may have a significant conductivity as shown by Cory and Bennett.[82]

Calculations were made to predict the increase in the extinction parameter due to free electrons. It was found that the effective work function for submicron-sized tungsten particles would probably have to be smaller than the 4.5 eV work function of large tungsten pieces before a significant number of electrons would be produced by thermionic emission at 1000°K to 2000°K. Even after enough electrons are present in the aerosol to increase the conductivity, the calculation of the increase in extinction parameter showed that the cross section for a free electron[85] (6.65×10^{-25} cm^2) is too small to be significant in the overall

extinction process.

A closer consideration of the particle-gas system at high temperature and pressure indicates that the concept of a free electron in the system may not be valid. The following parameters apply to an aerosol of 5×10^{-6} gm/cm^3 density formed from 0.1 micron diameter tungsten particles dispersed in 100 atmosphere hydrogen at 1000°K:

Particle diameter	0.1 micron
Particle surface area	3.14×10^{-10} cm^2
Density of particles in aerosol	4.9×10^8 particles/cm^3
Mean distance between particles	12.6 microns
Density of H$_2$ molecules	0.8×10^{21} molecules/cm^3
Mean distance between molecules	1.1×10^{-3} microns
Mean free path of H$_2$ molecules	2.36×10^{-3} microns
Collision frequency between H$_2$ and particle	1.85×10^{16} collisions/sec-particle
Average translational energy of H$_2$ molecule	0.129 eV

The hydrogen gas at 100 atmospheres and 1000°K is approximately 0.04 the density of liquid hydrogen. It may be possible for the free electrons *in the gas to form a radiant energy* absorption system with one or more hydrogen molecules under these conditions. There may be an even greater tendency for a molecule-electron unit to form if there is a high density of electrons surrounding a charged particle. Any absorption or scattering interactions of a photon with a molecule-electron system would tend to be pressure dependent.

Another process by which the extinction parameter could be expected to increase with temperature and pressure is the pressure induced broaden-

ing of tungsten spectral lines. Krascella[86] has calculated the Rosseland mean opacity for tungsten vapor as a function of temperature and pressure. This process would probably not be applicable unless it could be shown that a significant amount of tungsten atoms exists in the aerosol at moderate temperatures (below the vaporization temperature).

More information describing the tungsten-hydrogen aerosol at high pressure and temperature may be necessary before a particular photon absorption-scattering process can be cited with confidence. Knowledge of the electron density and electron distribution would permit a first order analytical study. The extension of the measurement of the extinction parameter to higher temperatures may also provide information that will indicate the predominance of one extinction process over the other possibilities.

Range of Operating Conditions

The experiment was originally designed with the objective of measuring the extinction parameter for refractory metal aerosols under pressures to 100 atmospheres and temperatures to 2800°K. Measurements of the extinction parameter were actually made at pressures to 115 atmospheres and temperatures to 2500°K. The limiting factors in reaching higher pressures were the regulator and the supply tank pressure.

Operation at temperatures higher than 2500°K was difficult for several reasons. At lower pressures the relatively poor heat transfer from the tungsten heating element to the hydrogen resulted in hot spots about two inches below the tip of the heating element. Radiation occurred from the tip of the heating element out the end of the boron

nitride heating tube. The tube itself was hot enough to prevent effective radiation from the tungsten heating strip along its sides. Therefore, the tip was cooler due to the heat lost by radiation than the sides of the heating strip. Melting at these hot spots occurred before the gas could be heated higher than $2500°K$. At the higher pressure the heat transfer appeared much better due to the greater heat capacity (per unit volume) of the hydrogen and the heating elements tended to burn out nearly at the tip. This indicated more uniform heating along the length of the tungsten heater strip. Higher operating temperatures were obtained at high pressures but the period of operation had to be limited. The higher heat capacity of the gas at high pressure increased the amount of heat transferred to the pressure vessel walls. At low pressures the main cooling coil and upper cooling coil could protect the pressure vessel wall from the intense heat but the cooling coil geometry and capacity were not sufficient for this purpose at the higher pressure. In order to operate at temperatures of $2000°K$ and higher it was necessary to heat up rapidly and make the measurements within a period of about 10 minutes to prevent the pressure vessel from overheating.

A further disadvantage of operating at high temperature was the increased probability of melting the tungsten heating element and incurring the one to two day replacement delay.

The thermocouple was enclosed in a 0.1 inch diameter boron nitride sheath to prevent tungsten particles from shorting out the wires leading to the junction. The difference between the thermocouple sheath temperature and the gas temperature due to conduction and radiation from the sheath was accounted for by using the following correlation[87,88] for

flow around cylinders

$$\frac{hD}{k}\,(P_r)^{-0.3} = 0.35 + 0.56\left(\frac{DG}{\mu}\right)^{0.52}$$

where h is the heat transfer coefficient in $BTU/(hr \cdot ft^2 \cdot {}^\circ F)$, D is the diameter of the cylinder in feet, k is the thermal conductivity of the gas in $BTU/(hr \cdot ft \cdot {}^\circ F)$, P_r is the Prandtl number, G is the mass flow rate in $lb_m/(ft^2 \cdot hr)$, and μ is the viscosity in $lb_m/hr \cdot ft$. This correlation has been shown to be valid for a number of liquids and gases provided that DG/μ is between 1 and 1000. For this work the value of this parameter varied from 32 to 146. The heat flux radiated from the sheath, q_r'', was calculated using an effective surrounding wall temperature equal to 75 percent of the sheath temperature, above room temperature. Observations of the interior of the heating chamber using an optical pyrometer and a consideration of the view factors related to the thermocouple location indicate that this figure is between 70 and 80 percent, so 75 percent was used. The heat (per unit surface area) conducted through the sheath to the wall, q_c'', was calculated using temperature dependent conductivity data from reference 89. Having calculated h, q_c'', and q_r'', the difference between the hydrogen and sheath temperature is given by $(q_r'' + q_c'')/h$. This difference is less than $54^\circ K$ for thermocouple sheath temperatures below $1000^\circ K$, but rises rapidly above $1000^\circ K$ due to radiation loses to $477^\circ K$ at $2000^\circ K$.

During the course of this research aerosols using carbon, silicon, silicon carbide, and tungsten carbide in hydrogen were investigated

in addition to the tungsten-hydrogen aerosol. The objective was to make exploratory investigations of the extinction parameters of these various aerosols at high pressures and high temperatures. No data were obtained at high pressures with carbon. However silicon, silicon carbide, and tungsten carbide aerosols were measured and values for the extinction parameter of between 60,000 cm^2/gm and 100,000 cm^2/gm were obtained. The data for tungsten carbide had a positive temperature dependence. The limited data for silicon and silicon carbide did not demonstrate a conclusive temperature trend.

The silicon, silicon carbide, and tungsten carbide aerosol data are not presented since the accuracy of the data was not very good. Also, the scope of operating conditions was very limited. The data values given are for guidelines to further research only and not proposed as useful engineering measurements.

CHAPTER VII

CONCLUSIONS AND RECOMMENDATIONS

Conclusions

A well-dispersed tungsten-hydrogen aerosol at room temperature was shown to have a spectrum averaged extinction parameter of approximately 20,000 cm^2/gm. Electron micrographs of this aerosol showed the average diameter of the tungsten particle agglomerates to be approximately 0.1 to 0.2 micron. In order to achieve this degree of dispersion the aerosol must be passed through a nozzle after mechanical agitation has mixed the tungsten agglomerates with the hydrogen carrier gas.

Since it was difficult to use a nozzle in the aerosol inlet tube at high pressures, the aerosol was formed by mechanical agitation only. The average diameter of the tungsten particle agglomerates formed by this method was about 0.2 to 0.5 micron. A spectrum averaged extinction parameter of approximately 8,000 cm^2/gm was measured for room temperature, high pressure aerosol. The reduction in the extinction parameter at high pressures and room temperature was the result of the larger particle diameter as predicted by Mie theory.

A plot of spectrum averaged extinction parameters as a function of temperature for aerosols at constant pressure showed an increase of the extinction parameter with temperature at temperatures above $1000°K$. The rate at which the extinction parameter increased became larger as

the pressure of the aerosol increased. A spectrum averaged extinction value of approximately 80,000 cm^2/gm was measured for tungsten-hydrogen aerosol at 100 atmospheres and 1520°K.

Partial deagglomeration of the tungsten particles can only account for about one fourth the increase in extinction parameter. Physical processes which have been considered as possible explanations for this phenomenon are the formation of an electron cloud around a thermionically emitting particle[82,84] (photon absorption by inverse bremsstrahlung[83]), the interaction of photons with an electron associated with one or more H_2 molecules, and pressure induced broadening of tungsten atom spectral lines.[86] The complexity of the aerosol system prevents any particular process from being cited as a dominant factor in the pressure and temperature dependent extinction parameter. The photon scattering by free electrons alone has been discounted as a possible explanation for the increase in extinction parameter with temperature and pressure. More information is needed on the electron density and electron distribution in order to make an analytical study of the relative importance of each photon interaction process. The measurement of extinction parameters at higher temperatures than reported in this work may provide useful insight into the nature of the process responsible for a pressure and temperature dependent extinction parameter.

The heat transfer in the gas core nuclear rocket concept will probably be enhanced by the pressure and temperature trends in these data. Since the extinction parameter represents the sum of absorption and scattering processes, it is not apparent whether the increase in the extinction parameter is due to an increase in only one, or, both processes.

An increase in either process will tend to reduce the percentage of seed material required in the propellant, but to different degrees.

The seeded aerosol in the actual gas core reactor will exhibit an additional photon absorption process, photoemission, when exposed to the extremely intense photon field from the uranium core. The extremely high levels of ionizing radiation present in the reactor will also contribute to ionization in the propellant.

The values of the extinction parameter plotted as a function of incident radiation wavelength at various pressure and temperature operating conditions showed a slight wavelength dependence. When the spectrum (2500 Å to 5800 Å) was divided into three regions (ultraviolet, violet-blue, and yellow-green) the average value of the extinction parameter for ultraviolet was slightly higher than the average values for the violet-blue and yellow-green regions.

Recommendations

The complete solution of the radiant energy heat transfer equation requires the knowledge of the extinction parameter, the scattering parameter, and the scattering amplitude function. The data determined in this research will be much more meaningful and useful if the scattering parameter and the scattering amplitude function are experimentally determined as a function of temperature and pressure.

The range in aerosol pressure and temperature was restricted in this experiment. The pressure could be varied over two orders of magnitude but the temperature could only be increased by a factor of two over the temperature at which the temperature and pressure dependence

began to occur. It is not likely that significant increases in temperature can be achieved with tungsten heating-elements beyond the present limits. As a result, the use of radio frequency induction heating is recommended to extend the temperature range over which the extinction parameter for aerosols can be measured. This is essential since there is a region ($2000°K$ to $9000°K$) which is not covered adequately by either experimental measurements or theoretical calculations. Operation at these higher temperatures will permit more accurate determination of the temperature dependent values of the extinction parameter.

APPENDICES

APPENDIX A

EQUIPMENT OPERATING PROCEDURE

The procedure for making an experimental run is given sequentially below. An "experimental run" consists of collecting transmitted light intensities as a function of wavelength for a specific pressure and temperature.

1. Plug in the 220 VAC plug and the two 110 VAC plugs.

2. Open the exhaust fan duct leading outside the building.

3. Turn on the electrical system interlock components (exhaust fan, 28 VDC power supply, 28 VDC relay power, and effluent blower switch) and pull out scram button. The red light near the scram button will come on.

4. Press the reset button; the red light will go off and the green light will come on indicating that electrical power is available to all of the instrumentation.

5. Turn on the oscillograph, digital voltmeters, picoammeters, and photomultiplier power supplies.

6. Turn on the sampling vacuum pump and set the sampling switch to "off" and the evacuation switch to "on".

7. Turn on the hydrogen and nitrogen gas bottles in the gas storage area.

8. Turn on the nitrogen cutoff valve at the control panel and purge the aerosol generator and furnace.

9. Install pre-weighed filters in the aerosol density sampling

system and pressure test the sampling system.

    10.   Connect the aerosol density sampling manifold to the furnace.

    11.   Turn off the backpressure throttling valve and pressurize the furnace with nitrogen in order to check for leaks.

    12.   Turn on and calibrate the hydrogen leak detector.

    13.   Depressurize the furnace, cut off the nitrogen flow and turn on the hydrogen flow. Allow the hydrogen to purge the nitrogen from the furnace and aerosol generator.

    14.   Calibrate the digital voltmeters, oscillograph and picoammeters after they have warmed up for 15 minutes.

    15.   Turn on the light source cooling fan.

    16.   Turn on the light source power supply and start the mercury arc lamp.

    17.   Adjust the gain on the picoammeters and the high voltage to the photomultipliers in order to achieve an optimum oscillograph trace.

    18.   Sample the experimental area periodically with the hydrogen gas detector.

    19.   Turn on the cooling water to the furnace.

    20.   Turn on the grating drive motor and start the spectrum scan. Determine from the trace the optimum amplification of the wavelength dependent signal.

    21.   Pressurize the furnace with hydrogen to the desired operating pressure. Check for leaks with bubble solution.

    22.   Adjust the backpressure throttling valve to give a small hydrogen flow through the furnace while it is being heated to the operating temperature.

23. Close the sight port flow valve and read the pressure drop across the main flow throttling valve. Adjust the main flow throttling valve to give approximately a three psi pressure differential.

24. Open the sight port flow valve until the pressure transducer across the main flow throttling valve decreases a fraction of a psi. This indicates the presence of sight port flow.

25. Turn on 220 VAC 3∅ power to Variac.

26. Increase Variac output to the 20 kW furnace power supply slowly as the temperature in the furnace rises to the desired operating temperature.

27. Open the desired filter valve on the aerosol density sampling manifold. Open the furnace-sampling isolation valve slowly. This allows high pressure gas to fill the line up to the sampling solenoid valve. Check for gas leaks with bubble solution.

28. Increase the main hydrogen flow rate to the predetermined value for the operating pressure. Readjust sight port flow if necessary.

29. Read the pressure in the sampled volume tanks from the manometers.

30. Turn off aerosol sampling system evacuation switch.

31. Start the grating drive motor. A green light on the control panel indicates the forward scan.

32. When the green light goes off and the adjacent red light comes on the reverse scan has started. Change the amplification of the wavelength dependent signal by a factor of ten.

33. After the "before" scan, divert the hydrogen flow from the bypass line to the aerosol generator. There are two valves located at

the control panel for this purpose.

34. Increase the voltage to the aerosol generator slowly until the desired speed is obtained.

35. Watch the intensity of the amplified signal from photo-multiplier 2. When the intensity decreases aerosol has reached the furnace.

36. Upon an indication of aerosol, start the grating drive motor and turn on the sampling switch simultaneously.

37. Change amplifications of the wavelength dependent signal when the reverse scan begins.

38. When the reverse scan ends turn off the sampling switch and the aerosol generator.

39. Read the pressure in the sampled volume tanks.

40. Redirect the hydrogen flow through the bypass line.

41. Record the operating pressure and temperature.

42. Isolate filter with sampled seed material and open a new filter.

43. Turn on sampling system evacuation switch.

44. Change operating conditions and repeat the above procedures.

45. When all filters have been used in the aerosol density sampling manifold, cutoff furnace-sampling isolation valve and replace filters.

46. Weigh used filters to determine density of the aerosol.

47. Spray oscillograph traces with yellow lacquer to prevent overdevelopment.

APPENDIX B

EQUIPMENT PHOTOGRAPHS
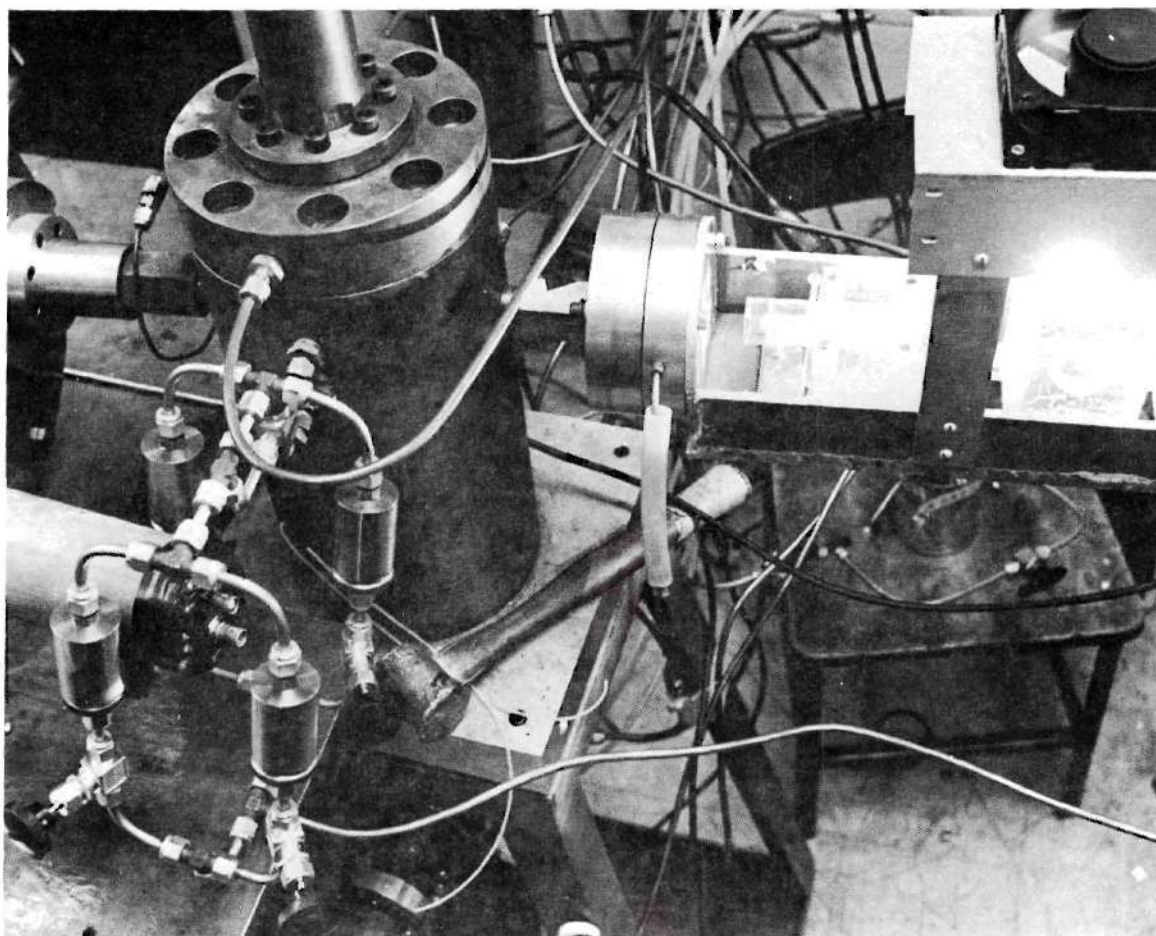
Figure 45. High Pressure Furnace and Light Source

(The high pressure furnace, light source, and sampling system can be seen in this photograph. The interconnecting tubing is part of the gas supply and water cooling systems. The equipment is inside the hood.)
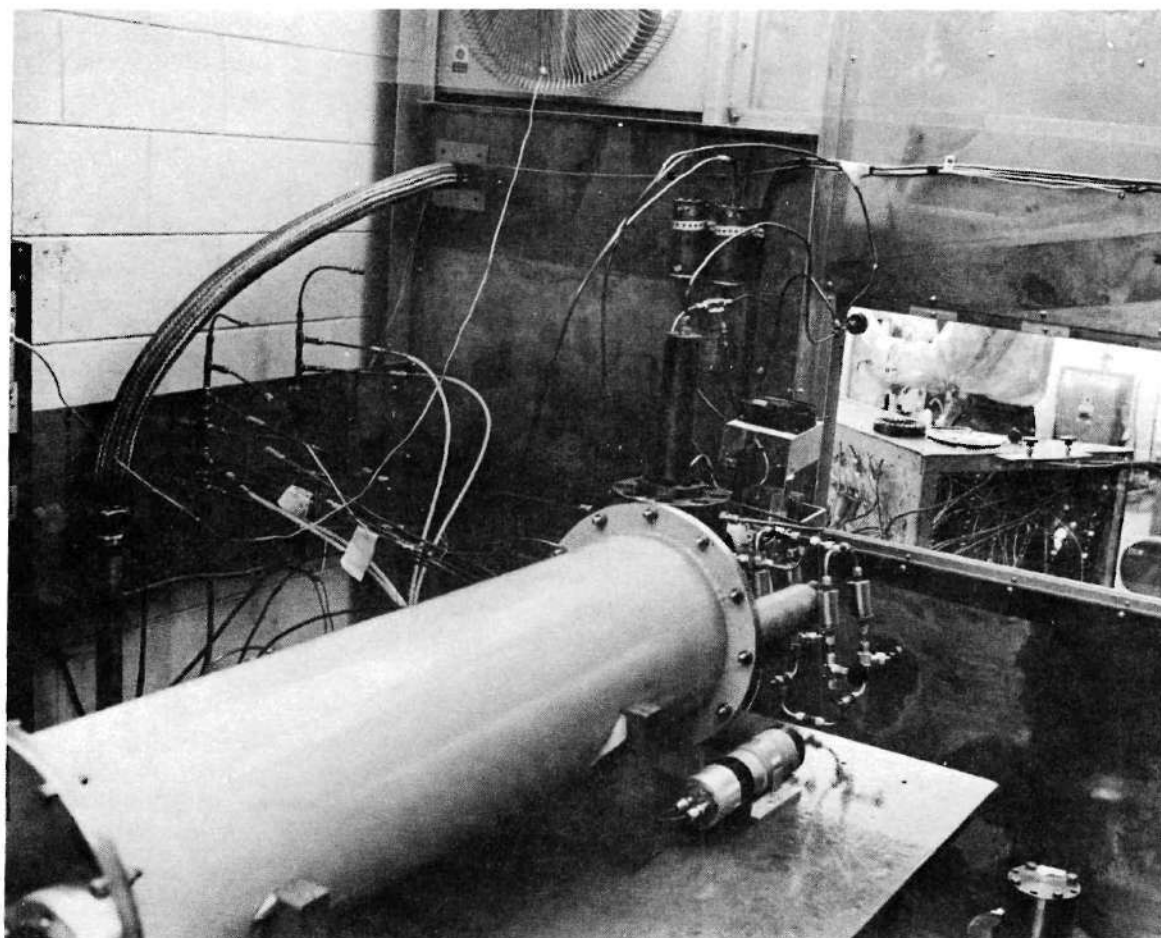
Figure 46.   Monochromator and Experimental Area
(An overall view of the experimental equipment showing the monochroma-
tor in the foreground and the furnace and light source in the hood.
Through the Plexiglas window in the hood can be seen the back of the
control panel.)
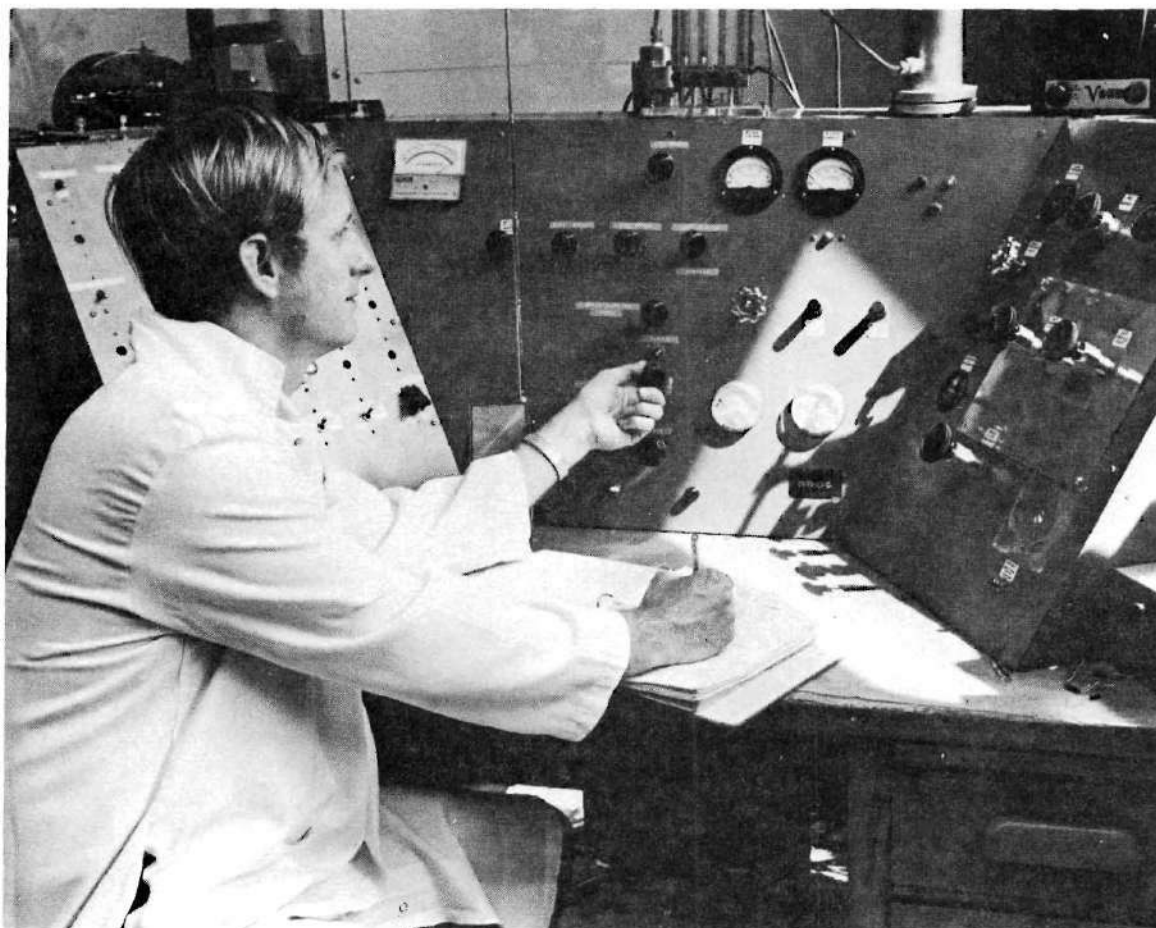
Figure 47. Control Panel

(The control panel is located in front of the hood and allows remote control of all gas flows and electrical equipment. Many of the electrical systems must be operated in sequence since electrical interlocks have been installed in the system for safety.)

Figure 48. Electronic Instrumentation

(The data recording instrumentation is on a table adjacent to the con-
trol panel. Shown in the photograph are the picoammeters required to
amplify the signals from the photomultipliers, the oscillograph and the
instrumentation tape recorder which record the amplified signals simul-
taneously, and the high voltage supplies for the photomultiplier tubes.)

REFERENCES

1. L. P. Hatch, W. H. Regan, and J. R. Powell, "Fluidized Solids as a Nuclear Fuel for Rocket Propulsion," *American Rocket Society Journal*, 31, 547 (1961).

2. Y. S. Tang, J. S. Stefanko, and P. W. Dickson, "The Colloid Core Concept - A Possible Forerunner for the Gaseous Core," University of Florida Symposium on Research on Uranium Plasmas and Their Technological Application, January 1970.

3. R. G. Ragsdale, A. F. Kascak, and L. F. Donovon, "Performance Potential of a Radiant Heat Transfer Liquid-Core Nuclear Rocket Engine," NASA TN-D4127, 1967.

4. R. V. Meghreblian, "Gaseous Fission Reactors for Booster Propulsion," *Amer. Rocket Soc. J.*, 32, 13 (1962).

5. E. E. Duke and W. J. Houghton, "Gas-Core Nuclear Rocket Engine," *Journal of Spacecraft*, 4: 12 (1967).

6. F. E. Rom, "Coaxial Flow Gaseous Nuclear Reactor Concept," *Proceedings of an Advanced Nuclear Propulsion Symposium*, Los Alamos Scientific Laboratory Report LA-3229, 177-179 (January 1965).

7. F. E. Rom, "Comments on the Feasibility of Developing Gas Core Nuclear Reactors," NASA TMX-52644, October 1969.

8. C. D. Lanzo, "A Flow Experiment in a Curved Porous Wall Gas-Core Cavity Geometry," *Nuclear Applications and Technology*, 8:1, 6 (1970).

9. G. H. McLafferty and J. W. Clark, "Summary of Research on the Nuclear Light Bulb Reactor," University of Florida Symposium on Uranium Plasmas and Their Technological Application, January 1970.

10. P. J. Marteney, A. E. Mensing, and N. L. Krascella, "Experimental Investigation of the Spectral Emission Characteristics of Argon-Tungsten and Argon-Uranium Induction Heated Plasmas," United Aircraft Research Laboratories Report No. G-910092-11, 1968.

11. A. G. Randol III, "Determination of High Pressure High Temperature Uranium Plasma Properties," Ph.D. Thesis, University of Florida, August 1969.

12.   A. S. Shenoy, "The Attenuation of Radiant Energy in Hot Seeded Hydrogen," Ph.D. Thesis, Georgia Institute of Technology, June 1969.

13.   W. L. Partain, J. R. Williams, and J. D. Clement, "Heat Transfer Parameters for Advanced Nuclear Propulsion Concepts," <u>Transaction of the American Nuclear Society</u>, <u>12</u>: 2, 6 (1969).

14.   D. E. Parks, G. Lane, J. C. Stewart, and S. Peyton, "Optical Constants of Uranium Plasma, Gulf General Atomic Report #8244, NASA-CR-72348, 1968.

15.   R. G. Ragsdale, "Relationship Between Engine Parameters and the Fuel Mass Contained in an Open-Cycle Gas-Core Reactor," NASA TM X-52733, 1970.

16.   N. L. Krascella, "Tables of the Composition, Opacity, and Thermodynamic Properties of Hydrogen at High Temperatures," NASA SP-3005, 1963.

17.   R. W. Patch, "Interim Absorption Coefficients and Opacities for Hydrogen Plasma at High Pressure," NASA TM X-1902, 1969.

18.   N. L. Krascella, "Theoretical Investigation of the Absorptive Properties of Small Particles and Heavy-Atom Gases," NASA CR-693, 1967.

19.   R. P. Main, "Optical Constants of Carbon-Hydrogen Mixtures," Heliodyne Corp., NASA CR-72570, 1969.

20.   R. W. Patch, "Status of Opacity Calculations for Application to Uranium-Fueled Gas-Core Reactors," University of Florida Symposium on Research on Uranium Plasmas and Their Technological Applications, January 1970.

21.   M. J. Monsler and J. L. Kerrebrock, "An Acoustic Instability Driven by Absorption of Radiation in Gases," University of Florida Symposium on Research on Uranium Plasmas and Their Technological Applications, January 1970.

22.   J. R. Williams, and S. V. Shelton, "Gas-Core Reactors for MHD Power Systems," University of Florida Symposium on Research on Uranium Plasmas and Their Technological Applications, January 1970.

23.   R. J. Rosa, "Advanced Nuclear MHD Power Plants," University of Florida Symposium on Research on Uranium Plasmas and Their Technological Applications, January 1970.

24. A. Sherman, "Gaseous Fission Closed Loop MHD Generator,"
     University of Florida Symposium on Research on Uranium Plasmas
     and Their Technological Applications, January 1970.

25. T. R. Brogan, "The Plasma MHD Power Generator," Advances in
     Plasma Physics, Vol. 1, Interscience Publishers, Somerset, N. J.
     1968.

26. R. Voshall and W. Emmerich, "MHD Power Generation with Photo-
     ionization," IEEE Transactions on Aerospace, 2: 2, 807-815 (1964).

27. A. T. Hooper, D. Newby, and A. H. Russell, "Closed-Cycle Nuclear
     MHD Studies Using Dust Suspensions," International Atomic Energy
     Agency Preprint No. SM-74/73, Magnetohydrodynamic Electrical
     Power Generation, 2nd International Symposium, Salzburg.

28. B. Waldie and I. Fells, "An Experimental Study of Gas Borne Suspen-
     sions of Thermionic Emitters as MHD Working Fluids," Royal
     Society (London) Philosophical Transactions, Series A 261, 490-5,
     (1967).

29. R. J. Rosa, Magnetohydrodynamic Energy Conversion, McGraw-Hill,
     New York, 1968.

30. W. C. Rochelle, "Review of Thermal Radiation from Liquid and
     Solid Propellant Rocket Exhausts," NASA TMX 53579, NASA/Marshall
     Space Flight Center, 1967.

31. D. J. Carlson, "Metalized Solid Propellants Exhaust Plumes,"
     AIAA Paper No. 66-652, Part II, 1966.

32. J. E. Fontenot, Jr., "Thermal Radiation from Solid Rocket Plumes
     at High Altitude," AIAA Journal 3: 5, 970-972 (1965).

33. C. D. Bartky and E. Bauer, "Predicting the Emittance of a Homo-
     geneous Plume Containing Alumina Particles," AIAA Journal of Space-
     craft and Rockets, 3: 10, 1523-1527 (1966).

34. R. P. Bobco and R. H. Edwards, "Radiation from an Absorbing
     Scattering Conical Dispersion with Non-Uniform Density," Aerospace
     Technology Research Report SSD 60571R, Los Angeles: Hughes Aircraft
     Company, 1966.

35. L. W. Stockham and T. J. Love, "Monte Carlo Solution of Radiative
     Heat Transfer from a Finite Cylindrical Cloud of Particles," AIAA
     Paper No. 68-69, 1968.

36. J. R. Williams, N. R. Byrn, W. R. Jacobs and J. D. Clement, "Monte
     Carlo Radiant Heat Transfer Analysis of Gas Core Reactors,"
     ANS Transactions, 13: 1, 13-15 (1970).

37. N. R. Byrn, "CAVEAT-A Revised Version of the General Purpose Monte Carlo Program, COHORT," Vol. I. Techniques and Validation, Brown Engineering Technical Note SE-292, October 1969; also, Vol. II. Users Manual, SE-290, August 1969.

38. D. E. Parks, G. Lane, J. C. Stewart and S. Peyton, "Optical Constants of Uranium Plasma," Gulf General Atomic Report No. 8244, NASA CR-72348, 1968.

39. B. J. Mitchel, "Re-Entry Radiation Scattering by a Boundary Layer Precipitate," AIAA Paper No. 70-156, 1970.

40. J. R. Howell, and H. E. Renkel, "Analysis of the Effects of a Seeded Propellant Layer on Thermal Radiation in the Nozzle of a Gaseous Core Nuclear Propulsion System," NASA-TN-D 3119, 1962.

41. C. N. Davies, Aerosol Science, Academic Press, New York, 1966.

42. H. L. Green and W. R. Lane, Particulate Clouds, Dust, Smokes, and Mists, D. Van Nostrand, New York, 2nd Edition, 1964.

43. C. Orr, Particulate Technology, MacMillan Co., New York, 1966.

44. E. Keng and C. Orr, "Light Boundary Effect in Photophoresis," Nature, 200, 352 (1963).

45. G. A. Mie, "Beiträge zur Optik Trüber Medien, Speziell Kolloidaler Metallösungen," Annal. d. Physik, 25, 377 (1908).

46. H. C. Van de Hulst, Light Scattering by Small Particles, John Wiley and Sons, New York, 1957.

47. J. A. Stratton, Electromagnetic Theory, McGraw-Hill Book Company, Inc., New York, 1941.

48. G. N. Plass, "Mie Scattering and Absorption Cross Sections for Absorbing Particles," Applied Optics, 5: 2, 279 (1966).

49. G. W. Kattanar and G. N. Plass, "Electromagnetic Scattering from Absorbing Spheres," Applied Optics, 6: 8, 1377 (1967).

50. M. Born and E. Wolf, Principles of Optics, 2nd Edition, Maxmillan Co., New York, 1964.

51. N. L. Krascella, "Theoretical Investigations of the Absorption and Scattering Characteristics of Small Particles," United Aircraft Research Laboratories Report C-910092-1, 1964.

52. A. L. Aden, "Electromagnetic Scattering from Spheres with Sizes Comparable to the Wavelength," Journal of Applied Physics, 22: 5, 601-5 (1951).

53. J. Svatos, "Light Scattering by Flattened Ellipsoids," Astronomical Institute of Czechoslavakia Bulletin, 18: 2, 114-19 (1967).

54. G. N. Plass, "Mie Scattering and Absorption Cross Sections for Aluminum Oxide and Magnesium Oxide," Applied Optics, 3: 7, 867-872 (1964).

55. R. Roback, "Thermodynamic Properties of Coolant Fluids and Particle Seeds for Gaseous Nuclear Rockets," NASA CR 212, 1965.

56. C. C. Masser, "Vapor-Pressure Data Extrapolated to 1000 Atmospheres (1.01 x 10^8 N/m^2) For 13 Refractory Materials With Low Thermal Absorption Cross Sections," NASA TN D-4147, 1967.

57. R. E. Duff and S. H. Bauer, "Equilibrium Composition of the C/H System at Elevated Temperature," J. of Chemical Physics, 36, 1754 (1962).

58. P. J. Marteney, "Experimental Investigation of the Opacity of Small Particles," NASA CR 211, 1965.

59. M. N. Plooster and T. B. Reed, "Carbon-Hydrogen-Acetylene Equilibrium at High Temperature," Jour. of Chemical Physics, 31: 1, 66 (1959).

60. W. A. Chupka and M. G. Inghram, "Direct Determination of the Heat of Sublimation of Carbon With the Mass Spectrometer," J. Physical Chemistry, 59, 100 (1955).

61. R. F. Baddour and J. L. Blanchet, "Reactions of Carbon Vapor with Hydrogen and with Methane in a High Intensity Arc," Industrial and Engineering Chemical Process Design and Development, 3, 258 (1964).

62. J. Drowart, et al., "Spectrometric Study of Carbon Vapor," J. of Chemical Physics, 31, 1131 (1958).

63. Zolta'n, Szabo, "The Examination of a System of Carbon and Hydrogen in the Temperature Range 1100-2600°," Journal of American Chemical Soc., 72, 3497 (1950).

64. E. A. Gulbransen, "Graphite-Hydrogen Reactions and Their Implications in Geochemistry," Nature, 212, 1920 (1966).

65. J. T. Clarke and B. R. Fox, "Reaction of Graphite Filaments with Hydrogen Above 2000°K," Jour. of Chemical Physics, 46, 827, (1967).

66. J. W. H. Chi and C. E. Landahl, "Hydrogen Reactions with Graphite Materials at High Temperatures and Pressures," Nuclear Applications 4 (1968).

67. V. R. Stull and G. N. Plass, "Emissivity of Dispersed Carbon Particles," Journal of the Optical Society of America, 50: 2 (1960).

68. N. L. Krascella, "Theoretical Investigation of the Absorption and Scattering Characteristics of Small Particles," NASA CR 212, 1965.

69. P. J. Marteney, N. L. Krascella and W. G. Burwell, "Experimental Refractive Indices and Theoretical Small-Particle Spectral Properties of Selected Metals," United Aircraft Corp. Research Laboratories, Report No. D-910092-6, 1965.

70. C. D. Lanzo and R. G. Ragsdale, "Experimental Determination of Spectral and Total Transmissivities of Clouds of Small Particles," NASA-TN-D-1405, 1962.

71. C. D. Lanzo and R. G. Ragsdale, "Heat Transfer of a Seeded Flowing Gas from an Arc Enclosed by a Quartz Tube," NASA TM X-52005, 1964.

72. C. D. Lanzo and R. G. Ragsdela, Proceedings of the 1964 Heat Transfer and Fluid Mechanics Institute, Stanford University Press, Palo Alto, Calif., 1964.

73. J. A. McAlister, J. A. Kocsis, and C. Orr, "Heat Transfer to a Gas Containing a Cloud of Particles," Semi-annual Status Report No. 8 Project A-635-002, Georgia Institute of Technology, E.E.S., Atlanta, Georgia, June 1966.

74. E. Keng and C. Orr, "Investigation of Radiant Heat Transfer to Particle-Seeded Gases for Application to Nuclear Rocket Engine Design," NASA-CR-953, 1967.

75. V. C. Burkig, "Theoretical Absorption in Seeded Gases," Douglas Report DAC-59985, NASw-1310, 1967.

76. J. R. Williams, "Radiative Heat Transfer in the Gaseous Core Nuclear Rocket," Ph.D. Thesis, Georgia Institute of Technology, Atlanta, Georgia, May 1967.

77. J. F. Klein, "Experiments for Simulating the Absorption of Thermal Radiation in the Propellant Duct of a Nuclear Light Bulb Reactor," University of Florida Symposium on Research on Uranium Plasmas and Their Technological Applications, January 1970.

78. T. J. Love, "An Experimental Investigation of Infrared Scattering by Clouds of Particles," Aerospace Research Laboratories Report ARL-64-109, June 1964.

79. J. R. Williams, "Thermal Radiation Transport in Particle-Seeded Gases," ANS Transactions, 12: 2 (1969).

80. J. R. Williams, and W. R. Jacobs, "Radiant Heat Absorption of Particle-Seeded Gases," Proceedings of the Sixth Annual Southeastern Serminar on Thermal Sciences, N. C. State Univ., Raleigh, N. C., 1970.

81. J. R. Williams, A. S. Shenoy, W. L. Partain and J. D. Clement, "Thermal Radiation Absorption by Particle-Seeded Gases," AIAA Paper No. 70-838, 1970. (to be published in Journal of Spacecraft and Rockets).

82. J. S. Cory and A. Bennett, "Thermal Absorption in Seeded Gases," DAC-60779, Donald W. Douglas Laboratories (February 1969).

83. S. Visvanathan, "Free Carrier Absorption Arising from Impurities in Semiconductors," Physical Review, 120: 2, 379-380 (1960).

84. S. L. Soo, "Gas-Solid Suspensions at High Temperatures," Journal of Applied Physics, 34: 6, 1689-1696 (1963).

85. L. Spitzer, Physics of Fully Ionized Gases, Interscience 2nd ed., 1965.

86. N. L. Krascella, "Theoretical Investigation of the Opacity of Heavy-Atom Gases," UAC Research Laboratories Report D-910092-4, September 1965.

87. W. M. Rohsenow and H. Y. Choi, Heat, Mass and Momentum Transfer, Prentice-Hall, Inc., New Jersey, p. 200, 1961.

88. W. H. McAdams, Heat Transmission, 3rd Ed., McGraw-Hill Book Co., New York, 1954.

89. J. E. Fredrickson and W. H. Redanz, "Boron Nitride for Aerospace Applications," paper presented to the Southern Materials Conference, American Society of Metals, Orlando, Florida, April 1964.

VITA

William Lee Partain, Jr. was born on September 22, 1942 in St. Louis, Missouri. He attended grammar school and two years of high school in Manchester, Georgia. In 1957 he moved to Titusville, Florida where he graduated from Titusville High School in 1960. In 1964 he received his Bachelor of Electrical Engineering degree from the Georgia Institute of Technology. He was commissioned an Ensign in the United States Navy after graduation and served aboard the USS Mullany (DD528) in the Western Pacific.

Mr. Partain left active duty in 1966 to work in the Electrical Systems Branch at the NASA/Kennedy Space Center. At the Kennedy Space Center Mr. Partain was engaged in the checkout and launch preparations of the Saturn V Instrument Unit Stage. While at the Kennedy Space Center he participated in the Graduate Engineering Extension System (GENESYS) administered by the University of Florida.

Mr. Partain entered graduate school at the Georgia Institute of Technology in 1967 and completed his Master of Science in Nuclear Engineering in 1968. In 1967 he became associated with a research grant investigating the radiant heat transfer in gas core nuclear rocket concepts and later began his Ph.D. work in this technical area. Mr. Partain is the author of "Measurements of the Extinction of Hydrogen Containing Particles at High Temperatures and Pressures," published in the Proceedings of the 6th Annual Southeastern Seminar on Thermal Sciences, N.C. State University, and of "A Study of Thermal Radiation Absorption Pro-

cesses in Gas Core Reactors," published in the Proceedings of a Symposium on Research on Uranium Plasmas and Their Technological Applications, University of Florida. He has also presented two papers at American Nuclear Society Conferences which have been published in the ANS Transactions.

Mr. Partain is married to the former Barbara Quinn of Chattanooga, Tennessee. He is a member of the American Nuclear Society and Sigma Xi.